DETECTION OF FOOD FRESHNESS AND PESTICIDES THROUGH CHEMICAL INTERACTION OF LIQUIDS OR GASES WITH SURFACES

Edoardo Donà

Doctoral Dissertation
Jožef Stefan International Postgraduate School
Ljubljana, Slovenia

Supervisor: Prof. Dr. Aleksandra Lobnik, IOS d.o.o, IPS and Faculty of Mechanical Engineering, University of Maribor, Maribor, Slovenia.
Co-Supervisor: Prof. Dr. Uroš Cvelbar, IPS and Jožef Stefan Institute, Ljubljana, Slovenia.

Evaluation Board:
Prof. Dr. Nives Ogrinc, Chair, IPS and Jožef Stefan Institute, Ljubljana, Slovenia.
Prof. Dr. Ester Heath, Member, IPS and Jožef Stefan Institute, Ljubljana, Slovenia.
Prof. Dr. Lidija Fras Zemljič, Member, Faculty of Mechanical Engineering, University of Maribor, Maribor, Slovenia.

MEDNARODNA PODIPLOMSKA ŠOLA JOŽEFA STEFANA
JOŽEF STEFAN INTERNATIONAL POSTGRADUATE SCHOOL

Edoardo Donà

DETECTION OF FOOD FRESHNESS AND PESTICIDES THROUGH CHEMICAL INTERACTION OF LIQUIDS OR GASES WITH SURFACES

Doctoral Dissertation

UGOTAVLJANJE SVEŽINE ŽIVIL IN PESTICIDOV S KEMIČNO INTERAKCIJO TEKOČIN ALI PLINOV S POVRŠINAMI

Doktorska disertacija

Supervisor: Prof. Dr. Aleksandra Lobnik

Co-Supervisor: Prof. Dr. Uroš Cvelbar

Ljubljana, Slovenia, May 2025

To . . .

Lorenzo Vendruscolo

"Conceiving freedom as the multiplication and quick gratification of desires, men distort their own nature as they generate in themselves many senseless and foolish desires and habits, many foolish fantasies. They live only to envy one another, out of lust and ostentation. Dining, travelling, owning carriages, ranks and servants to look after them, these are all considered needs for which it is worth sacrificing even one's life, honour, love of one's neighbour; and men are ready to kill themselves if they cannot satisfy these needs."

Fëdor Michajlovič Dostoevskij
The Brothers Karamazov

Acknowledgments

This PhD thesis would not have been possible without the assistance, guidance and motivation provided by numerous individuals and institutions. I am sincerely grateful to all those who have contributed to this significant journey.

First and foremost, I wish to express my deepest gratitude to my supervisor, Prof. Dr. Aleksandra Lobnik, for the opportunity she offered me, her trust, invaluable guidance, and insightful feedback throughout my PhD journey. Her expertise and unwavering patience have been instrumental in shaping my research, ultimately leading to the successful completion of this thesis. Special thanks also go to my co-supervisor, Prof. Dr. Uroš Cvelbar, for welcoming me into his laboratory, where I was able to grow scientifically under his guidance, support, and advice.

I sincerely thank my co-authors, Dr. Gerhard J. Mohr, Dr. Neelakandan Marath Santhosh, Dr. Vasyl Shvalya, Dr. Martin Košiček and Ardita Kurtishaj Hamzaj for their valuable contributions, dedication, and scientific acumen throughout our collaboration. Their efforts and expertise have been crucial in the research that underpins this thesis

I am profoundly grateful to the European Union's Horizon 2020 research and innovation program, which, through the Marie Sklodowska-Curie grant agreement no. 956265 (FoodTraNet project) provided the essential financial support for my research.

A special mention goes to everyone who worked tirelessly to make FoodTraNet a reality. This initiative offered me the unique opportunity to learn from and engage with scientists and experts from all over the world, fostering a network of knowledge that is indispensable for conducting research in today's interconnected world.

To my fellow ESRs who participated in this project, I am hugely indebted. Together, we explored not only scientific challenges but also engaged in enriching discussions on cultures and religions from around the globe. The light-hearted and joyful moments we shared gave me, unforgettable memories and renewed energy throughout this long journey.

My deepest thanks go to the IOS team, where I conducted most of the laboratory work for my thesis and where I was warmly welcomed and supported. Equally, I am grateful to the Jožef Stefan Postgraduate School, where I will defend this thesis, an institution that nurtures brilliant minds from all over the world and has enriched me with its knowledge and inspiration.

A heartfelt thank you to my family for always believing in me, encouraging me to explore the vast ocean of human knowledge, and supporting me at every step of this journey. Without them, I would not be where I am today. A special mention to my fiancée, Lea Calliku, who embarked on this adventure alongside me, offering me unconditional trust, love, and support. Thank you.

Finally, I am thankful to my friends, both near and far, for their trust, support, and for reminding me to approach life with humour and lightness.

Edoardo Donà

Abstract

Food, water, and sleep form the foundation of human needs, all of which are indispensable. However, unlike sleep, food and water have historically been beyond direct human control. Since ancient times, hunter-gatherers have migrated in search of these essential resources. The advent of agriculture marked a turning point, allowing humans to settle in one place, solving the challenge of food acquisition but introducing new problems. Food preservation and protection from pests became critical issues, and despite over 12,000 years of progress, some challenges still remain. While refrigeration and pesticides have significantly mitigated these challenges, food spoilage persists, and pesticide residues continue to contaminate our food. In this context, sensors present a promising solution, enabling real-time monitoring of food spoilage and pesticide contamination.

In this work, we developed two fluorescent probes for the detection of the pesticides chlorpyrifos and dimethoate, as well as a sensor for ammonia, a common byproduct of food spoilage. The first probe leverages a naturally occurring phenomenon, the hydrolysis of organophosphates pesticides. By accelerating this reaction using concentrated NaOH, we detected the hydrolysis byproduct rather than the pesticide itself. While organophosphates are relatively unreactive, their breakdown products are much easier to identify. Specifically, we employed a coumarin-based dye to detect methylamine, achieving a detection limit of 3.2 µg/L, well below globally established regulatory limits in USA, China, Brazil, Russia and India. The probe was also tested in green tea, yielding a recovery rate of 95.4%.

The second probe was inspired by medical applications, where oximes are commonly used as antidotes for OP poisoning. We selected a fluorescent dye featuring an oxime functional group, which, when deprotonated, acts as a potent nucleophile. Since the oxime in water would compete with hydroxide ions (necessary for the oxime activation) for the pesticide, we employed a non-nucleophilic phosphazene base, P4, to facilitate the reaction. This approach enabled the detection of chlorpyrifos at concentrations as low as 15.5 µg/L, a value below regulatory limits in several countries (India, China, Brazil and Russia). The method was further validated using a tap-water extracted matrix.

Additionally, we developed a sensor based on reduced graphene oxide for ammonia detection. Reduction of graphene oxide was achieved using low-pressure H_2 plasma, and we systematically investigated the effect of reduction time on sensor performance. Our findings revealed a transition from chemisorption-dominated to physisorption-driven sensing with prolonged reduction times. The optimal sensor, obtained after 20 seconds of plasma treatment, exhibited the highest sensitivity (relative resistance change), reaching 23.9% at 100 ppm and 47.1% at 1049 ppm, while maintaining good reversibility. Furthermore, tests conducted in ambient air confirmed the sensor's reliability.

This work demonstrates the potential of fluorescence-based probes and graphene-based sensors in addressing food safety challenges, providing innovative approaches for pesticide detection and spoilage monitoring.

Povzetek

Hrana, voda in spanje predstavljajo temeljne človeške potrebe, ki so vse nepogrešljive. Vendar pa sta hrana in voda, za razliko od spanja, zgodovinsko gledano ostali izven neposrednega nadzora človeka. Od pradavnine so se lovci in nabiralci selili v iskanju teh ključnih virov. Pojav kmetijstva je pomenil prelomnico, saj je ljudem omogočil naselitev na enem mestu, s čimer so rešili izziv pridobivanja hrane, vendar pa so se pojavile nove težave. Ohranjanje hrane in zaščita pred škodljivci sta postali ključni vprašanji in kljub več kot 12.000 letom napredka nekatere težave še vedno ostajajo. Čeprav so hladilniki in pesticidi znatno omilili te izzive, je kvarjenje hrane še vedno prisotno, ostanki pesticidov pa še naprej onesnažujejo našo prehrano. V tem kontekstu predstavljajo senzorji obetavno rešitev, saj omogočajo sprotno spremljanje kvarjenja hrane in kontaminacije s pesticidi.

V tem delu smo razvili dve fluorescenčni sondi za detekcijo pesticidov klorpirifos in dimetoat ter senzor za amonijak, ki je pogost stranski produkt kvarjenja hrane. Prva sonda izkorišča naravno pojavnost, hidrolizo organofosfatnih pesticidov. S pospeševanjem te reakcije z uporabo koncentrirane NaOH smo zaznali produkt hidrolize namesto samega pesticida. Čeprav so organofosfati razmeroma nereaktivni, je njihove razgradne produkte veliko lažje identificirati. Posebej smo uporabili barvilo na osnovi kumarina za detekcijo metilamina in pri tem dosegli mejo zaznave 3,2 µg/L, kar je bistveno pod svetovno določenimi regulatornimi mejami v ZDA, na Kitajskem, v Braziliji, Rusiji in Indiji. Sondo smo testirali tudi v zelenem čaju in dosegli izkoristek 95,4 %.

Druga sonda je bila navdihnjena z medicinskimi aplikacijami, kjer so oksimi pogosto uporabljeni kot protistrupi pri zastrupitvah z organofosfati. Izbrali smo fluorescenčno barvilo z oksimsko funkcionalno skupino, ki v deprotoniranem stanju deluje kot močan nukleofil. Ker bi oksim v vodi tekmoval s hidroksidnimi ioni (ki so potrebni za aktivacijo oksima) za pesticid, smo uporabili nenukleofilno fosfazensko bazo P4 za pospešitev reakcije. Ta pristop nam je omogočil zaznavo klorpirifosa v koncentracijah že od 15,5 µg/L, kar je pod mejami, določenimi v več državah (Indija, Kitajska, Brazilija in Rusija). Metoda je bila dodatno potrjena z uporabo matriksa, ekstrahiranega iz vodovodne vode.

Poleg tega smo razvili senzor na osnovi reduciranega grafenskega oksida za zaznavanje amoniaka. Redukcijo grafenskega oksida smo izvedli s pomočjo nizkotlačne H_2 plazme ter sistematično preučili vpliv časa redukcije na zmogljivost senzorja. Naše ugotovitve so pokazale prehod od kemisorpcije k fizisorpcijsko dominiranemu zaznavanju pri daljših časih redukcije. Optimalni senzor, pridobljen po 20 sekundah obdelave s plazmo, je izkazal najvišjo občutljivost, dosegel 23.9 % pri 100 ppm in 47.1 % pri 1049 ppm, hkrati pa ohranil dobro reverzibilnost. Poleg tega so testi v zraku potrdili zanesljivost senzorja.

Ta študija prikazuje potencial fluorescentnih sond in grafenskih senzorjev pri reševanju izzivov varnosti hrane ter ponuja inovativne pristope za zaznavanje pesticidov in spremljanje kvarjenja hrane.

Contents

List of Figures

Abbreviations

FAO	...	Food and agriculture organization
GHG	...	Greenhouse gases
DDT	...	Dichlorodiphenyltrichloroethane
EPA	...	United States Environmental Protection Agency
OC	...	Organochlorine
DNA	...	Deoxyribonucleic acid
RNA	...	Ribonucleic acid
ATP	...	Adenosine triphosphate
OP	...	Organophosphate
ACh	...	Acetylcholine
Ch	...	Choline
AChE	...	Acetylcholinesterase enzyme
EU	...	European Union
IoT	...	Internet of Things
ICT	...	Intramolecular charge transfer
TICT	...	Twisted intramolecular charge transfer
DFP	...	Di-isopropyl fluorophosphate
GR	...	Graphene
2D	...	2 Dimensions
GO	...	Graphene oxide
rGO	...	Reduced graphene oxide
RF	...	Radio frequency

ICP	...	Inductively coupled plasma
MS	...	Mass spectrometry
HPLC	...	High-performance liquid chromatography
GC	...	Gas chromatography

Symbols

CO_2	...	Carbon dioxide
CH_4	...	Methane
N_2O	...	Nitrous Oxide
NH_3	...	Ammonia
NH_4^+	...	Ammonium cation
Ca^{2+}	...	Calcium (II) ion
K_{OC}	...	Organic carbon-water partition coefficient
CaF_2	...	Calcium Fluoride
ΔE_d	...	Dissipation energy between two excited states.
Φ	...	Fluorescence Quantum Yield
τ	...	Lifetime of a generic fluorophore
K_r	...	Rate of radiative decay
K_{nr}	...	Rate of non-radiative decay to S_0
sp^2	...	Hybrid orbital with 33% s and 67% p character

Chapter 1

Introduction

1.1 Food Supply: From a Local to a Global Challenge

1.1.1 Evolution of human nutrition

Throughout history human survival and societal development have been deeply intertwined with food acquisition. Around 80,000 years ago, early humans began migrating from Africa [1-2], adapting to new environments through foraging and hunting [3-4]. The transition to agriculture, beginning roughly 12,000 years ago, marked a pivotal shift, enabling permanent settlements and fostering the rise of civilizations [5-7].

Agriculture developed independently in multiple regions. In the Fertile Crescent, wheat and barley were cultivated, while rice and millet thrived in Asia [8-9], and maize and potatoes were domesticated in the Americas [10]. The domestication of animals (around 32,000 years ago [11]) such as cattle and horses further enhanced food production, trade, and transportation, strengthening economies and social structures. Early civilizations, from Mesopotamia to Mesoamerica, established food storage systems and large-scale processing techniques, ensuring sustenance for growing populations [12].

Trade played a crucial role in food distribution. The exchange of crops and goods, such as salt, spices, and grains, connected distant regions and influenced culinary traditions [13], [14]. The Columbian Exchange of the 15th and 16th centuries accelerated global food integration, introducing new crops and livestock across continents, reshaping diets and economies. However, this globalization also introduced vulnerabilities, as reliance on trade and monoculture farming led to food shortages and economic instability [15].

The industrialization of food in the 19th and 20th centuries revolutionized production, preservation, and distribution. Advances such as canning [16-17] refrigeration [18], and large-scale agriculture reduced costs and improved food accessibility. However, the modern agriculture came with several drawbacks, deepened in the next paragraph, that are unsolved today: environmental degradation, loss of dietary diversity [19], pesticide pollution, rising health concerns related to processed foods [20-22] and the increasing issue of food waste. In addressing these challenges, technology has always played a critical role, and sensor development, although in its infancy at the time of early industrialization, has now emerged as a powerful tool. As we will explore, modern sensor technologies have the potential to tackle these persistent food-related problems by improving supply chain efficiency, monitoring food quality, and reducing waste. Today, agricultural trade is valued at over $1.75 trillion annually (FAO 2021), and food-processing technologies have enabled unprecedented global movement of food products. While international food trade is still a small part of the food consumed worldwide, the spread of global brands, culinary

knowledge, and advancements in nutrition science has arguably had a more profound impact.

Despite technological progress, food insecurity remains a global challenge. Climate change, population growth, and economic disparities threaten stable food supplies, making collaboration essential. Throughout history, humanity has overcome food crises through innovation and cooperation. Today, just as our ancestors adapted and worked together, we too must come together to deal with the complexity of food production and distribution.

1.1.2 Feeding the future: strategies for sustainable food production

By 2050, the global human population is projected to reach approximately 9.8 billion [23], an increase of nearly 20% from the current 8.2 billion, in 25 years. This population growth, combined with climate change and shifts in agricultural practices, poses a significant threat to future food security. Given the multidimensional nature of this issue, a comprehensive approach is required to mitigate these risks. The World Resources Institute has outlined key strategies to ensure sustainable food security, which should be prioritized [24]:

1. Reduce growth in demand for food and other agricultural products;
2. Increase food production without expanding agricultural land;
3. Protect and restore natural ecosystems;
4. Increase fish supply;
5. Reduce greenhouse gases (GHG) emissions from agricultural production.

These interrelated objectives present numerous challenges. The first strategy, reducing demand for agricultural products, may appear counterintuitive given population growth. However, it is crucial to recognize that between one-quarter and one-third of all food produced is wasted annually [25]. This amounts to approximately 1.3 billion tons, a quantity sufficient to feed an additional 2 billion people [26]. Consequently, current food production levels could adequately support the projected 2050 population if waste is minimized.

One approach to reducing food demand is the adoption of more sustainable diets, incorporating increased consumption of plant-based foods and alternative protein sources such as insects. This dietary shift would reduce land use and GHG emissions, since animal product produce more GHG and requires more soil compared to plants to provide the same amount of kcal [27-29]. Additionally, mitigating competition between food and bioenergy production is essential. Contrary to popular belief, biofuels are not inherently carbon-neutral; their production consumes land and water resources, increases pesticide use, and contributes to GHG emissions upon combustion [30-32].

Another viable measure to reduce food demand is stabilizing fertility rates at approximately two children per woman, thereby limiting future food requirements. While direct interventions to regulate fertility rates may be ethically contentious, research has demonstrated a strong correlation between higher levels of education, particularly among women, and lower fertility rates [33-35]. Thus, investments in education not only contribute to the development of women itself, but also play a crucial role in global food security and broader environmental sustainability.

The second objective, enhancing agricultural productivity, necessitates improvements in livestock management, fertilization, feed quality, and veterinary care. Selective breeding [36], rotational grazing [37-39] and optimized pesticide application (as only 1% of pesticides effectively target pests) are also critical strategies [40].
Additionally, advancing crop breeding through genomic selection [41-42] and enhancing water and soil management techniques, such as rainwater harvesting and agroforestry, are vital components of sustainable agricultural intensification [43-44].

The third priority, protecting and restoring natural ecosystems, has become increasingly critical in the context of climate change. Governments can influence land-use patterns through predictive models that assess crop yields, biodiversity impacts, and climate effects. These tools should guide regulatory frameworks for land use, infrastructure development, and public land management. Strategies should include directing agricultural expansion toward low-impact areas, reforesting degraded farmland, and conserving peatlands, which currently account for 5–10% of global anthropogenic carbon dioxide emissions due to land-use changes and drainage [45-46].

The fourth goal, enhancing fish supply, faces significant challenges, including overfishing [47-49] and rising ocean temperatures. Achieving this objective requires improved wild fishery management, particularly in underutilized regions, alongside the expansion of aquaculture [50]. In 2020, aquaculture accounted for 46% of global fish production. Sustainable aquaculture practices, including selective breeding, improved feed formulations, disease management, water recirculation systems, pollution control measures, and spatial planning for new marine farms, are essential for meeting future protein demands while minimizing environmental impact [51-53].

Finally, mitigating GHG emissions from agriculture is a central challenge of the 21st century. Currently, food production accounts for approximately one-quarter of global GHG emissions [54-55]. While drastic reductions in emissions are unlikely due to rising food demand, mitigation strategies aim to maintain current emission levels through 2050. Ruminant livestock are responsible for approximately half of all agricultural emission [56], primarily due to enteric fermentation, which releases mainly methane, that has 28 times greater global warming potential than CO_2 on a 100-year timescale. Reducing these emissions can be achieved by improving ruminant productivity [57-58] and incorporating methane-reducing feed additives [36-39]. Manure management is another critical area where government policies and financial incentives can promote technological advancements and best practices [63-64]. Enhancing fertilizer efficiency, particularly nitrogen (N) fertilizers, is also crucial, as current nitrogen use efficiency ranges from 30% to 53%, leading to significant losses [65]. Excessive nitrogen application, low plant density, and inefficient application methods contribute to these losses [66].

Furthermore, rice cultivation is a significant source of CH_4 and N_2O emissions. Methane emissions arise from the anaerobic decomposition of organic material in flooded rice fields, while N_2O emissions result from excessive nitrogen availability in soils and manure applications [67-68]. Addressing these emissions requires improved water and nutrient management. Additionally, transitioning agricultural energy sources toward renewables for ploughing, irrigation, fertilization, and harvesting [69], is a critical step toward sustainability. Achieving these transformations will necessitate not only technological innovations but also systemic socio-economic transitions in a co-evolutionary manner [70].

These challenges require the creation and enhancement of models to predict and monitor the impact of our decisions and also to provide information to the end user, to minimize waste production and understand the impact of our choices. To ensure these models remain reliable and to provide up to date information, an increasing amount of data will be produced and needed. This is where sensors can play a crucial role. Their miniaturization and relatively low cost enable widespread deployment, allowing them to become part of the Internet of Things (IoT), where they continuously transmit data and provide real-time information. In this thesis, I aimed to contribute to these innovation pathways by developing new sensors for food safety and quality.

1.2 Food Spoilage

To achieve the goal of reducing food demand, one of the most effective actions individuals can take is minimizing food waste. In Europe, households account for an astonishing 53% of food waste within the supply chain [71]. While this may be surprising, it also underscores the significant impact that each individual can have in addressing this issue. But why does this happen? As with most complex challenges of the modern era, there is no single, straightforward answer. Several factors contribute to food waste, including purchasing or cooking excessive amounts, failing to create or adhere to a shopping list, inadequate meal planning, neglecting to conduct a food inventory before shopping, making impulse purchases, and discarding food that has exceeded its shelf life [72-73]. While some of these issues cannot be easily addressed through natural sciences, the expiration date of a product is something that can be scientifically determined. Over the years, significant advancements have been made in this field, providing consumers with improved food management systems. However, these systems have inherent limitations, as their predictive models rely on a strictly maintained cold chain and packaging integrity [74]. Additionally, fresh produce, home-cooked meals, and certain refrigerated foods do not come with a predetermined expiration date. A potential solution to this problem is a "smart" refrigerator equipped with artificial intelligence, capable of assessing the shelf life of stored items and suggesting meal plans to minimize food waste. Research is actively moving in this direction, with the development of sensors that can detect signs of spoilage in real time and determine when food is no longer safe for consumption [75]. To create these sensors, it is first necessary to understand the chemical compounds produced during food aging. To do so is important to know the food composition which is biological raw materials that inevitably deteriorate over time. The food composition changing over time is crucial in the creation of sensors, since they have to precisely understand when the food is spoiled. But when is it spoiled? Generally, it is deemed spoiled when it becomes unacceptable to consumers. In the worst-case scenario, consumption poses a health risk. However, spoilage can also occur in less severe forms, such as changes in colour [76] (fig. 1), flavour, texture, or aroma that render the food unappetizing. Additionally, the depletion of essential nutrients may cause the product to no longer meet its declared nutritional value [77].

In this thesis, I have focused on the gases produced during the decomposition of food, since measuring their concentration can provide clear indications of the aging of certain type of food, and consequently whether if it is still safe for consumption.

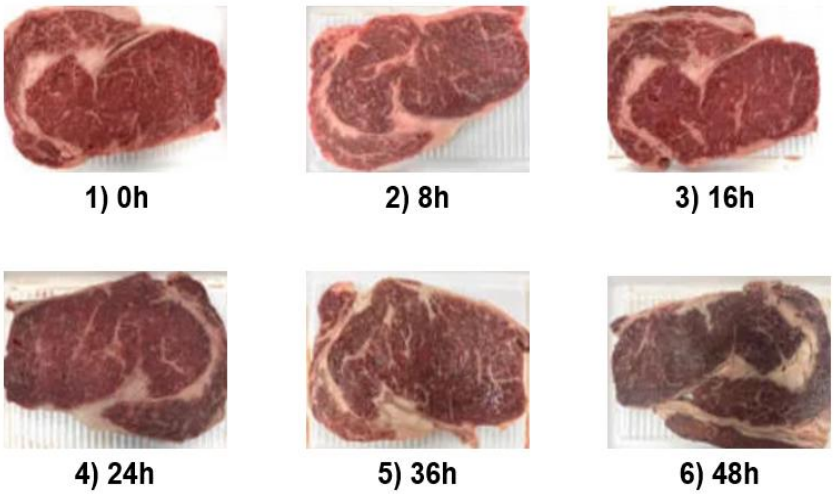

Figure 1: Meat colour changes due to spoilage.

1.2.1 Gas production due to food spoilage

Food spoilage and ripening are influenced by multiple factors, but monitoring these processes can help reduce food waste. A key aspect of food degradation is the release of various gases, which can be detected and correlated with spoilage. This presents an opportunity for effective monitoring and early intervention [78]. Fruits, for example, can be categorized into two main groups: climacteric and non-climacteric. The key distinction between them is that climacteric fruits produce ethylene during ripening, whereas non-climacteric fruits do not [79]. This explains why bananas can continue to ripen after harvesting, while pineapples can only mature while still attached to the plant. Ethylene is not only responsible for ripening but can also be used to accelerate the process in fruits such as apples, avocados, kiwis, pears, and tomatoes. Additionally, ethylene detection allows for better monitoring of fruit maturation [80-81]. Another important indicator of food spoilage is hydrogen sulphide, which is particularly relevant in fish and rotten eggs. This gas is released due to enzymatic degradation and microbial reduction of sulphate [82]. Similarly, carbon dioxide is produced during meat spoilage, making it another gas that can be monitored [83-84]. Interestingly, carbon dioxide can also help slow down spoilage by inhibiting the proliferation of aerobic microorganisms [85]. Both meat and fish spoilage share the common by-products of ammonia [86] and biogenic amines [87] which are generated through the decarboxylation of amino acid precursors. Unlike carbon dioxide and ethylene, these compounds are highly reactive and significantly contribute to the distinct odours associated with spoilage. Ammonia formation occurs due to the activity of deaminase enzymes, which remove amino groups from amino acids. This process not only produces unpleasant odours but also alters the pH of the food, affecting both its quality and safety.

1.2.1.1 Ammonia (NH_3)

For these reasons, and given that ammonia is one of the most widely produced gases globally, reaching 235 million tonnes in 2019 [88], I have focused part of my research on developing a sensor capable of detecting ammonia. At room temperature, ammonia is a colourless gas with a highly irritating, pungent odour. It possesses alkaline and corrosive properties and is also hygroscopic. Approximately 80% of industrially produced ammonia, synthesized through the Haber-Bosch process [89], in enormous industrial plant (fig. 2) and is used in agriculture as a fertilizer. Beyond this, ammonia serves various purposes, including its use as a refrigerant gas, in water purification, and in the production of plastics, explosives, textiles, pesticides, dyes, and other chemicals. It is also a key component in many household and industrial-strength cleaning solutions [90].

The properties of ammonia stem from its molecular structure, which adopts a trigonal pyramidal shape. The central nitrogen atom has five valence electrons and forms three bonds with hydrogen atoms, resulting in a total of eight electrons, or four electron pairs, arranged in a tetrahedral configuration. However, one of these pairs is a lone pair, which exerts greater repulsion than bonding pairs, reducing the bond angle from the expected 109.5° (typical of a regular tetrahedral structure) to 106.8°. This shape gives the ammonia molecule a dipole moment, making it polar. Its polarity, particularly its ability to form hydrogen bonds, allows ammonia to be highly miscible with water. The lone pair also makes ammonia a nucleophile and a base, enabling it to act as a proton acceptor in water and form the ammonium cation $[NH_4]^+$.

In the food industry, ammonia is primarily recognized for its role in fertilizer production. It is commonly combined with nitric acid to produce ammonium nitrate or with carbon dioxide to form urea. However, ammonia is not solely a human-made compound, various microorganisms generate it by breaking down food sources [91], particularly fish [92]. Hence

detecting ammonia in food can provide clear information about the degradation level of the food, preventing spoilage and provide consumers with reliable indication about the status of stored food.

Given these considerations, a sensor based on reduced graphene oxide, designed to detect ammonia efficiently and contribute to improved food safety has been developed.

Figure 2: Ammonia production plant. Created by Dall-E.

1.3 Chemical Pesticides

Since the end of World War II, synthetic pesticides have played a central role in the intensification of agriculture, particularly during the "Green Revolution". This period saw the rapid modernization of farming, supported by significant investments in agricultural research and development by both governments and industry. However, the widespread use of synthetic pesticides also introduced new, often unseen, risks [93]. The large-scale application of agrochemicals resulted in forms of "slow and invisible violence" that affected farmworkers and consumers alike. These chemicals were released into the environment in massive quantities, millions of tonnes, before their harmful effects were fully understood or adequately controlled. Like other pollutants, pesticides have created an unequal distribution of health and environmental hazards, disproportionately affecting vulnerable populations and ecosystems.

Dichlorodiphenyltrichloroethane, commonly known as DDT stands out as a landmark compound in the history of pesticides. The compound's global spread during the 1950s and 1960s (Figure 3, [94]), was fuelled by a confluence of factors, including the efforts of transnational institutions, Cold War geopolitical strategies, the chemical industry's growing influence, and the rise of intensive monoculture farming. Media outlets, government officials, and networks of scientific experts enthusiastically promoted DDT for its dual promise: fighting disease and improving agricultural yields. It became a symbol of modern technology's triumph over pests and disease, and its use was framed within an urgent wartime and philanthropic narrative.

However, this widespread adoption overshadowed early toxicological warnings about DDT's harmful effects on mammals and other wildlife. Public scepticism about its safety was met with significant resources devoted to reassuring the public, including campaigns that portrayed DDT as harmless and suitable for use not only in agriculture but also in homes and hospitals [95]. In the United States, concerns about DDT eventually shifted focus to its environmental impact. One of the most alarming indicators of its ecological damage was the sharp decline in the bald eagle population, a consequence of the compound's bioaccumulation in the food chain [96]. The issue with DDT was the extremely long half-life in the environment (in the soil from 2 to 15 years) leading to unacceptable accumulation levels that were causing the thinning of eagle eggs. These concerns were brought to the forefront by Rachel Carson's seminal 1962 book, "Silent Spring", which exposed the ecological and health risks associated with pesticides. Carson's work sparked widespread public awareness and galvanized the environmental movement. This growing advocacy culminated in a landmark decision: in 1972, the United States Environmental Protection Agency (EPA) banned DDT for agricultural use.

The ban symbolized a turning point in how society evaluated the trade-offs between technological progress and environmental stewardship, underscoring the importance of rigorous scrutiny in the use of chemical agents.

Figure 3: Advertising campaign for DDT in the 1950s. [94]

1.3.1 Organophosphates rise

The decline of DDT and many other organochlorine (OC) pesticides in the 1970s, due to their toxic effects on mammals, paved the way for the adoption of a new class of pesticides: organophosphates (OP). The term "organophosphate" refers to a broad variety of chemical compounds and biomolecules that feature a central phosphate molecule with alkyl or aromatic substituents. Examples of such compounds include DNA, RNA, ATP, triphenyl phosphate (used as a flame retardant), and tricresyl phosphate (employed as a plasticizer).

However, the most widely produced and used OPs are pesticides, with glyphosate being perhaps the most well-known.

Initially, OPs suffered from the same high mammalian toxicity issues as their OC counterparts. However, the introduction of malathion by American Cyanamid in 1950 marked a breakthrough [97]. Malathion combined effective insecticidal properties with low mammalian toxicity and much faster environment degradation (about 17 days in soil). The subsequent development of even less toxic compounds, coupled with growing concerns over pest resistance and the environmental persistence of OCs, ushered in a new era for OP pesticides. By 1970, annual production of OPs had already exceeded 50,000 tonnes [98]. Nowadays they still represent around 40% of the worldwide use of pesticides [99].

1.3.1.1 Organophosphates in the environment

OPs application in fields and crops has significant environmental and health implications. These chemicals primarily enter the environment through agricultural runoff, direct application to crops, accidental spills, and improper handling. Once applied, OP pesticides leach into the soil, seep into groundwater, and are carried into surface water bodies through irrigation runoff. Additionally, these compounds can volatilize into the atmosphere, particularly under high temperatures and windy conditions, contributing to air contamination. These pathways expose various ecological and human systems to pesticide residues [100]. The pervasive nature of OP pesticides means they pollute multiple environmental matrices as can be seen in fig. 4. In aquatic ecosystems, they harm microbial populations, disrupt photosynthesis in algae, and reduce biodiversity, affecting the entire food chain. In soils, OP pesticides degrade the microbial community, acidify the environment, and threaten soil fertility. The compounds also pose risks to terrestrial organisms through direct contact or ingestion of contaminated water and plants. In the air, pesticide drift and volatilization can lead to respiratory and neurological disorders in humans and animals. Chronic exposure has been linked to severe health issues, including reproductive problems, genetic mutations, and neurological disorders [101].

Degradation of OP pesticides occurs through both abiotic and biotic processes. Abiotic factors such as hydrolysis, photolysis, and chemical reactions can break down these compounds into by-products, that can be also detected to monitor pesticide concentration and degradation [102]. The efficiency of these processes depends on environmental conditions such as temperature, pH, and the presence of sunlight. Biotic degradation primarily involves microbial activity, where bacteria and fungi metabolize the pesticides into harmless substances [103]. Some species, such as Pseudomonas and Bacillus, have been engineered to enhance the breakdown of specific OP compounds. Despite these degradation pathways, many OP pesticides are semi-persistent, with half-lives ranging from days to months, depending on their chemical structure and environmental conditions. Chlorpyrifos, for example, has a half-life in soil of up to 120 days under certain conditions, highlighting the risk of long-term contamination [104]. But the fate of a pesticide does not always end when the degradation is completed, since several other byproducts are produced. Notably, some of these degradation products can be as toxic, if not more so, than the original compounds. For instance, the breakdown of chlorpyrifos results in metabolites such as chlorpyrifos-oxon and 3,5,6-trichloro-2-pyridinol, both of which exhibit higher toxicity levels compared to their parent compound [105]. Similarly, the degradation of glyphosate [106], produces aminomethylphosphonic acid (AMPA), a metabolite that is more persistent in the environment and can be more toxic than glyphosate itself. Also, dimethoate [107], undergoes degradation in soil, leading to the formation of metabolites such as omethoate, which is even more toxic than the parent compound. Furthermore, dimethoate degradation can also produce other toxic byproducts that may persist in the soil for extended periods,

potentially affecting soil microbial communities and reducing soil fertility. For these reasons it is important to monitor also degradation compounds.

In summary, while OP pesticides play a critical role in agricultural productivity, their environmental and health costs necessitate urgent attention. Comprehensive efforts combining innovative remediation technologies and preventive measures are essential to manage their impact effectively and safeguard ecosystems and human health. However, after more than 50 years of activity, alternatives like pyrethroids are in the market, especially in the more developed countries, due to their less toxicity. But every chemical sprayed bring environmental consequences so now more than ever sustainable alternatives are urgent.

Figure 4: Indian man spraying pesticides in a field.

1.3.1.2 Organophosphates mechanism of action

OPs based their toxicity for insects but also for human on the inhibition of the acetylcholinesterase enzyme (AChE). To understand the mechanism of action it is important to understand the role of acetylcholine (ACh) functions and chemical properties. It is a neurotransmitter composed by an acetyl group bound to a choline (Ch) moiety, making it a quaternary ammonium compound. It is a hydrophilic and positively charged at physiological pH, which influences its interaction with receptors. The function of a neurotransmitter is to transmit signal across synapses, the junctions between neurons or between neurons and target cells (e.g. muscle cells). These molecules enable communication within the nervous system and between the nervous system and other parts of the body. As a result, we are able to contract our muscles and ultimately live.

OPs interfere with the termination phase of neurotransmission by inhibiting AChE. Within the active site of AChE lies a catalytic triad (esteratic site) consisting of serine, histidine, and glutamate. This triad plays a central role in hydrolysing ACh under normal conditions.

When an OP molecule enters the active site of AChE, its highly reactive phosphorus atom binds covalently to the serine hydroxyl group as showed in fig. 5. The oxygen of the serine is electron-rich due to the proximity with the N of histidine, and the result is a very good nucleophile capable to attack the phosphate group. This reaction produces a phosphorylated enzyme intermediate, which is far more stable than the acetyl-enzyme

intermediate typically formed during ACh hydrolysis. Over time, the phosphorylated enzyme undergoes a process known as "aging", during which one of the alkyls or alkoxy groups attached to the phosphorus atom is lost. This structural rearrangement stabilizes the bond between the OP and AChE, rendering the enzyme irreversibly inactivated. Once aged, even antidotes like oximes, which are designed to cleave the bond, are ineffective at reactivating the enzyme as can be seen in fig. 5 [108].

As a result of AChE inhibition, ACh accumulates in the synaptic cleft. This causes continuous stimulation of cholinergic receptors, leading to a phenomenon known as a cholinergic crisis. The excessive activation of these receptors produces a range of symptoms, including salivation, lacrimation, urination, diarrhoea, gastrointestinal distress, and muscle twitching, collectively referred to as "sludge" syndrome. In severe cases, this overstimulation can lead to respiratory paralysis and failure of the autonomic nervous system, potentially resulting in death.

Luckly, if caught in time this poisoning is not fatal, since antidote like oxime can help to reverse the binding between AChE and the OP. Oximes, such as pralidoxime (2-PAM), obidoxime, and asoxime, are a class of antidotes designed to reactivate AChE by cleaving the covalent bond between the phosphorus atom of the OP and the serine residue in the enzyme's active site as can be seen in fig. 5. These compounds work through their nucleophilic properties, exploiting their oxime (-C=NOH) functional group. When an oxime is administered, it binds to AChE near the phosphorylated serine residue. The oxime group, with its strong nucleophilicity, attacks the phosphorus atom of the OP-enzyme complex. This reaction displaces the serine residue and restores the free, active enzyme as can be seen in fig 5. The success of this reactivation depends on the structural compatibility of the oxime with the phosphorylated enzyme and the time elapsed since OP exposure.

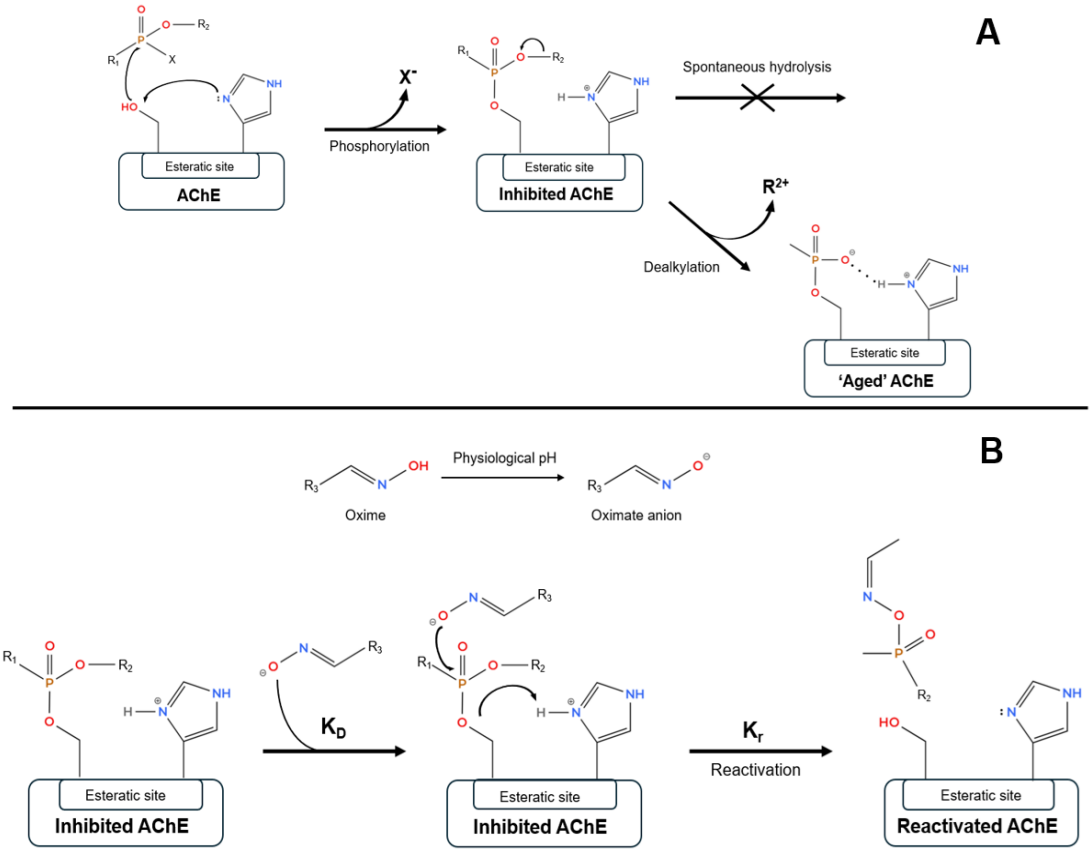

Figure 5: (a) OP inhibition of AChE (b) subsequent reactivation with oxime [108].

Once "*aging*" occurs, structural rearrangements in the phosphorylated enzyme result in a more stable complex, making it resistant to reactivation by oximes. So, oximes are most effective when administered promptly after exposure, before significant enzyme "*aging*" has occurred. However, their effectiveness varies depending on the specific OP compound involved, as some OPs "*age*" more rapidly than others. By restoring AChE activity, oximes alleviate the toxic effects of OPs and help normalize cholinergic signalling, underscoring their critical role in the management of OP poisoning.

1.3.1.3 Organophosphates classification and detection methods

OPs can be broadly divided into various categories based on their chemical structure and functional groups as can be seen in fig. 6:

- Phosphates: Compounds where the phosphorus atom is bonded to four oxygen atoms, either directly or through organic groups. These are the simplest form of OPs;
- Phosphorothioates: A subgroup where one of the oxygen atoms attached to phosphorus is replaced by a sulphur atom. This substitution has significant implications for the compound's activity and toxicity;
- Phosphorodithioates: Compounds with two sulphur atoms replacing oxygen atoms in the structure. These compounds are often pro-pesticides, requiring metabolic activation to exert their toxic effects;
- Phosphonates: In these compounds, one of the oxygen atoms is replaced by a direct carbon-phosphorus (C-P) bond. These are less common in pesticide applications.
- Phosphoramidates: As the name suggests, one of the oxygen atoms is replaced by a direct nitrogen-phosphorus (N-P) bond;
- Phosphoramidothioates: These compounds are a combination of two previous group, where two oxygen atoms are replaced by a sulphur-phosphorus (S-P) and nitrogen-phosphorus (N-P) bonds;
- Phosphonofluoridates: These compounds are the most toxic one, and there is a bond between fluorine and phosphorus (F-P).

OPs are usually distinguished by the presence or not of heteroatoms different from oxygen. When only oxygen is present (oxon compounds), the effect is a pesticide more reactive and more potent AChE inhibitors. The sulphur substitution serves dual purposes: it reduces the pesticide's toxicity to non-target species and enhances its environmental stability during storage. However, this pro-pesticide required bioactivation in the target organism by oxidative enzymes (e.g. cytochrome P450), into more toxic oxon derivatives, which is crucial in determining their selectivity and overall toxicity.

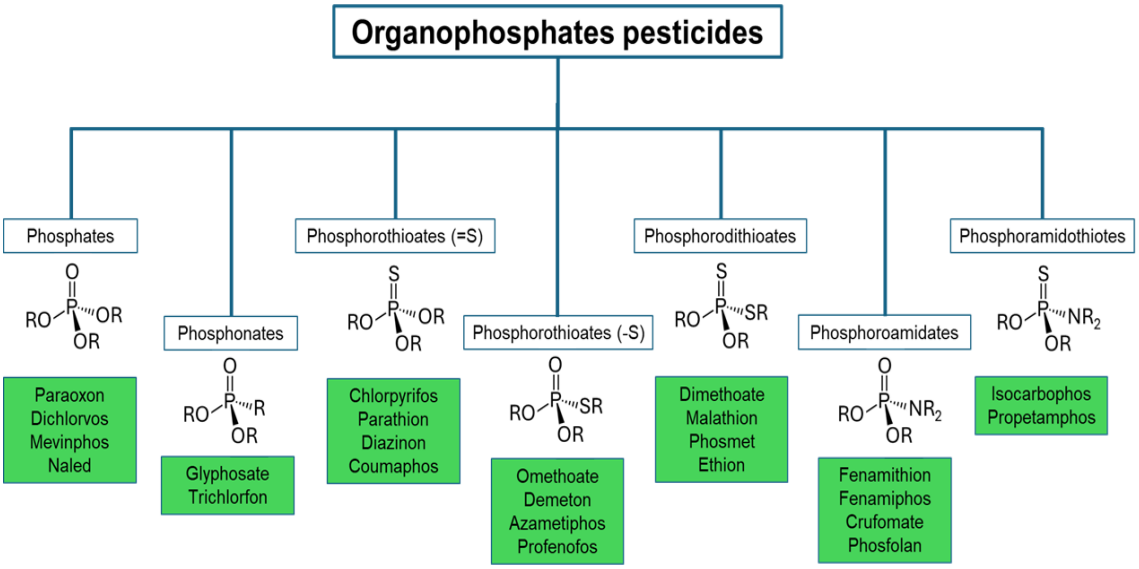

Figure 6: Main categories of OPs pesticide.

Nowadays, when it comes to detecting these compounds in food, chromatographic and mass spectrometry (MS) methods stand as the gold standard. Techniques like gas chromatography-mass spectrometry (GC-MS) and liquid chromatography-tandem mass spectrometry (LC-MS/MS) offer unparalleled sensitivity, specificity, and accuracy. These methods can detect even trace amounts of pesticides, ensuring food safety and compliance with strict regulations. However, despite their precision, they are time-consuming, expensive, and require specialized labs. This means we can't test every single food sample in the supply chain [109]. That's why we need alternative sensors and biosensors, rapid, cost-effective tools that can provide on-site detection, helping bridge the gap where chromatographic methods fall short. Together, these approaches would ensure a safer, more efficient food monitoring system.

1.3.1.3.1 Chlorpyrifos

Chlorpyrifos belongs to the category of phosphorothioates due to the presence of a double bond between phosphorus and sulphur (P=S) as can be seen in fig. 7. Introduced to the market in 1966, chlorpyrifos gained prominence during a period when the insecticide DDT was being criticized for its detrimental environmental effects. Its effectiveness, affordability, and broad-spectrum action compared to alternative products quickly made it one of the most widely used insecticides [110]. It is sprayed on the crops (on the stem or on the leaf) and affect the insects when they come in direct contact with the pesticide, so spraying point and distribution are crucial for the effectivity.

The mode of action of chlorpyrifos involves bioactivation by oxidative enzymes, converting it into its active oxon form, which then exerts its toxic effects. It is a broad-spectrum insecticide employed to control a wide variety of insect pests, including household pests such as cockroaches, fleas, and termites, as well as livestock pests like cattle ticks. It is also widely used in agriculture on crops such as maize, nuts, soybeans, and tree fruits [111]. Before 2001, chlorpyrifos was extensively used for residential pest control, including lawn treatments, termite management, and flea and tick control on pets. However, its residential applications were phased out in the United States in 2001 due to mounting evidence of its toxic effects on humans, particularly children. Several studies have highlighted the long-term health risks associated with chlorpyrifos exposure, including neurological damage, where prenatal exposure has been linked to neurocognitive deficits in

children [112]. It has also been implicated as an endocrine disruptor and associated with an increased risk of cardiovascular diseases [113].

From an environmental perspective, chlorpyrifos has been reported to degrade relatively quickly through hydrolytic and photolytic processes under neutral pH conditions. However, studies have observed its persistence in natural water bodies for up to eight weeks [114], and its half-life can be up to 120 days under certain conditions [104]. Chlorpyrifos binds to aquatic sediments, with dissipation rates in sediment comparable to those in soil [115]. Degradation is slower under conditions of low temperature, anaerobic environments, and high salinity, contributing to its environmental impact. Non-target species, including birds [116], fish [115], and pollinators like bees, have been adversely affected by its use [117]. Due to these concerns, the European Union (EU) decided not to renew chlorpyrifos authorization in 2020. In the United States, an initial ban was proposed for 2017. However, a political shift under the Trump administration delayed the decision until August 2021, when the pesticide was finally banned. This ban was partially overturned in November 2023 when a federal appeals court deemed the decision "arbitrary and capricious." As a result, in February 2024, the EPA implemented a partial ban, exempting 11 crops, including apples, cherries, peaches, and strawberries. In all other countries, chlorpyrifos remains permitted. Despite these regulatory changes, monitoring chlorpyrifos residues in food remains crucial, particularly as the EU imported €158 billion worth of agri-food products in 2023 [118]. To address this concern, I focused part of my research on developing a probe capable of detecting this pesticide.

1.3.1.3.2 Dimethoate

Dimethoate is classified as a phosphorodithioate due to the presence of a double bond between phosphorus and sulphur (P=S), as well as a single bond between phosphorus and an additional sulphur atom (P-S) as shown in Figure 7. Introduced to the market in 1956, dimethoate has been widely utilized for the control of various insect pests, including mites, flies, aphids, and plant hoppers [119]. Its mechanism of action is similar to that of chlorpyrifos, as both require enzymatic oxidation to become biologically active.

Dimethoate gained popularity not only due to its direct spraying effectiveness, comparable to that of chlorpyrifos, but also because it is a systemic pesticide. This means it is absorbed by plants and translocated throughout their tissues, providing protection to the entire plant, including new growth, against sap-feeding pests [120]. Dimethoate is approximately three orders of magnitude more soluble in water than chlorpyrifos (2.5 g/L compared to 0.0014 g/L), and it exhibits relatively poor soil absorption ($K_{oc} = 20$) [121], depending on environmental conditions. As a result, it is susceptible to leaching, which can pose risks to groundwater, particularly in areas with frequent pesticide application. However, its relatively short half-life in soil and water reduces the potential for long-term environmental contamination. The degradation products of dimethoate, such as omethoate, remain biologically active and contribute to its overall toxicity [122]. If the pH of the soil is basic, dimethoate tends to hydrolyse giving methylamine, thioglycolic acid and thiophosphate [123].

Despite its limited persistence, dimethoate is highly toxic to non-target organisms, including bees, fish, and aquatic invertebrates, raising concerns regarding its impact on ecosystems [121]. In 2019, dimethoate was banned in the EU due to its potential human health risks, adverse environmental effects on non-target organisms, pesticide residues on crops exceeding safe levels, and the availability of less toxic alternatives. However, since dimethoate continues to be used in other parts of the world, and imported food products may still contain residues, monitoring for this pesticide remains crucial. To address this concern, a probe capable of detecting dimethoate has been developed.

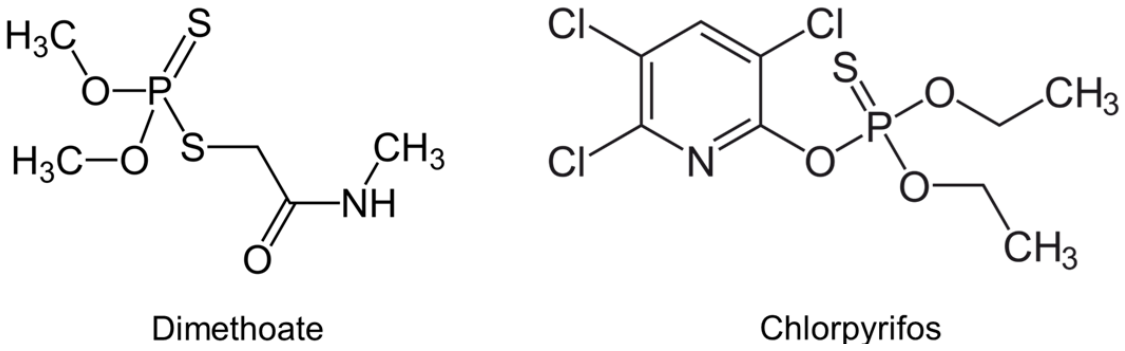

Dimethoate Chlorpyrifos

Figure 7: Dimethoate and Chlorpyrifos molecular structure.

1.4 Sensors

In general terms, a sensor is a device that detects some physical property and records, indicates or otherwise responds to it. Living organisms on this planet have developed different ways of perceiving the reality around us, such as the five senses of the human being. Therefore, every living being can be considered a sensor in some way. Modern man, however, has gone much further, enhancing the perception of reality with objective and replicable instruments that are part of today's world, such as thermometers, barometers, accelerometers, etc.

It was the 20th century that paved the way for the modern sensor concept, with its rapid technological progress leading to diversification and miniaturization of sensors. The advent of electronics and semiconductor technology revolutionized sensing mechanisms, enabling the development of highly sensitive and reliable sensors across multiple domains. Optical sensors emerged with the discovery of the photoelectric effect (fig. 8), which Albert Einstein explained in 1905, leading to the creation of photodetectors, cameras, and light-based sensors used in automation, imaging, and communication systems. Chemical and electrochemical sensors, based on selective ion detection and catalytic reactions, gained prominence in medical diagnostics, environmental monitoring, and industrial safety applications. The pH sensor, developed in the early 20th century, remains a cornerstone in analytical chemistry, facilitating precise measurements in various scientific and industrial processes [124].

The miniaturization of sensors, particularly with the advent of microelectromechanical systems (MEMS) in the late 20th century, significantly enhanced their efficiency, sensitivity, and application scope. Thermal sensors, originally based on liquid expansion, evolved into infrared thermometers and bolometers, widely used in medical imaging, meteorology, and security systems [125]. Resistance-based sensors, such as strain gauges, became crucial in structural health monitoring, aerospace, and automotive industries, offering precise measurements of stress, force, and displacement. In contemporary technological landscapes, sensors have become ubiquitous, integrating seamlessly into everyday life and high-end scientific applications. Optical sensors, now incorporating advanced photonics and laser technologies, play a pivotal role in spectroscopy, biomedical imaging, and autonomous systems [126]. Chemical and electrochemical sensors have advanced towards lab-on-a-chip devices, enabling rapid diagnostics and personalized healthcare solutions.

As sensor technology continues to evolve, the integration of artificial intelligence, nanomaterials, and wireless communication further enhances their capabilities, fostering the development of smart sensing systems. These innovations pave the way for highly autonomous, adaptive, and energy-efficient sensing networks that are crucial in fields such as environmental monitoring, space exploration, and the IoT [127].

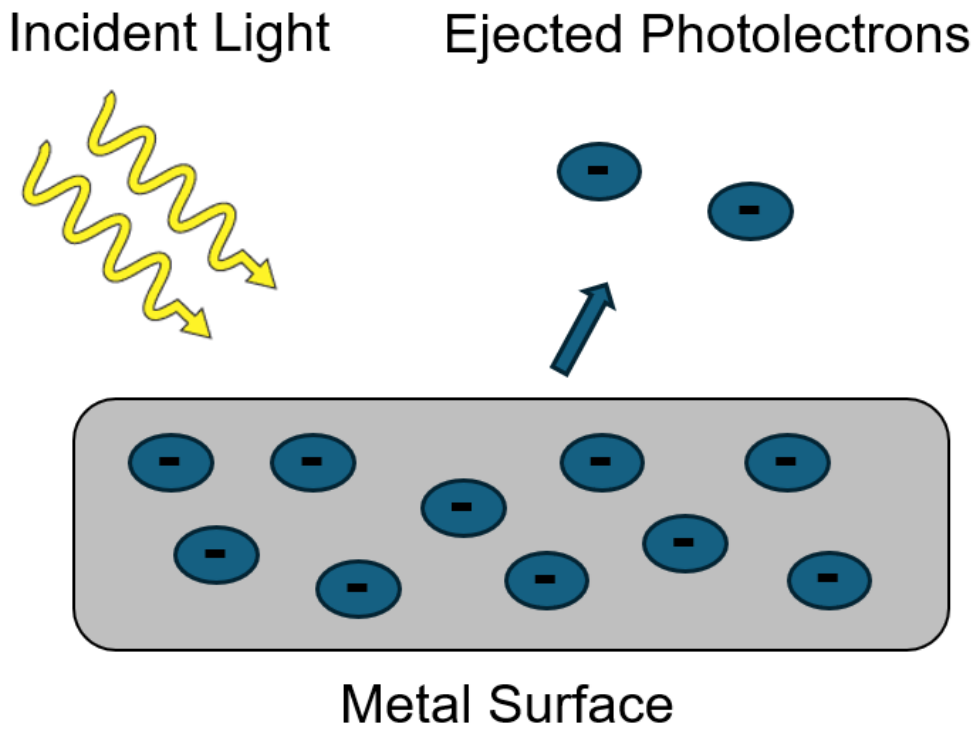

Figure 8: Photoelectric effect: when photons (usually from a UV light source) hit the metal surface with enough energy (depending on the metal) electrons are emitted.

1.4.1 Optical sensors

The historical evolution of optical sensors traces its roots to the early exploration of light and its interactions with matter. Early methods of optical observation, grounded in the principles of infrared absorbance, emissive properties such as those utilized in flame spectroscopy, and fluorescence, can be traced back to the 16th and 17th centuries [128]. However, it was not until the 19th century that these phenomena were systematically linked to the chemical composition of materials.

As the 19th century progressed into the early 20th century, scientists such as Coblentz further refined the categorization of materials based on their spectroscopic features [129]. These developments cemented the critical link between optical properties and chemical composition, forming the bedrock of modern optical sensing technologies. Instrumentation improved steadily, but it was the invention of the laser in the 1960s that marked a transformative moment for optical sensors. Lasers provided unparalleled precision and control over light, enabling advanced methods such as Raman spectroscopy and laser-induced breakdown spectroscopy (LIBS). These techniques facilitated highly sensitive and selective chemical analyses [130].

The advent and maturation of fibre optics in the latter half of the 20th century represented another leap forward. Fiber optic technology allowed for the efficient manipulation and transmission of light, unlocking new possibilities for sensing applications.

Fiber optic sensors became pivotal in diverse fields, including the detection of gases and vapours, environmental monitoring, medical diagnostics, industrial process control, and even automotive systems [131]. Today, optical sensors continue to evolve, driven by advancements in nanotechnology, materials science, and integrated photonics.

Optical sensors operate through a series of interrelated stages, each playing a crucial role in detecting and analysing target chemicals. These stages typically include the introduction of the sample or analyte, signal transduction, signal processing, and ultimately the quantification or identification of the desired chemical species [132]. Central to the operation of these sensors is the ability to recognize the target analyte, a feature that may be embedded in the transduction mechanism, the signal processing stage, or both, depending on the specific method employed. Transduction methods in optical sensing are broadly categorized into direct and indirect approaches. Direct methods, such as fluorescence, absorbance (both visible and infrared), and Raman spectroscopy, rely on the intrinsic optical properties of the analyte. These methods measure changes in light intensity, wavelength, or scattering that occur due to direct interactions between the analyte and the light source [133]. For instance, fluorescence-based sensors exploit the emission of light at specific wavelengths following excitation, while Raman spectroscopy detects shifts in scattered light caused by vibrational transitions within the target molecule. Indirect methods, on the other hand, often involve a mediated process that modifies the sensor's optical properties. These techniques might utilize indicators or chemical reactions to produce a measurable change. Examples include colorimetric methods, where a visible colour change indicates the presence of the analyte, and changes in a fluorophore's emission lifetime or wavelength due to environmental factors [134]. Other indirect approaches detect alterations in physical properties, such as the refractive index, which can vary in response to molecular binding or other interactions [135]. The transduction mechanism is complemented by advanced signal processing techniques, which enhance the sensitivity and specificity of the sensor. Modern optical sensors often integrate computational algorithms and machine learning to interpret complex data, enabling them to distinguish between closely related chemical signatures and reduce the impact of background noise. In practical applications, optical sensors have demonstrated remarkable versatility. They are widely employed in environmental monitoring, where they detect pollutants and gases; in medical diagnostics, for the identification of biomarkers; and in industrial processes, for real-time quality control. Their ability to combine precision, adaptability, and non-invasive measurement has established optical sensors as indispensable tools across scientific and technological domains.

1.4.1.1 Fluorescence sensors and principles

Fluorescence optical sensors are becoming increasingly popular compared to other optical sensing technologies, such as absorbance and Raman-based sensors, due to their high sensitivity, rapid response times, and strong signal-to-noise ratios. Unlike absorbance sensors, which rely on detecting small changes in transmitted light intensity and can suffer from background interference, fluorescence sensors amplify signals through emission, allowing for the detection of extremely low analyte concentrations. Additionally, compared to Raman sensors, which require expensive and complex instrumentation, fluorescence sensors are generally more cost-effective and easier to implement in a variety of applications, including biomedical diagnostics, environmental monitoring, and industrial process control.

Despite these advantages, fluorescence sensors have some limitations. Photobleaching, where fluorophores degrade with prolonged exposure to excitation light, can reduce signal intensity over time, limiting long-term measurements. Additionally, environmental factors

such as pH fluctuations, temperature variations, and oxygen levels can influence fluorescence efficiency and lead to measurement variability. Nonetheless, ongoing advancements in fluorophore chemistry, sensor miniaturization, and data processing techniques continue to improve their reliability and expand their applicability, making them a preferred choice in many optical sensing applications.

These sensors exploit the principle of photoluminescence, a subset of the broader luminescence family, encompasses both fluorescence and phosphorescence. These phenomena share the fundamental mechanism of photon emission following the absorption of electromagnetic radiation at specific wavelengths [136]. While fluorescence and phosphorescence may appear visually indistinguishable, they exhibit distinct differences in their emission characteristics and underlying electronic transitions. Fluorescence emission is typically short-lived, occurring on a timescale of nanoseconds to microseconds, whereas phosphorescence persists from milliseconds to hours due to the phenomenon known as afterglow, where light emission continues even after the excitation source has been removed, which does not occur in fluorescence. Additionally, fluorescence arises from the relaxation of an excited electron within a singlet state, whereas phosphorescence involves a transition from a triplet state to the ground state. The latter process is significantly slower due to spin-forbidden transitions [137] thereby prolonging the emission duration. These distinctions are illustrated in fig. 9.

Fluorescence is now widely recognized as the property of certain substances to re-emit absorbed electromagnetic radiation, typically at a longer wavelength and therefore lower energy. The process begins when incident light excites electrons within the atoms of the substance, elevating them to higher, less bound energy levels. Within mere nanoseconds, these excited electrons return to their ground state through a series of transitions, often involving intermediate states, releasing photons in the process. The mechanics of this absorption and emission process are best understood using the Jablonski diagram shown in fig. 9, a tool named after Alexander Jablonski, a pioneer in fluorescence research. The diagram in fig. 9 delineates two primary electronic states: S_0, the ground state, and S_1, the first excited state. Each of these states includes several vibrational sub-levels, labelled as 0, 1, 2, 3, and so forth. At room temperature, the available thermal energy is insufficient to populate excited electronic or vibrational levels; thus, external light is required to induce fluorescence. Upon irradiation, an electron transitions from the ground state to an excited electronic and vibrational state in approximately 10^{-15} seconds, too rapid for nuclear

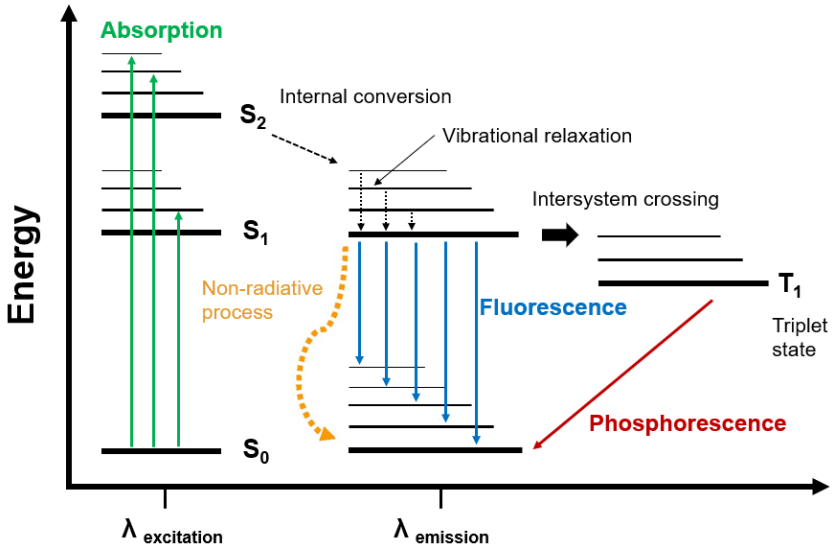

Figure 9: Jablonski diagram.

displacement to occur, as described by the Franck-Condon principle. Over the next 10^{-12} seconds, the system undergoes internal conversion, a non-radiative process that relaxes the electron to the lowest vibrational level of the excited state. Fluorescence emission occurs as the electron returns to the ground state, often passing through an excited vibrational level before achieving thermal equilibrium. One notable characteristic of fluorescence, also illustrated in the Jablonski diagram, is that the emitted light generally has a longer wavelength, and thus lower energy, than the absorbed light. This energy difference, known as the Stokes shift, is a defining feature of the phenomenon and underpins its numerous applications in scientific and industrial fields.

1.4.1.1.1 Stokes shift, mirror image and Kasha's rule

The phenomenon where fluorescence occurs at longer wavelengths than the incident radiation is known as the "*Stokes shift*", a term coined after its discovery by G. G. Stokes in 1852. The Stokes shift, that can be seen in fig. 10 [138] arises due to several factors, including [139]:

- Rapid relaxation to the lowest vibrational level of the first excited electronic state (S_1);
- Relaxation to higher vibrational levels in the ground state (S_0), resulting in thermal dissipation;
- Solvent interactions;
- Excited-state chemical reactions;
- Complex formation;
- Energy transfer between molecules.

Another intriguing feature of fluorescence is the "*mirror image rule*". This principle states that the absorption and emission spectra of a molecule are often mirror images of each other. This symmetry occurs because electronic excitation generally does not alter the nuclear geometry. Consequently, the spacing between vibrational levels in the ground (S_0) and excited (S_1) states remains similar, resulting in analogous vibrational structures in both spectra as can be seen in fig. 10 [140]. For instance, perylene exemplifies this rule, as its emission and absorption spectra closely resemble each other [141]. This happens because a transition with a high probability during absorption will also have a high probability during emission, producing a near-mirror symmetry [142].

However, exceptions exist, such as in the case of quinine [143]. In its spectrum, the first absorption peak corresponds to a transition from the ground state (S_0) to the second excited state (S_2), while subsequent peaks reflect the S_0 to S_1 transition. Fluorescence predominantly arises from the S_1 state due to the rapid, non-radiative relaxation of electrons from higher excited states (e.g., S_2, S_3) to S_1, a process faster than fluorescence

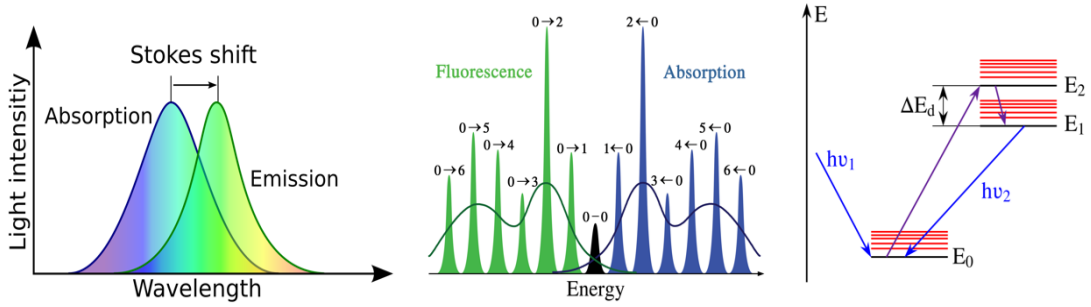

Figure 10: Stokes shift [138], mirror image [141] and Kasha's rule.

emission. Consequently, fluorescence spectra primarily represent the S_1 to S_0 transition rather than the total absorption spectrum.

This leads to Kasha's rule, a fundamental property of fluorescence, which asserts that the emission spectrum of a fluorophore is independent of the excitation wavelength, provided that sufficient energy is supplied for the transition. As can be seen in fig. 10 a photon with energy hv_1 excites an electron of fundamental level, of energy E_0 up to an excited energy level (e.g. E_1 or E_2) or on one of the vibrational sub-levels. Vibrational relaxation then takes place between excited levels, which leads to dissipation of part of the energy (ΔE_d), taking the form of a transition (internal conversion) towards the lowest excited level. Energy is then dissipated by emission of a photon, which allows the system to go back to its fundamental state. Since higher excited states decay non-radiatively before fluorescence occurs, the emission always reflects the S_1 to S_0 transition. Notably, exceptions to Kasha's rule include certain fluorophores with two ionized states that exhibit distinct emission and absorption spectra, as well as rare molecules capable of emitting directly from the S_2 state [144].

These principles, the Stokes shift, the mirror image rule, and Kasha's rule, provide essential insights into the behaviour of fluorophores and the fundamental mechanisms of fluorescence.

1.4.1.1.2 Quantum yields and fluorescence lifetimes

The fluorescence quantum yield (Φ) represents the ratio of emitted photons to the total number of absorbed photons. This relationship can also be expressed in terms of the rates of radiative and non-radiative processes. Here, signifies radiative processes, which result in the emission of light, while encompasses non-radiative processes such as internal conversion, intersystem crossing, and energy transfer. Quantum yield values range from 0 to 1, with 1 representing the theoretical maximum emission efficiency, a value unattainable by any known substance. Essentially, the quantum yield reflects the likelihood that an excited system will return to its ground state through a radiative process [137].

Another crucial parameter in fluorescence studies is the excited state lifetime, which indicates the average duration a molecule remains in its excited state before returning to the ground state. Typically, this lifetime is approximately 10 nanoseconds. By measuring this value, one can infer the time available for the excited state to interact with and diffuse within its environment, thereby gaining insights into the information conveyed by its emission. For a generic fluorophore, the lifetime (τ) is defined as: $\tau = 1/ (K_r + K_{nr})$ where K_r is the constant of radiative decay, and k_{nr} the constant of non-radiative decay. As fluorescence is a random process, very few molecules emit at time: $t = \tau$. Fluorescence is inherently a stochastic process, and only a small fraction of molecules emit light precisely at τ. To achieve shorter lifetimes and consequently lower quantum yields, heavy atoms like iodine are often incorporated into the molecular structure [137]. These atoms enhance non-radiative processes, effectively reducing the fluorescence efficiency.

1.4.1.2 Coumarin dyes

The result of fluorescence emission is invariably electromagnetic radiation; however, the mechanisms giving rise to this emission are diverse. Here, the focus will be on coumarin fluorescent dyes that, when excited at the appropriate wavelength, exhibit the phenomenon of fluorescence. Coumarin dyes hold a significant place in the history of chemistry and their applications in fluorescence technology. These fascinating molecules were first isolated in 1820 by the German chemist Alfred Vogel from Tonka beans and sweet clover, marking the beginning of nearly two centuries of exploration. The name "coumarin" originates from "coumarou," the French term for Tonka beans. In 1868, W. H. Perkin achieved the first synthetic production of coumarin through the reaction of salicylaldehyde with acetic acid,

a milestone in the development of organic synthesis [145]. This synthesis not only demonstrated the versatility of coumarins but also laid the foundation for their application in numerous scientific domains.

The basic structure of coumarin dyes consists of a 1-benzopyran-2-one core (fig. 11 central structure), a framework that provides immense opportunities for chemical modification and that already shown fluorescence properties [146]. This adaptability has enabled scientists to fine-tune their physical and photophysical properties as shown in fig. 11. Coumarins exhibit excellent biocompatibility, strong fluorescence emission, and remarkable photostability, characteristics that make them particularly useful as fluorescent probes. Depending on the substitution patterns on the coumarin core, their fluorescence can be shifted to emit in different regions of the visible spectrum, ranging from blue to red. This tunability is achieved by introducing electron donating or electron-withdrawing groups at specific positions, which modulate the electronic properties of the molecule [147].

The applications of coumarin dyes are vast and impactful. In the fluorescence domain, they have been harnessed in the design of small-molecule fluorescent chemo sensors, playing a vital role in molecular imaging and analytical chemistry. Coumarin-based sensors are frequently used to detect metal ions [148], anions [149], and reactive species, offering a sensitive and selective means of monitoring these substances in biological and environmental systems. Beyond sensing applications, coumarins serve as active components in optical brighteners, laser dyes, and organic light-emitting diodes (OLEDs) [150]. These dyes are integral to technological advancements in energy-efficient lighting and display technologies, as well as in enhancing the efficiency of solar cells [151].

Among the derivatives of coumarins, the 7-aminocoumarin family stands out for its extraordinary fluorescence properties. These compounds, characterized by the presence of an amino group at the 7^{th} position of the coumarin core (fig. 12), exhibit high fluorescence quantum yields and strong emission intensities [152]. Their photophysical behaviour is primarily governed by intramolecular charge transfer (ICT) mechanism [153]. Upon excitation, 7-aminocoumarins form a planar excited state where charge separation occurs

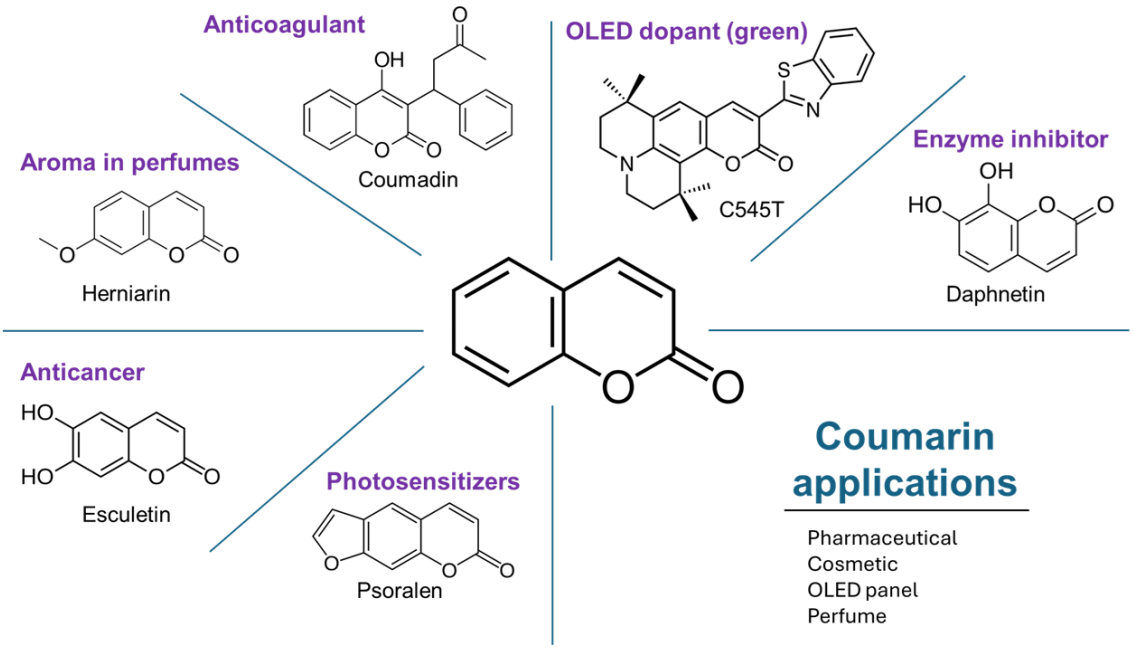

Figure 11: Coumarin family applications.

between electron-donating and electron-accepting parts of the molecule as shown in fig. 12. This state is highly emissive and responsible for their characteristic fluorescence.

However, the fluorescence efficiency of 7-aminocoumarins can be influenced by the surrounding environment and the molecular structure. In some cases, the ICT state may transition to a non-fluorescent twisted intramolecular charge transfer (TICT) state, where the molecule adopts a twisted geometry that dissipates energy non-radiatively [154] as can be seen in fig. 12. Such transitions are more likely in polar environments or when the substituents allow for greater flexibility in the molecular structure [155]. Researchers have found that restricting this twisting motion, either by chemical modifications that rigidify the structure or by embedding the dye in a less polar environment, can significantly enhance fluorescence quantum yields [156]. The ICT-TICT interconversion in 7-aminocoumarins is a pivotal area of study, as understanding and controlling this mechanism can lead to the development of more efficient dyes and sensors. By designing derivatives that favour the emissive ICT state and suppress the non-emissive TICT state, scientists can create highly sensitive fluorescent probes. Such probes are invaluable in applications ranging from medical diagnostics to environmental monitoring [147]. For these reasons a coumarin as a probe for our study on pesticides was employed.

1.4.1.3 Oxime dyes

If coumarins take their popularity due to their scaffold 1-benzopyran-2-one, it is also possible to categorize dyes based on functional groups. This is because usually the backbone of a dye gives the fluorescence properties, but to prepare chemo-sensors is usually very important to have the right functional group capable to react with the target analyte [157]. Oximes are organic compounds characterized by the functional group -C=NOH as can be seen in Figure 13. Their unique structure equips them with exceptional nucleophilic properties, allowing them to act as antidotes in OP poisoning by reactivating AChE that has been inhibited by OP compounds [158] as shown in Figure 13. Beyond medical treatment, oximes have found applications in detecting OPs, owing to their reactivity and adaptability when incorporated into various sensing platforms. Additionally, oximes have been employed in other fields, such as organic synthesis, where they serve as intermediates in the formation of various compounds [159], and as ligands in coordination chemistry [160]. Their ability to form stable complexes and participate in diverse chemical reactions highlights their broad utility.

Oximes exhibit a range of properties that make them ideal for detecting OP compounds. High reactivity is one of their defining features, as oximes can readily deprotonate to form oximates, which are super nucleophiles capable of reacting with phosphorylated OP species [161], attacking the P which behave as an electrophile species. This property is central to their use in both antidotal and sensor applications. They also possess stability and versatility, enabling chemical tailoring to exhibit desired solubility, stability, and reactivity characteristics. This adaptability allows them to integrate seamlessly into diverse detection platforms, from optical sensors to surface-based devices [159-160]. Furthermore, oxime functional group play a significant role in fluorescence modulation. When incorporated into fluorescent chemo-sensors, it can modulate fluorescence signals upon reaction with OP compounds, providing a basis for real-time detection.

The development of oxime-based detection systems for OPs has gained traction due to their rapid response and specificity. Oxime-containing fluorescent sensors have been developed to detect OP nerve agents like Sarin and Soman. For instance, oxime-

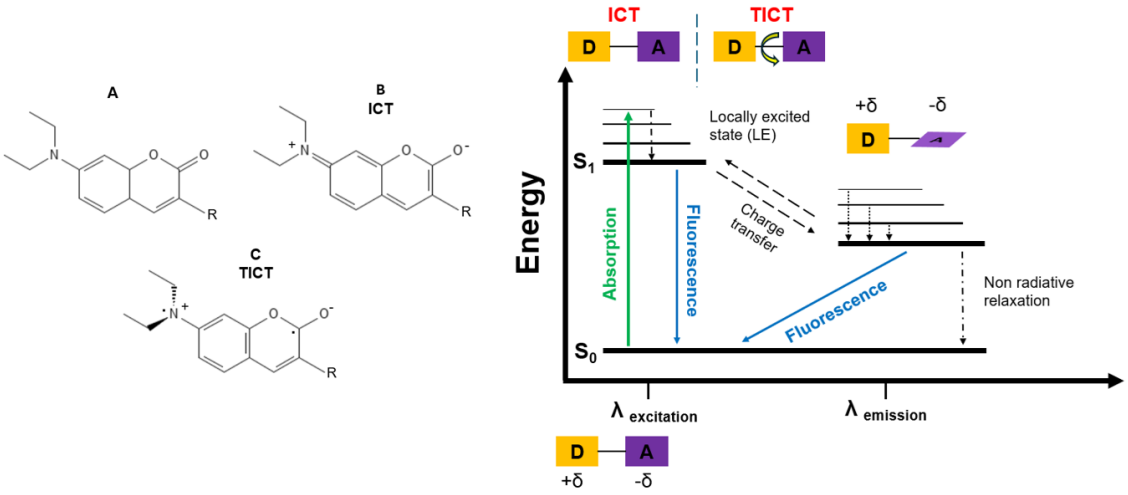

Figure 12: TICT mechanism [152] and scheme [154].

functionalized dipyrrinone probes demonstrate a dramatic colorimetric response upon interaction with dimethoate, a pesticide analogue of OP nerve agents [164]. The reaction triggers a fluorescence "turn-on" mechanism due to the disruption of photoinduced electron transfer (PET) pathway, that we will discuss further in this thesis. Hydroxy-oxime probes incorporate a β-hydroxy oxime moiety capable of undergoing cyclization upon interaction with OP compounds, forming highly fluorescent aryl isoxazole derivatives. Such systems show enhanced sensitivity and rapid response times, critical for detecting volatile OP agents like di-isopropyl fluorophosphate (DFP) and sarin [165]. Oxime-based sensors immobilized on substrates such as cellulose acetate films have proven effective for in-field detection [166]. These sensors can identify simulants like DFP through emission shifts, even under ambient conditions. Beyond fluorescence, oxime-functionalized systems have also been developed for colorimetric detection. These probes rely on visible colour changes upon phosphorylation reactions, enabling naked-eye detection without sophisticated instrumentation [167].

Despite significant advancements, challenges remain. Sensitivity to environmental factors, the need for selective reactivity, and limitations in detecting a broad spectrum of OPs highlight areas for further development. However, the search for oxime sensors has focused almost exclusively on nerve gases and has almost completely neglected OPs used as pesticides. These are the reasons why the possible applications of fluorescent oximes for detecting OPs pesticides were investigated.

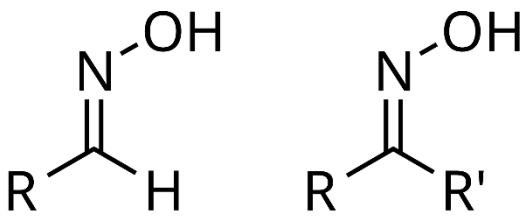

Figure 13: Oxime generic structure.

1.4.2 Graphene

The development of science often starts with unexpected experimental discoveries, which are even inconsistent with previous theories. However, it is through these unexpected discoveries that science has often advanced. For a long time in the past, scientists have believed that at room temperature, free-standing graphene could not exist due to the minimization of its surface energy [162-163]. But in 2004, Konstantin Novoselov and Andre Geim proved that those assumptions were wrong. They discovered one of the most studied materials in the last 20 years: graphene [170].

Graphene (GR) is a two-dimensional allotrope of carbon, structured as an atomic-scale hexagonal lattice where each vertex hosts a carbon atom with sp^2 hybridization. The C-C bond length measures approximately 0.142 nm. Within the lattice, each carbon forms three σ-bonds, creating a robust and stable hexagonal framework. The material's impressive electrical conductivity primarily arises from its π-bonds, which extend perpendicular to the lattice plane. GR's remarkable stability stems from its densely packed carbon atoms and sp^2 hybridization, where the s, p_x, and p_y orbitals combine to form σ-bonds, while the p_z electron contributes to π-bonding as can be seen in Figure 14 [171]. These π-bonds interact, generating π and π* bands, which play a key role in GR's extraordinary electronic properties by enabling the movement of free electrons through a partially filled band [172].

GR has garnered immense attention due to its extraordinary properties, groundbreaking potential applications, and the challenges that accompany its integration into modern technologies. As a single layer of carbon atoms arranged in a two-dimensional honeycomb lattice, GR exhibits a large specific surface area (2600 m^2/g, Zeolite Y has 500-600), high electron mobility (200,000 cm^2/Vs, crystalline silicon has 1400) with low joule effect, enhanced thermal conductivity (3000-5000 W/mK, copper has 401), and exceptional mechanical strength, with a Young's modulus of 1 TPa (steel has 0.2) [173]. Being a quasi-2D material, GR's thickness is measured at only 0.345 nm. All these features in a single material have made it so special, but there is still a long way to go to exploit its full potential.

One particularly intriguing area of GR research lies in sensing technologies. The material's sensitivity to even minute environmental changes is tied to its high conductivity and large surface area, allowing for efficient interaction with gases [174], biomolecules [175], or other analytes. This makes GR a prime candidate for applications in chemical, biological, and environmental sensors, where precision and rapid response are crucial.

Graphene oxide (GO) and reduced graphene oxide (rGO) have also emerged as critical derivatives in research. GO, which contains oxygen functional groups, is hydrophilic and easily dispersible in water, making it ideal for applications such as biomedical devices, drug delivery systems, and water purification. Meanwhile, rGO, with reduced oxygen content, retains many of GR's electronic properties while being more cost-effective to produce. These derivatives are extensively studied because they can be tailored chemically, enabling fine control over properties such as hydrophilicity, conductivity, and reactivity.

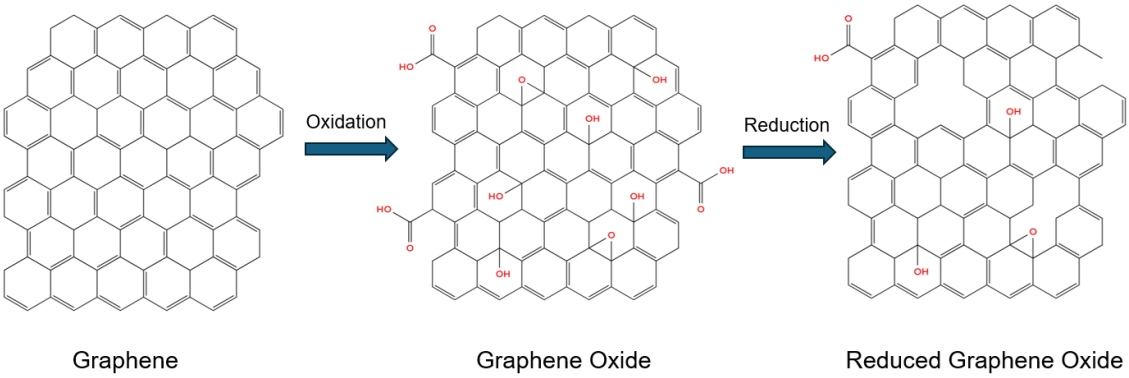

Figure 14: Structure of graphene, graphene oxide and reduced graphene oxide.

Despite its promise, GR faces challenges in scalability, consistent quality during production, and integration into existing systems. Suffice it to say that the price of GR fluctuates between 50 and 1000 $ per kg, depending on several factors including purity (closely linked to the application), production method and market logic such as purchase quantity [176]. Large-scale production methods often introduce defects, compromising its properties. Additionally, the cost-effective, sustainable fabrication of GO and rGO must be refined to ensure widespread adoption. Addressing these challenges will unlock GR's full potential, particularly in transformative areas like sensing, energy storage, and next-generation electronics.

1.4.2.1 Graphene oxide

GO is an oxidized derivative of GR, distinguished by its two-dimensional structure decorated with various oxygen-containing functional groups such as epoxy, hydroxyl, and carboxyl groups. This composition makes GO hydrophilic and highly dispersible in water, in contrast to the hydrophobic nature of pristine GR. The presence of these functional groups significantly alters its chemical and physical properties, rendering GO a material of immense interest across multiple disciplines, including electronics, materials science, and sensing technologies [177].

GO is primarily produced through the chemical exfoliation of graphite using methods such as the Hummers or modified Hummer's method, which involve strong oxidizing agents [178]. This process is scalable, cost-effective, and less resource-intensive compared to the production of high-quality GR, which often requires mechanical exfoliation or chemical vapor deposition. The lower production cost and greater ease of processing make GO a more accessible option for a broad range of applications. One of its primary advantages compared to GR is its abundance of oxygenated functional groups, which act as active sites for chemical interactions. This property enables GO to achieve better dispersion in aqueous and polar organic solvents (Figure 15) and facilitates functionalization for specific applications. However, these same functional groups disrupt the sp^2 hybridized carbon lattice, introducing defects that reduce electrical conductivity, transforming GO into an electrical insulator rather than a conductor [179]. This contrasts with GR, renowned for its exceptional electrical conductivity, mechanical strength, and thermal properties.

The unique properties of GO are particularly valuable in gas sensing applications, where its chemical reactivity and ability to form hydrogen bonds enhance the adsorption of gas molecules [180]. For ammonia sensing, GO demonstrates superior sensitivity compared to GR, primarily due to its interaction with ammonia molecules through its hydroxyl and epoxide groups [181]. Density functional theory (DFT) calculations reveal that these functional groups enable GO to achieve strong binding energies and efficient charge transfer

with ammonia molecules. Furthermore, the tuneable band gap introduced by the functional groups in GO allows for improved signal modulation compared to the zero-band-gap nature of GR [182].

Despite these advantages, the insulating nature of GO presents a significant limitation in sensing applications that rely on electrical signal transduction. Strategies such as partial reduction to rGO have been explored to restore partial conductivity while retaining sufficient functional groups for adsorption. This trade-off highlights the delicate balance between functionalization and electrical performance in the design of GO-based sensors.

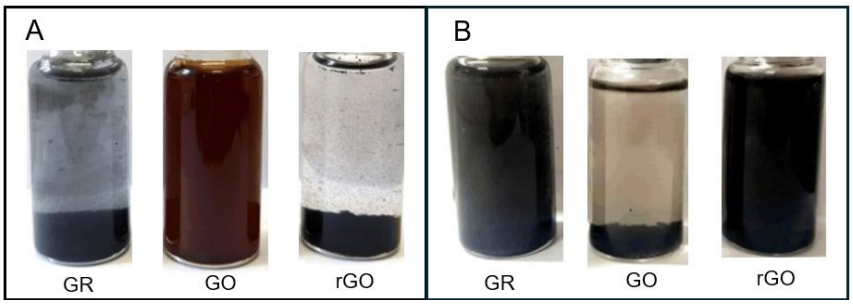

Figure 15: GR, GO and thermally rGO in (a) water (b) hexane.

1.4.2.2 Reduced graphene oxide

rGO is a modified form of GO that regains many of GR's original properties through reduction processes. GO is highly oxidized and hydrophilic, but upon reduction, it becomes more conductive while retaining certain functional groups that enhance its chemical reactivity. This transformation makes rGO a practical compromise between GO and pristine GR, offering both ease of fabrication and desirable electronic properties. rGO has found extensive applications in sensor technology due to its unique structure and electronic properties. The presence of residual oxygen functional groups and defects in rGO enhances its interaction with gas molecules, making it an effective material for detecting various chemical analytes [183]. Compared to GR, rGO is easier and cheaper to produce in large quantities while still offering high sensitivity and fast response times in sensing applications. While GR boasts superior electrical conductivity and structural integrity, its production is expensive and often requires specialized techniques such as chemical vapor deposition. rGO, on the other hand, can be synthesized from GO through a variety of reduction methods, making it more accessible for industrial applications. However, the quality of rGO depends significantly on the reduction technique used [184]. Some methods may leave behind residual oxygen groups, which can be both an advantage and a disadvantage depending on the intended application [185]. While these functional groups improve dispersion in solvents and enhance chemical interactions, they also reduce overall conductivity compared to pristine GR.

The effectiveness of rGO in ammonia sensing is attributed to its ability to interact with ammonia molecules through physisorption and chemisorption. The defects and functional groups in rGO provide active sites for ammonia adsorption, which leads to measurable changes in electrical resistance. This interaction makes rGO an excellent candidate for low-power, highly sensitive ammonia sensors that operate at room temperature [180-181]. Studies have demonstrated that modifying the reduction conditions can optimize rGO's response time, recovery, and selectivity, making it adaptable to various sensing applications. The reduction of GO into rGO can be achieved through different methods, each influencing the final material properties as we are going to see in the next paragraphs.

1.4.2.2.1 Reduction methods of graphene oxide

Reduction of GO into rGO employs various techniques, each tailored to balance efficiency, scalability, and environmental impact. Among these, chemical, thermal, biological, photochemical, microwave, hydrothermal, and electrochemical methods, shown in Figure 16, all have unique advantages and challenges [188].

Chemical reduction remains a cornerstone, utilizing agents like hydrazine, sodium borohydride, and ascorbic acid. Hydrazine offers one of the highest reduction efficiencies, yielding rGO with superior electrical conductivity and a high C/O ratio. However, its high toxicity and environmental risks significantly hinder its scalability. Sodium borohydride is a milder chemical alternative but often requires catalysts, such as silver nanoparticles, to enhance its efficiency. Ascorbic acid, a green and biocompatible reducing agent, is increasingly popular for applications requiring eco-friendly processes. However, it sometimes produces rGO with less consistent electrical and structural properties [189].

Thermal reduction utilizes high temperatures, often exceeding 800°C, under inert conditions [190]. This approach efficiently removes oxygen groups, restoring GR's sp^2 lattice and enhancing its conductivity. However, the process may introduce lattice defects at very high temperatures, compromising mechanical stability. While excellent for large-scale applications, the energy demands and equipment requirements can limit its use in resource-constrained settings [191].

Photochemical reduction encompasses several subcategories, including plasma-based methods. Plasma reduction is particularly promising as it uses highly energetic ions and electrons to selectively remove oxygen groups at room temperature or slightly elevated conditions. Plasma methods are advantageous due to their rapid processing, absence of harmful chemicals, and precise control over the degree of reduction, making them highly suitable for applications like patterned rGO films for electronics [192]. Another subset of photochemical techniques involves ultraviolet (UV) or visible light [193], often combined with photocatalysts, though these methods typically have lower reduction efficiency compared to plasma.

Microwave reduction exploits rapid, volumetric heating to achieve fast and uniform reduction of GO. This method is notable for its scalability and energy efficiency, making it appealing for industrial applications. However, the high power involved can cause agglomeration or uneven reduction if not properly controlled [194].

Hydrothermal reduction relies on high-temperature and high-pressure water environments to reduce GO. This method can be tuned by adjusting parameters such as temperature, pressure, and reaction time. It is highly effective for producing rGO with functional groups retained for specific applications, such as supercapacitors, though the energy input and long reaction times can be limitations [195].

Electrochemical reduction offers a clean and controllable method by applying a voltage across a GO-coated electrode in an electrolyte solution. This approach avoids the need for toxic chemicals and allows for precise tuning of rGO properties by adjusting the applied voltage and reaction time. However, it is relatively slower and less suitable for large-scale production [196].

Overall, each reduction method provides unique benefits and trade-offs. For applications requiring high electrical conductivity and scalability, chemical or thermal methods remain preferred. In contrast, plasma, hydrothermal, and electrochemical methods offer greener, tuneable alternatives suited for specialized applications. The continued evolution of these techniques focuses on optimizing the trade-offs between efficiency, environmental

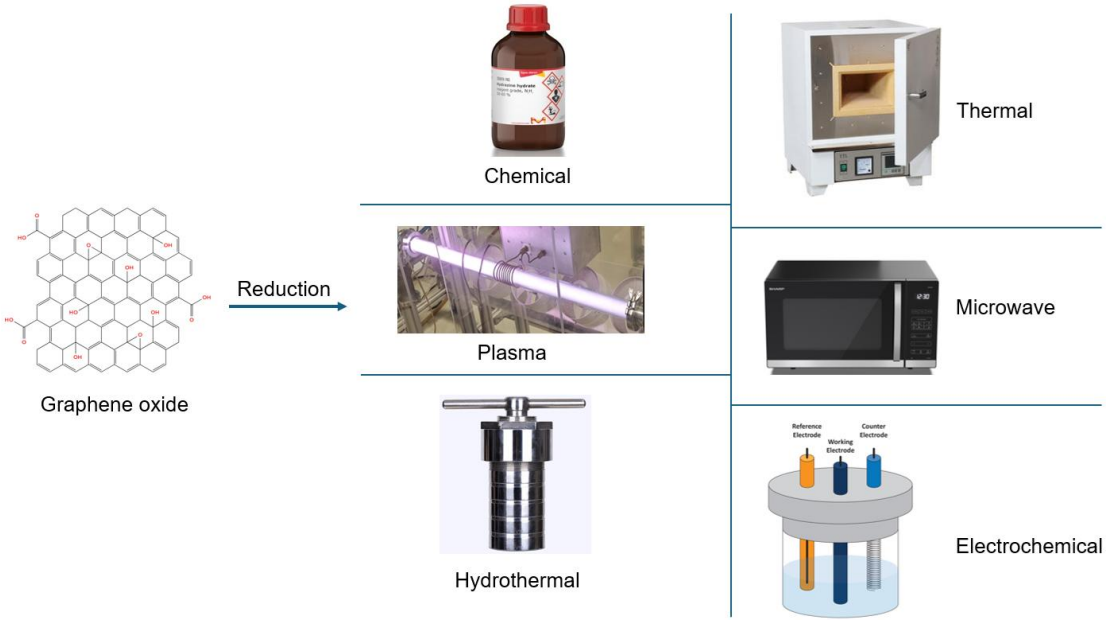

Figure 16: Graphene oxide main reduction method.

sustainability, and cost-effectiveness. However, among the many reduction techniques, the attention was focused into low-pressure plasma reduction. It is an underexplored field, especially for ammonia sensing, and it is a clean and very fast technique which is aligned with environmental needs and with possibilities to upscale it at an industrial level.

1.4.2.2.1.1 Plasma reduced graphene oxide

Plasma, often referred to as the fourth state of matter, has a rich and dynamic history. Its scientific journey began in the early 20th century when Irving Langmuir coined the term in 1928, drawing an analogy to blood plasma due to its capacity to carry various charged particles.

At its core, plasma is an ionized gas composed of free electrons and ions, exhibiting collective electromagnetic behaviours that distinguish it from neutral matter. While it may seem exotic on Earth, plasma dominates the universe, constituting more than 99% of visible matter. Nowhere is this more apparent than in stars, which are colossal spheres of hydrogen plasma. In the Sun's core, temperatures reach millions of degrees, providing the extreme conditions necessary for nuclear fusion. Hydrogen nuclei, or protons, collide with such energy that they overcome their natural electrostatic repulsion, fusing to form helium in the proton-proton chain reaction. This process not only sustains the Sun's brilliance but also serves as the foundation for life on Earth, providing the heat and light essential for our planet's ecosystems [197].

The sun's influence extends beyond its core. Streams of plasma, known as the solar wind, emanate from the sun, filling the space between celestial bodies. These charged particles interact with planetary magnetic fields, creating phenomena like Earth's auroras. Even these mesmerizing displays owe their origin to the fundamental dynamics of hydrogen plasma, the primary constituent of both the Sun and its emissions. This highlights plasma's dual role as both a cosmic and terrestrial force, shaping the universe while offering inspiration for scientific advancement [198].

On Earth, harnessing plasma's properties has led to technological innovations that define modern life. From lighting and plasma screens to advanced semiconductor manufacturing, plasma plays a critical role. But perhaps its most transformative potential lies in nuclear fusion research. Here, scientists seek to replicate the processes of stars, using

hydrogen plasma (mainly deuterium and tritium) as fuel. Within experimental reactors, such as tokamaks and stellarators, magnetic fields confine the plasma, heating it to temperatures rivalling the sun's core to initiate fusion. This pursuit, though fraught with challenges, represents humanity's effort to turn the power of the stars into a boundless source of clean energy [199].

The generation of plasma has been achieved using various methods, each tailored to specific applications and conditions. One of the most fundamental approaches is through the application of electric fields to a neutral gas, where collisions between accelerated electrons and neutral molecules initiate ionization. Among the methods, direct current (DC) discharges [200], capacitively coupled radio frequency (RF) discharges [201], inductively coupled plasma (ICP) [202], microwave discharges [203], and dielectric barrier discharges stand out as distinct technologies [204], each with unique operating principles and advantages.

In particular ICP techniques have revolutionized analytical chemistry by enabling precise elemental analysis and material processing. ICP-MS is widely used for ultra-trace metal detection in environmental, pharmaceutical, and food safety applications due to its high sensitivity and multi-element capability. ICP-AES/OES (Atomic/Optical Emission Spectroscopy) allows rapid and accurate quantification of metals in geological, industrial, and biological samples. ICP-RIE (Reactive Ion Etching) is essential in semiconductor fabrication, creating high-aspect-ratio microstructures with excellent precision. These techniques can work either at low or high pressure driven by RF fields and are highly versatile for generating stable and uniform plasma. In such systems, an alternating RF current passes through a coil, creating a time-varying magnetic field that induces electric fields within the gas. These electric fields accelerate electrons, which ionize the gas molecules upon collision, sustaining the plasma as can be seen in fig. 17 [205-206]. This electrode-less design minimizes contamination and allows precise control over the plasma parameters, making it ideal for surface treatments, thin-film deposition, and material reduction processes [207].

The application of hydrogen plasma in ICP systems holds significant promise, especially in reducing GO to rGO. Hydrogen, as a reducing agent, offers unique advantages due to the reactivity of atomic hydrogen generated within the plasma. Unlike other gases such as argon or nitrogen, hydrogen plasmas not only ionize but also produce highly reactive species like H radicals and H^+ [208]. These species selectively target oxygen-containing functional groups on GO, efficiently removing oxygen atoms while preserving the sp^2-hybridized carbon structure [209]. When comparing hydrogen to other gases in plasma processes, hydrogen's reducing properties are unparalleled. While argon and nitrogen plasmas are often used for physical sputtering or introducing nitrogen functionalities, they lack the chemical reactivity required for effective reduction. This makes hydrogen plasma the preferred choice for applications demanding high-quality GR derivatives with minimal defect formation [210]. In the case of GO, hydrogen plasma treatment achieves an optimal balance between reduction efficiency, process simplicity, and material preservation, paving the way for its use in advanced electronics and energy storage technologies.

Compared to conventional reduction methods, such as chemical treatments with hydrazine or high-temperature annealing, hydrogen plasma offers a gentler yet effective alternative. Chemical agents are often hazardous and leave residual contaminants, while thermal methods risk introducing structural defects due to carbon loss. Moreover, both methods are time consuming (at least 10 minutes to hours) [188], and industrially this would mean a slow process, one of the main reasons that usually increase the price of a product. Hydrogen plasma circumvents these issues by operating at relatively low temperatures and avoiding harsh chemicals. For instance, studies have shown that hydrogen cold plasma can achieve reductions comparable to chemical techniques, lowering

oxygen content significantly without compromising the integrity of the material [186, 202]. It doesn't produce waste and it is very fast, as reduction can be efficiently done in seconds.

For these reasons the plasma potentials were exploited to reduced GO in order to sense NH_3 as we will see in the next chapter.

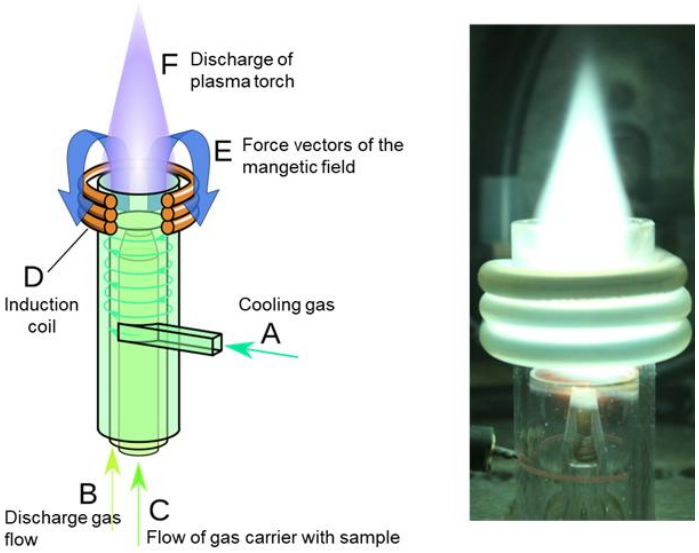

Figure 17: Scheme [206] and real image [205] on how ICP torch at 1 atm works.

1.5 Summary of the Research Framework

This introduction emphasizes how ensuring sufficient food production remains a pressing challenge, with the risk of this issue escalating in the future if effective countermeasures are not adopted. This problem is deeply intertwined with contemporary global issues, particularly climate change. Addressing these challenges will depend heavily on predictive models that can identify, monitor, and guide the actions necessary to achieve sustainable food production for the global population. Sensors will be indispensable in this process, as they provide the crucial data required for these models to deliver accurate and actionable forecasts.

In particular, monitoring food spoilage and pesticide residues demands more widespread sensor deployment, as current technologies sample only a small fraction of total production. This PhD work aimed to advance the field by developing fluorescence-based sensors for pesticide detection and leveraging rGO's unique properties to monitor ammonia levels related to food spoilage.

Chapter 2

Aims and Hypothesis

This dissertation aims to develop and implement innovative sensor technologies to address harmful chemical contamination and prevent food spoilage. The ability to detect contaminants quickly and cost-effectively is crucial for public health. Rapid detection technologies could allow food producers, distributors, regulatory agencies and consumers to swiftly identify and remove contaminated products from the market, thereby safeguarding health and restoring confidence in food safety.

In addition to chemical detection, food freshness sensors could provide significant benefits to the food industry by optimizing supply chains and reducing waste. Consumers would also benefit from these sensors, as they would enable real-time evaluation of food freshness both in supermarkets and at home, empowering them to make informed purchasing decisions

Aims of the dissertation in realm of food quality and safety:

1. To develop a novel ammonia sensor based on rGO;
2. To investigate environmental degradation of OPs and identify their byproducts;
3. To develop and select suitable fluorescent dyes capable of detecting OPs at concentrations in the µg/L range with high specificity;
4. To understand the detection mechanisms of the sensors;
5. To validate the developed sensors by detecting OPs and ammonia in real environmental samples.

Based on these aims, the research was driven by the following hypotheses:

1. Plasma treatment can modify the surface of GO, making possible the quantification of ammonia effectively;
2. OP hydrolysis will produce simpler byproducts that are easier to detect;
3. Dicyanovinyl coumarin can react with nucleophiles produced during OP hydrolysis, enabling quantification;
4. Deprotonated oxime dyes can directly attack the phosphorus in OPs pesticides, leading to their quantification.

Chapter 3

Publications

3.1 General Overview

This chapter presents the work that validated the hypotheses outlined in Chapter 2. In the first article, it was demonstrated how plasma can rapidly and efficiently reduce GO without waste, also revealing the influence of treatment duration on sensor performance towards ammonia, addressing hypotheses 1. The second article focuses on optimizing the natural degradation process (hydrolysis in basic media) of dimethoate, enabling its quantification with a coumarin dye addressing hypotheses 2 and 3. Finally, the third article explores how a class of compounds (oximes), traditionally used as antidotes for OP warfare agents, can be repurposed for detecting OP pesticides addressing hypotheses 4.

3.2 Ammonia Sensing

Ammonia, among one of the most produced gases every year and produced during food spoilage, due to its chemical properties it is reactive towards electrophile species. GO presents exactly this feature, it is a hydrophilic material and its production is cost-effective, enabling scalable fabrication. However, its inherently insulating nature presents a critical limitation for practical applications, particularly in sensing technologies, necessitating reduction processes to enhance its electrical conductivity. Conventional thermal and chemical reduction techniques, while effective, pose challenges related to environmental sustainability and scalability. Consequently, alternative reduction methods have been actively explored.

Plasma-assisted reduction offers a rapid, environmentally friendly, and scalable approach to enhancing the electrical conductivity of GO while preserving its structural integrity. In particular, hydrogen plasma treatment has demonstrated high efficacy in selectively removing oxygen functional groups, thereby significantly improving GO's conductivity and making it a promising candidate for gas sensing applications. Among various analytes, ammonia (NH_3) detection is of particular interest due to its widespread industrial use and emission in food spoilage. The presence of residual functional groups on rGO surfaces plays a crucial role in facilitating ammonia adsorption and influencing sensor performance through measurable resistance variations.

3.2.1 Plasma-Modification of graphene oxide for advanced ammonia sensing

This study fills a key gap in the literature by systematically exploring how the duration of low-pressure hydrogen plasma treatment impacts ammonia adsorption (ranging from 100 to 1049 ppm) within the rGO lattice. GO films were deposited onto clean copper electrodes using drop-casting and then exposed to plasma treatment for varying durations (10, 20,

40, 120, and 240 seconds). The results show a clear shift in the adsorption mechanism: shorter treatment times lead to chemisorption-dominated behaviour, while longer plasma exposure favours physisorption-dominated interactions. This shift has a major effect on sensor sensitivity and reversibility, with the best performance seen at 20 seconds of treatment, where both adsorption mechanisms coexist. Sensitivity increased from 23.9% at 100 ppm to 47.1% at 1049 ppm. These findings highlight how fine-tuning plasma treatment duration can optimize sensor response.

Beyond confirming the effectiveness of plasma treatment in modifying rGO properties, this study provides important insights into the relationship between reduction time, surface chemistry, and gas sensing performance. The results validate plasma-assisted reduction as a scalable, sustainable approach for the next generation of gas sensors. Real-world testing in open-air conditions confirmed our initial hypothesis, emphasizing the need for more studies on plasma-induced modifications of GR-based materials to further expand their use in environmental monitoring and industrial safety. Compared to existing literature, this work improves treatment speed by at least one order of magnitude while achieving similar sensitivity. With this article, I successfully confirmed Hypothesis 1.

In this article I contributed in: writing - original draft, methodology, investigation, formal analysis, data curation.

Applied Surface Science 660 (2024) 160006

Contents lists available at ScienceDirect

Applied Surface Science

journal homepage: www.elsevier.com/locate/apsusc

Full Length Article

Plasma-Modification of graphene oxide for advanced ammonia sensing

Ardita Kurtishaj Hamzaj [a,b,1], Edoardo Donà [b,c,1], Neelakandan M Santhosh [a,b], Vasyl Shvalya [a], Martin Košiček [a], Uroš Cvelbar [a,b,*]

[a] Department of Gaseous Electronics (F6), Jožef Stefan Institute, Jamova cesta 39, Ljubljana SI-1000, Slovenia
[b] Jožef Stefan International Postgraduate School, Jamova cesta 39, Ljubljana SI-1000, Slovenia
[c] Institut for Environmental Protection and Sensors, Beloruska ulica 7, Maribor SI-2000, Slovenia

ARTICLE INFO

Keywords:
Graphene oxide
Plasma reduction
Hydrogen plasma
Ammonia sensing
Gas sensor

ABSTRACT

The exceptional tailoriability of electrical properties in reduced graphene oxide (rGO) is a pivotal factor in unleashing its advanced gas sensing capabilities. Amidst various chemically/thermally-driven techniques, plasma reduction emerges as the fastest method with the potential for scalable treatment. This paper demonstrates a controlled plasma-enabled approach for swift and green surface reduction of graphene oxide (GO) films, specifically tailored for room-temperature ammonia (NH_3) detection at ppm levels. Employing a mild hydrogen plasma treatment on a thin GO layer deposited on copper electrodes by drop casting, we were able to tailor the sensor's sensitivity and reversibility due to the great impact of treatment time. The GO reduction experiments were conducted in a low-pressure mild hydrogen plasma discharged at 100 W, and the treatment time varied between 10 and 240 s. Structural and chemical analyses reveal an instantaneous reduction in oxygen content, dropping from approximately 30 to 20 atomic percentages within the initial 20 s. Sensitivity and recovery trade-offs are explored for different treatment durations, with the 'rGO - 20 s' sensor demonstrating the highest sensitivity at 23.9 % (100 ppm) and 47.1 % (1049 ppm) of NH_3, albeit with a recovery time approximately four times longer than the '240s-rGO' sample. This double-play behavior, attributed to chemisorption-dominated and physisorption-dominated interactions of NH_3-rGO, elucidates the sensitivity and recovery time dynamics. Proposing a scalable, environmental-friendly and room-temperature H_2-plasma reduction process enables one of the fastest approaches for designing advanced rGO sensors with controllable sensing behaviour towards ammonia.

1. Introduction

Considering the increasing environmental pollution and safety issues, the research interest is in developing advanced gas sensors to detect toxic and harmful gases in minute concentration. Owing to the high surface-to-volume ratio and large surface area, nanoscaled materials have been widely used as promising materials for gas sensors. Such nanomaterial-based devices reduce the size of the sensors and minimise energy consumption. Among the different sets of nanomaterials used for gas sensors, graphene [1] and its derivatives have been considered a frontrunner because of their unique mechanical, chemical, physical and electrical properties [2]. Graphene comprises a single layer of carbon atoms arranged in a honeycomb lattice [3,4] with a thickness of 0.34 nm, and superior conductivity, enabling electrons to traverse its perfect lattice structure at a speed of one million meters per second [2]. This exceptional mobility, with a peak value of 200,000 cm^2/V s, set graphene apart from conventional materials. Besides, the easy functionalisability of graphene makes it attractive to tailor the electrical properties for the desired applications by altering the concentration of free electrons - a rise for donor species and a decrease for acceptor species [5]. Such a phenomenon enhances the sensitivity of graphene that could detect even a single molecule, pushing the limits of measurement to quantum scales [6].

However, one of the major challenges to using pristine graphene as an advanced sensor material is the lack of the necessary surface functional groups for the selective and effective chemisorption of gas and vapor. Surface functionalisation of graphene by introducing functional groups, polymers, metals, or other modifiers has been widely used to address this limitation [7–9]. By such methods, functionalised layers acted as trapping centers, facilitating the adsorption of target species and inducing local changes in graphene's electrical resistance—a fundamental principle in graphene-based sensors [10]. Among the

* Corresponding author at: Department of Gaseous Electronics, Jožef Stefan Institute, Jamova Cesta 39, Ljubljana SI-1000, Slovenia.
E-mail address: uros.cvelbar@ijs.si (U. Cvelbar).
[1] Equal contribution.

https://doi.org/10.1016/j.apsusc.2024.160006
Received 24 January 2024; Received in revised form 15 March 2024; Accepted 28 March 2024
Available online 29 March 2024

varieties of graphene derivatives, GO has gained research interest. [11] This graphene derivative holds two key advantages. Firstly, it could be produced cost-effectively using readily available graphite as a raw material [12]. The utilisation of inexpensive chemical methods ensured high yields, making GO an attractive choice for large-scale production. Secondly, GO exhibits remarkable hydrophilicity, allowing for the formation of stable aqueous colloids [13]. This characteristic facilitated the assembly of macroscopic structures using simple and affordable solution-based processes—a crucial aspect for the practical implementation of graphene in diverse applications.

Though GO have been showing good potential for sensing applications, a critical drawback lies in its inherently insulating nature, limiting its practical application [7]. The direct approach to improve the conductivity of GO to restore the original conductivity, as observed in pristine graphene, is the reduction of oxygen groups; thus, various techniques were explored to reduce the oxygen content on the GO surface [14]. Thermal annealing [15–18] and chemical reduction [19–22] were traditional methods employed for this purpose, but being environmentally unfriendly and time-consuming chemical reactions restrict their large-scale applications. Owing to the fast and facile processing, dry soft-chemistry surface treatment and environmental friendliness, plasma-assisted reduction techniques [23–28] are gaining research interest to reduce graphene oxide, while preserving its structural integrity. The plasma surface treatment techniques allow GO reduction by removing oxygen atoms from GO without disrupting the carbon lattice and the surface. Commonly, hydrogen-containing plasma with mild treatment conditions has been reported for plasma-assisted GO reduction, which also ensures an energy-efficient alternative to the existing complex procedures. Such a reduction process could improve the electrical conductivity of reduced graphene oxide (rGO) and tailor the surface properties, which can be efficiently used for gas sensing applications. Besides, a reverse approach has also been reported to functionalise graphene using oxygen plasma, which has proven effective in the field of gas sensing [29].

Among all the major industrial gases produced yearly (N_2, O_2, CO_2, He, Ar, etc.) ammonia is among the most harmful gases. With a global production volume reaching millions of tons per year (253 in 2021 [30]), ammonia found widespread use in fertiliser production. As far as safety is concerned, our sense of smell is in itself an excellent sensor, as it can detect ammonia as low as 5 ppm [31]. However, safety regulations permit individuals to work in environments containing ammonia concentrations up to 25 ppm for extended periods. Beyond this threshold, concentrations exceeding 300 ppm posed immediate harm to the human body. Therefore, the need for real-time ammonia sensors capable to accurately detect its concentration became increasingly crucial. Multiple studies have been reported on applying thermally or chemically reduced GO for ammonia sensing [32–36]. However, the reduction time, sensor response and environmental impact are still a concern and demand an alternative fast approach to reduce GO for sufficient ammonia detection.

Therefore, in this study, we aim to address this demand by developing an rGO-based sensor, which is reduced by a fast and green plasma technique for the sufficient detection of ammonia at room temperature. The sensors were designed by drop casting the GO solution on the conventional sensor chip, which was exposed to a hydrogen plasma for the controlled reduction of the GO surface. Through systematic experimentation, we investigated the effect of plasma treatment time on the GO reduction by varying the time between 10 s and 240 s and analysed the response of the designed sensor towards different ammonia concentrations. The experimental observations suggest that the plasma-reduced GO sensors show excellent performance towards ammonia sensing at room temperature. To best of our knowledge, such plasma enabled reduction reveals one of the fastest GO reductions techniques. By combining the advantage of plasma for the surface reduction of GO, the cost-effectiveness and environmental friendliness of the method, and the significant improvement in the detection of ammonia at room temperature, this study will contribute to the development of efficient and real-time ammonia sensors for industrial applications.

2. Materials and methods

2.1. Sensor preparation

The active surface of the sensor comprised of interdigitated copper electrodes printed on an insulating substrate. A hydrogen plasma flow was used to enhance the contact between the electrodes and the graphene oxide (GO) by eliminating the oxide layer from the copper surface. The process utilised a low-pressure radio-frequency inductively coupled plasma system (Fig. 1, left panel). This system, operating at 100 W power, 100 sccm H_2 flow rate, and a total pressure of 32 Pa, was applied for 60 s in intervals of 20 s. Subsequently, the sensor chips underwent an Argon treatment to cool the sensor and to impede the risk of surface contamination upon re-exposure to ambient air.

After this pre-treatment, the chips were primed for the deposition of the graphene oxide ink. The GO ink was prepared by diluting a GO suspension in water (concentration 2 mg/mL) into a 40 % ethanol/distilled water solution. The resulting concentration of GO was 1 mg/mL in approximately 2 mL of the 40 % ethanol/distilled water solution. To obtain a homogenous GO suspension, it was immersed in an ultrasonic bath for 60 s. Then, precisely measured, 100 µL of this GO suspension was drop-casted onto the surface of the plasma-cleaned chip. To remove the residues of the solvent, the sensor chips were stored in a fume hood overnight, at a constant room temperature.

2.2. Plasma-assisted GO reduction

The as-prepared sensor chips exhibited high initial resistance, proving to be impractical for the purpose of ammonia sensing. To improve the conductivity, a plasma-assisted reduction mechanism was established. This mechanism involved a low-pressure radio-frequency inductively coupled plasma system consisting of an 80 cm long tube with a 9-turn inductive coil connected to the RF generator.

The sensor chips were subjected to hydrogen plasma treatment, utilising specific discharge parameters. The latter included a power of 100 W, a hydrogen flow at a rate of 100 sccm and a pressure of 32 Pa. The sensors were positioned in the post-glow region of the plasma (10 cm away from the centre of the coil), and the treatment durations included 10 s, 20 s, 40 s, 120 s, and 240 s. The treatments were conducted incrementally with a period of 10 s to prevent overheating and surface damaging. Hence, a total of six sensors were developed and tested, each named based on the duration of the plasma treatment. They include the untreated or control GO sensor labelled ‘GO−0 s’, and the GO sensors reduced after plasma treatment named ‘rGO − 10 s’, ‘rGO − 20 s’, ‘rGO − 40 s’, ‘rGO − 120 s’, and ‘rGO − 240 s’.

2.3. Sensing measurements

After plasma treatment, the sensors were soldered onto a home-built holder. This holder was placed inside a vacuum chamber and connected to a 2-point high current source meter (Keithley 2460). After the holder was firmly positioned inside the chamber, the system (Fig. 1, right panel) was evacuated until an overall pressure of 1 Pa was reached. As per necessity, the system was also flushed with N_2 gas to establish the desired vacuum conditions.

The sensing tests commenced by introducing a continuous N_2 gas flow at a rate of 1000 sccm (resulting in a total pressure of 450 Pa), with simultaneous recording of resistance changes. Nitrogen was used to create a controlled environment and detect the targeted analyte without any other gas interference. Once the resistance stabilised, NH_3 gas was introduced into the chamber, producing no significant changes in total pressure. Firstly, resistance variation measurements were conducted at a constant NH_3 concentration to investigate the reproducibility and

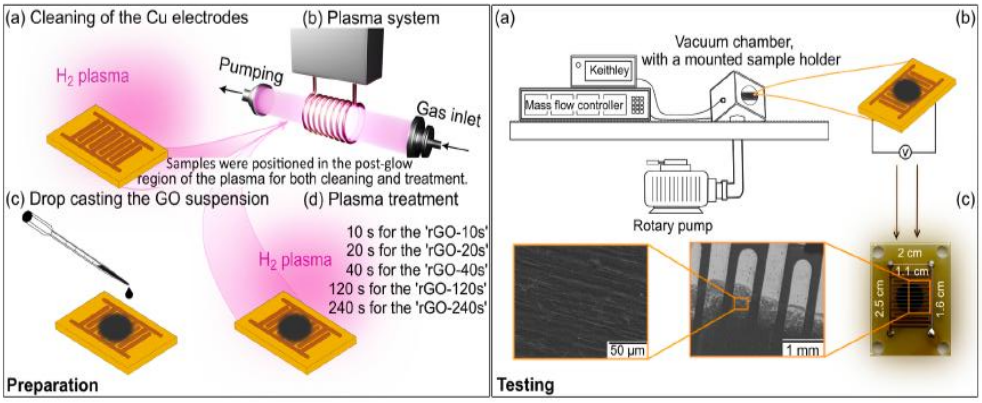

Fig. 1. Left panel: Schematic representation of the steps undertaken for the sensors' preparation and treatment. Right panel: (a) – Scheme of the system employed for NH_3 sensing measurements; (b) – A drawing that symbolises the sensor's connection to the Keithley multimeter; (c) – Digital image of the sensor, with magnified sections featuring SEM images of the drop-casted GO suspension, providing visual evidence of the even distribution of GO suspension and electrode coverage.

reliability of the prepared sensors. Additionally, the sensor response was evaluated for various NH_3 concentrations, ranging from 100 ppm to 1049 ppm. The concentration of ammonia was calculated based on the different flow of analyte to the environmental gas, fed through the mass flow controllers (accuracy ± 0.25 % of full scale). In both cases, the sensor response and recovery were observed for a fixed interval of 600 s in order to see the effect of plasma reduction time on sensor response.

2.4. Characterisation techniques

The effect of plasma treatment on the surface morphology of the GO structures was analysed by Prisma E scanning electron microscope (from Thermo Fisher Scientific Inc.). The surface properties and chemical modification of the GO after the plasma reduction were investigated by the X-ray photoelectron spectroscopy (XPS, PHI-TFA XPS spectrometer, Physical Electronics Inc) using an Al-monochromatic X-ray source with an energy of 1486.6 eV. A confocal μ-Raman setup (NT-MDT, model NTegra Spectra II) accompanied by a Peltier-cooled CCD device was used to measure the samples in a back-scattering regime using a10 × objective lens with NA = 0.40. Measurements were conducted with a 488 nm laser with an acquisition time of 10 s and a number of 5 accumulations. Three different surface spots were analysed for each sample and then averaged for better statistical accuracy. PerkinElmer (USA) spectrometer in ATR mode was used to probe samples in a range of 3700 cm^{-1} to 500 cm^{-1} with a resolution of 2 cm^{-1} and accumulated 10 scans from 3 different spots with their following averaging.

3. Results and discussion

3.1. Sensor properties

Resistance measurements were conducted on non-treated and plasma-treated sensors to understand the effect of plasma surface treatment on GO sensors. The drop-casted GO without any plasma

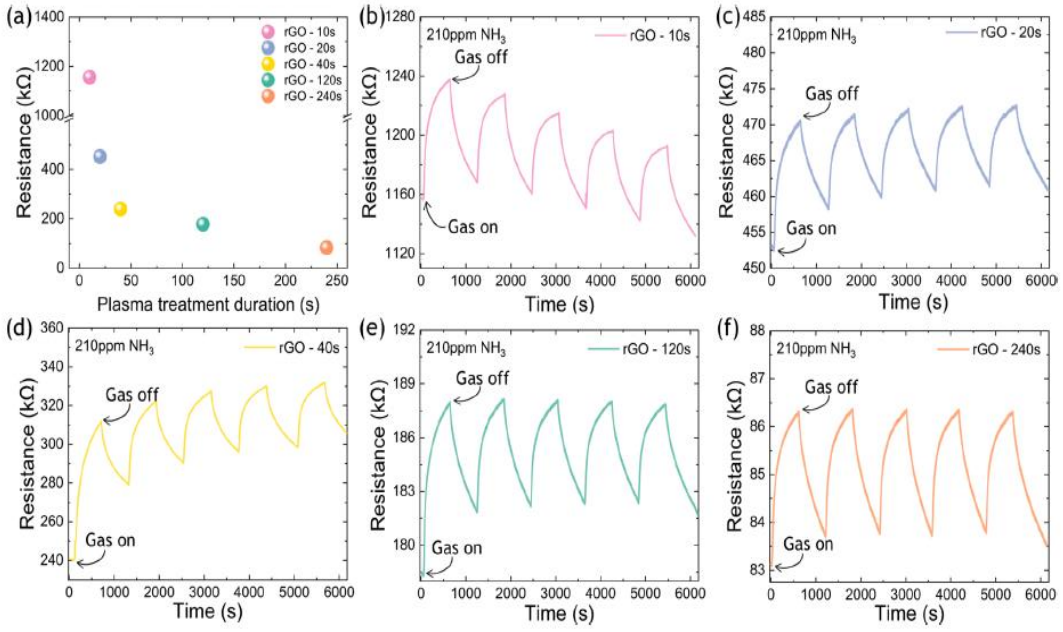

Fig. 2. (a) - Initial resistance of all rGO sensors, prior to NH_3 exposure; Resistance variation and repeatability of NH_3 sensing on (b) – 10 s, (c) – 20 s, (d) – 40 s, (e) – 120 s and (f) – 240 s H_2 plasma reduced GO sensors. All sensors were exposed to 210 ppm of NH_3 in a N_2 environment, at room temperature.

treatment, 'GO – 0 s', exhibited very high resistance (>200 MΩ), confirming the insulating behaviour of non-treated GO. Consequently, the as-prepared GO sensors weren't used for any further sensor studies. On the other hand, the resistance measurements on the plasma-treated GO sensors revealed a clear trend of decreasing resistance with increased plasma treatment duration, as presented in Fig. 2(a).

It is well-known that the presence of higher concentration oxygen functional causes the low conductivity of GO and reduction of such groups could enhance the conductivity 4–5 orders of magnitude [37,38]. The decrease in resistance of the GO along with plasma treatment indicates the surface reduction of GO to rGO. Hydrogen plasma treatment effectively removes the oxygen groups from the surface layer and partially restores the sp^2-bounded carbon network, resulting in an improved conductivity. Moreover, hydrogen is known for the etching of the amorphous phase [39,40]. Thus, it helps eliminate the amorphous phase and remove oxygen termination from the GO surface during the plasma reduction process. As all the sensors demonstrated significant changes in the resistance after the plasma reduction, their response towards ammonia was evaluated. During sensing measurements, the response and recovery time was fixed to 600 s to identify the best responsive sensor. The sesnsor response and the repeatability of all the plasma-reduced rGO sensors are presented in Fig. 2(b-f).

To assess reliability and repeatability, response measurements were performed for each sensor over five cycles at a constant NH_3 concentration of 210 ppm. All the sensors responded instantaneously to the ammonia exposure, e.g., gas on stage, and the response started to drop as soon as the ammonia gas was off. The resistance response studies show that sensors treated with longer plasma durations exhibit excellent repeatability. On the other hand, the sensors with lower plasma treatment duration show lower repeatability, likely due to minimal reduction of GO. The repeatability of the 'rGO – 10 s' sensor, (Fig. 2(b)), decreases with time, and a similar behaviour is observed for the 'rGO – 20 s' and 'rGO – 40 s' sensors (Fig. 2(c) and (d)), but with an improved repeatability. As the sensor response changes with the plasma reduction time, the shorter reduction times seem to result in an insufficient reduction of oxygen functional groups. Such groups are active towards the chemical modifications and might potentially facilitate the chemisorption of NH_3 molecules, which leads to incomplete desorption during the recovery process and, thus, the initial resistance values for the repeated sensing cycles are not attained. On the other hand, the GO sensors exposed to longer plasma durations, the 'rGO – 120 s' and 'rGO – 240 s' sensors (Fig. 2(e) and (f)), exhibit good recovery and stability, suggesting that the higher reduction of oxygen groups favors the physisorption dominated response, allowing for easier desorption of the NH_3 molecules during the recovery period. All these findings indicate that the plasma-enabled removal of oxygen functional groups from GO promotes enhanced sensor recovery and stability.

To evaluate the sensitivity towards different NH_3 concentrations, the sensors were subjected to a range of ammonia concentrations, varying from 100 to 1049 ppm (Fig. 3(a)). All the plasma rGO sensors exhibited increased response with the increase in NH_3 concentration. Additionally, these measurements unveil that the sensitivity of sensors at different concentration of NH_3 decreases as the duration of plasma reduction increases. The sensors treated for shorter times attain the

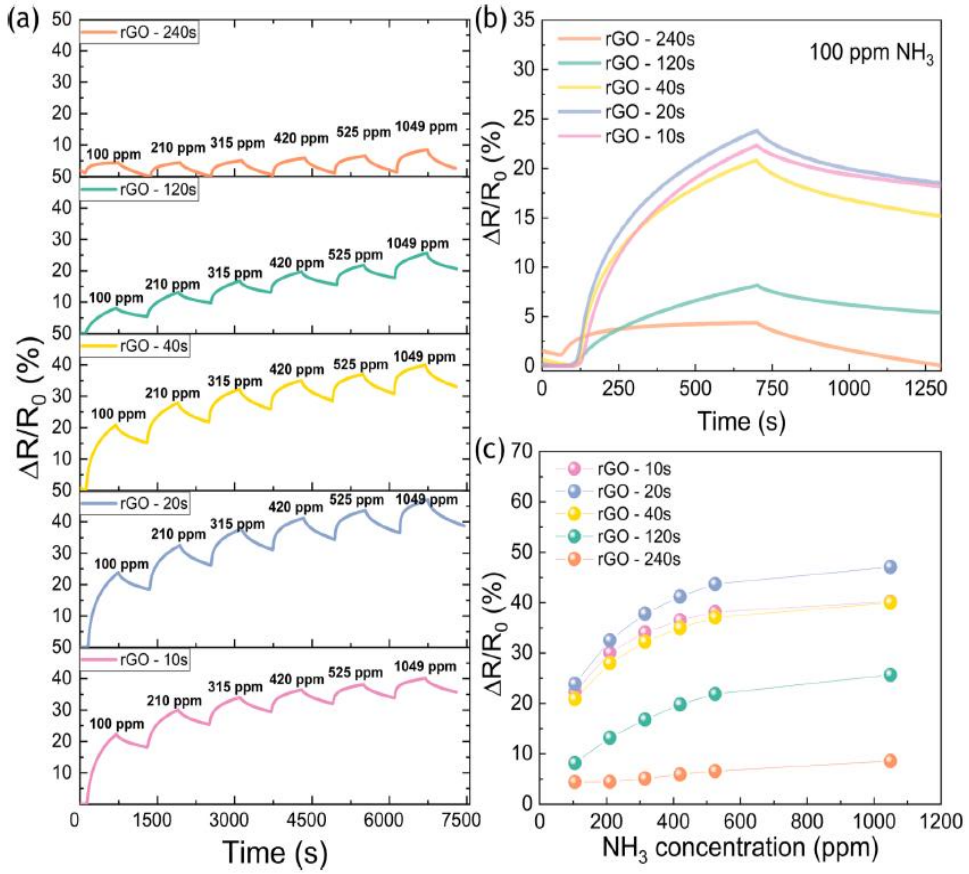

Fig. 3. (a) - Response of all five sensors to various NH_3 concertation, ranging from 100 up to 1049 ppm; (b) - extracted response curves for each sensor at an ammonia concentration of 100 ppm; (c) - Maximum recorded response of each sensor in terms of NH_3 concentration.

highest sensitivity by exceeding 40 % at 1049 ppm of NH_3, while the sensors with longer treatment durations possess the lowest sensitivity at a high concentration of NH_3. For comparison, the sensitivity of the sensors during the first cycle of measurements with 100 ppm of NH_3 is depicted in Fig. 3(b). The 'rGO – 10 s' sensor exhibits a maximum recorded sensitivity of 22.3 %, followed by 'rGO – 20 s' with 23.9 %, 'rGO – 40 s' with 20.8 %, 'rGO – 120 s' with 8.2 %, and finally, the 'rGO – 240 s' sensor with 4.4 %. Fig. 3(c) further compares the maximum recorded sensitivity in terms of NH_3 concentration for all sensors. It denotes that the 'rGO – 20 s' sensor provides the highest sensing response, while the 'rGO – 10 s' sensor closely resembles the response of the 'rGO – 40 s' sensor. The higher sensitivity of the 'rGO – 20 s' sensor compared to the 'rGO – 10 s' sensor, suggests the presence of a threshold or a minimum reduction time required to achieve the maximum sensing response. Conversely, the 'rGO – 120 s' sensor exhibits significantly lower sensitivity, followed by the 'rGO – 240 s' sensor, which is the least sensitive. Such sensor characteristics could be ascribed as the combined effect of irreversible chemisorption influenced by the surface functional groups and reversible physisorption stimulated by the surface of plain graphene.

Additional tests were conducted to investigate the selectivity, sensitivity towards ammonia in ambient conditions, plasma treatment reproducibility and long-term stability of sensors. CH_4, CO_2, CF_4, and synthetic air N_2/O_2 (80/20) were used as interference gases to address the selectivity of the 'rGO – 20 s' sensor. Figure S1 shows that the sensor's response towards NH_3 was at least four times greater than for the other tested gases. To understand how different humidity levels influence the sensors' response, tests were conducted under ambient conditions. The behaviour of the 'rGO – 240 s' sensor in air at atmospheric pressure, 21 ± 1 °C and under different humidity conditions is reported in Figure S2. The response increased proportionally with NH_3 flow, and the changes in sensitivity in different relative humidity conditions were negligible. Moreover, to investigate the reproducibility of plasma treatment conditions to provide consistent sensing results, the sensitivity of 'rGO – 240 s' sensors was compared at various NH_3 concentrations (Supporting Information, Figure S3). A comparable sensitivity was recorded in all sensors. Lastly, the performance of 'rGO – 10 s', 'rGO – 20 s', and 'rGO – 240 s' (stored in ambient conditions) after one year was tested to evaluate the effect of ageing and the sensor performance is presented in Figure S5. Even though a reduction in the sensitivity was observed, all the sensors were still reactive towards ammonia. To understand the difference in the sensing behavior of our sensors, changes in the surface morphology and chemical compositions of GO after the plasma surface treatment were further investigated.

3.2. Physical and chemical characterisation

Surface Morphology. The overview SEM micrographs of the non-treated, least-treated and most-treated sensors are presented in Fig. 4. Higher resolution SEM micrographs are presented in Figure S4. The 'GO – 0 s' sensor's surface displays mild wrinkles, and these features persist without noticeable modifications after the plasma treatment for 'rGO – 10 s' and 'rGO – 240 s' sensors, as shown in Fig. 4(b-c).

Surface analysis and chemical composition by XPS. The direct information on the surface reduction of GO is the changes in the oxygen concentration in the material. Therefore, to evaluate the changes in the chemical composition of GO after the plasma treatment, the materials were analysed by XPS. The XPS survey spectra of the non-treated and plasma-treated GO structures are presented in Fig. 5(a), and all the spectra are featured with carbon at 284.6 eV and oxygen at 532 eV. A minor peak around 400 eV, corresponding to nitrogen, is also observed in the non-treated GO and could be adsorbed from the atmosphere. The significant changes observed in the survey spectrum are the decrease in oxygen concentration along with the plasma treatment time, which indicates the removal of the oxygen group from the surface of GO and the fast reduction of GO to rGO. To gain a better understanding of the carbon and oxygen bonding environments after the plasma treatment, high-resolution C 1s and O 1s regions were observed. The normalised C 1s region of GO and plasma rGO is presented in Fig. 5 (b). The C 1s spectra of 'GO – 0 s' featured two major peaks around 284.6 and 286.5 eV, corresponding to C-C and C-O groups.

However, the peak intensity of C-O groups lowers after the initial 10 s plasma treatment and tends to diminish with longer plasma treatment time. This characteristic feature implies that plasma treatment removes the O groups from the surface and reduces them to other functional groups, resulting in improved electrical conductivity, as seen in the different sensors. Therefore, the O 1s spectra of all the samples, which possess a similar peak shape, were also investigated in detail. The peak position was changed to the lower binding energies, indicating the changes in the chemical bonding of GO after the plasma reduction. To get insight into the bonding environments of carbon, the high-resolution C 1s regions were further deconvoluted to better understand the chemical bonding changes after the plasma reduction. The non-treated GO and plasma rGO featured the peaks: sp^2 C = C (284.6 eV), sp^3 C-C/C-N (285.5 eV), C-O (286.5 eV), C = O (287 eV), O-C = O (288.2 eV), a broad satellite peak (289.5 eV) and the defect peak at 283.3 eV (Fig. 5 (d-f)) [41,42]. This indicates that the structural quality of GO improves after the plasma reduction as the peak assigned to structural defects and the C-O groups are lowered after plasma treatment. The significant difference observed in these regions could be due to the removal of oxygen and amorphous phase, suggesting that most of the oxygen groups (C = O or C-O) were either removed or reduced to OH groups, which opened more conductive routes in the GO after plasma reduction. The GO structures exhibited more pronounced oxygen groups singly bonded to carbon (C-O/C-OH) compared to the C = O groups. While after the plasma reduction, the C-O groups to C = O group intensity ratio become lower than the non-treated GO. The observed changes in peak area of deconvoluted C 1s spectra with plasma treatment time are presented in Supporting Information, Table S1. These features suggest that the removal of weakly bonded oxygen from the surface, leads to the enhancement in the electrical conductivity and structural quality of the materials. All these effects could significantly contribute to the improved sensing performance of the plasma rGO sensors.

Structural stability and reduction efficiency by Raman and FTIR

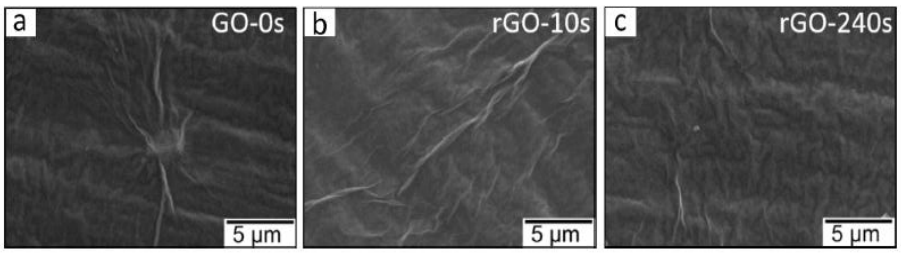

Fig. 4. SEM micrographs: (a) – 'GO – 0 s' sensor, (b) – 'rGO – 10 s sensor', (c) –'rGO – 240 s' sensor, pinpointing no apparent damages of the sensor surface after plasma treatment.

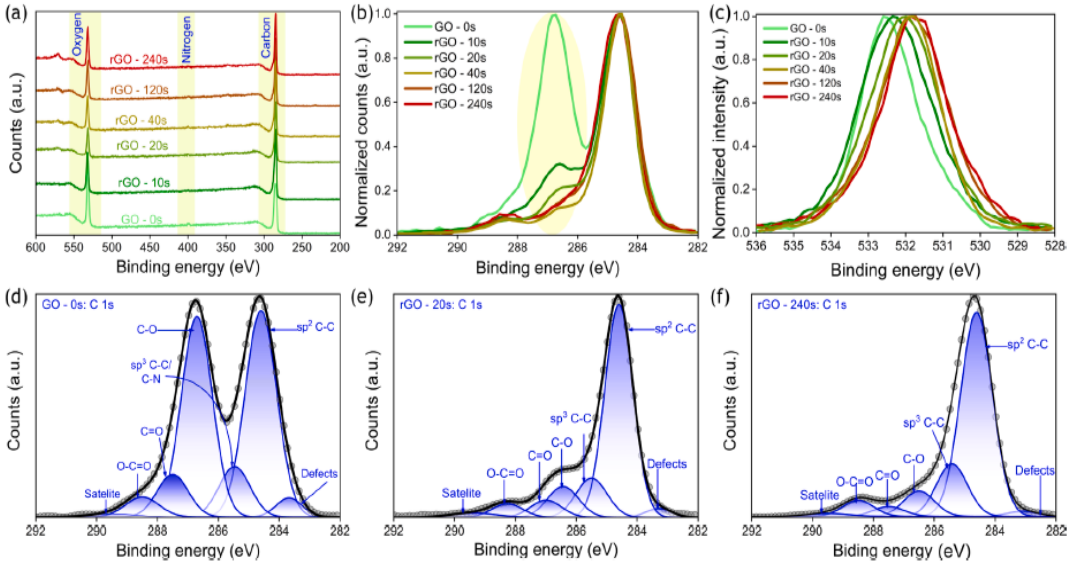

Fig. 5. Surface composition of GO and plasma rGO (a) - XPS survey spectra, (b) - normalised high-resolution C 1s spectra and (c) - normalised O 1s spectra of GO and rGO as a function of plasma treatments time; deconvoluted C 1s spectra of (d) – GO, (e) - rGO after 20 s plasma treatment and (f) - rGO after 240 s plasma treatment.

analysis. Raman study was undertaken to evaluate the structural stability and modification of GO under plasma reduction. As a graphene derivative, GO spectra consist of first-order (1000–1800 cm^{-1}) and second-order Raman modes (2400–3400 cm^{-1} [43–46]) (Fig. 6(a)). Considering the lower frequency 'fingerprint' range, the spectrum profile reveals two intense peaks centred at 1357 cm^{-1} (D) and other at 1600 cm^{-1} (G), which are much broader comparing to graphene. D-peak is assigned to the breathing phonon mode of A_{1g} at Brillouin zone boundary *K*-point, and its intensity and width change are linked to the number and type of disorder/defects in the graphene plane. The G peak stands for the first-order E_{2g} optical mode corresponding to in-plane C = C stretching vibrations. A closer look at this mode displays an asymmetric type feature that indicates the contribution of an additional defect-related (intravalley double-resonance process activated when graphene structure is defected) D'-band component typically observed around 1615 cm^{-1} (Fig. 6(a), inset). Two more peaks were added at 1200 cm^{-1} (D*) and 1500 cm^{-1} (D") to describe the first-order (1000–1800 cm^{-1}) profile, where D* can be linked to the disordered graphitic lattice at the edges caused by sp^2-sp^3 bonds, and D" often referred as a contribution of interstitial defects related to amorphous lattices with sp^2-bonded carbon that functionalised with other molecules. The phonons in the second-order spectral part are overtones and combinations of the first-order ones, where 2D mode at 2700 cm^{-1} (also called G') is an overtone of D-phonon, and its activation requires scattering of a phonon pair having opposite wave vectors obeying conservation of momentum. The D + G combined overtone mode located at ~2940 cm^{-1} is the most intense overtone within a region. Lastly, the 2G band, being an overtone of G-peak placed at ~3170 cm^{-1}, was found to be the smallest one [43–46].

After treatment in cold hydrogen plasma afterglow, the second-order region starts to be reduced gently at 10 s and 20 s, with no further changes at longer exposure times. A similar, but stronger trend in overtones reduction was observed in GO under local laser heating [43] and under an effect of controlled annealing between 100 and 800 °C [45]. No apparent changes are observed within the first-order region after plasma reduction. Minor variations within a valley (~1500 cm^{-1},

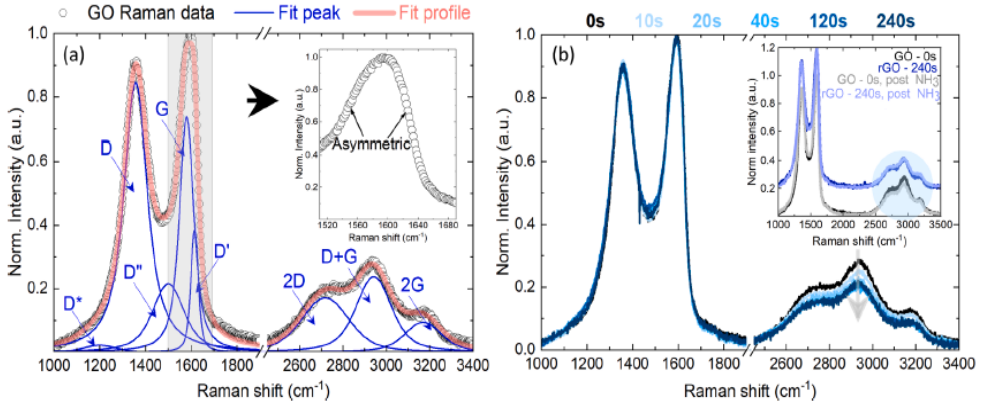

Fig. 6. (a) - Raman study of GO accompanied by Gaussian fit function with vibrational modes assignment. Inset shows the zoomed section of G peak; (b) – Normalised and superimposed Raman spectra of GO exposed to H_2-plasma treatment, with inset revealing spectra of control GO and most treated sample rGO-240 s before and after NH_3 sensing.

peak D") are related to the contribution of interstitial defects in the sp^2 lattice. The changes in $I_D/I_G = 0.91 \pm 0.02$ are not significant as well, and they are even less prominent compared to those found by Ma et al. [43] and Claramunt et Al. [45], the where effect of heat was investigated. Considering these reports, Raman indicates that plasma reduction approaches employed in this study do not provide thermal-induced damages to the bulk of GO layers and most of the chemical and structural changes occur mainly at the surface (Fig. 6(b)). After exposing samples to NH_3, the Raman features of control and plasma-treated samples remain similar (Fig. 6(b), inset), implying the structural stability of rGO to be used in a real-case sensing scenario.

In correlation with the Raman spectra, a direct comparison of the intensity reduction in the Raman second-order region and the resistance of the plasma-treated rGO sensors (Fig. 7(a)) reveals no significant changes after 20 s of plasma reduction. Similarly, when examining the C 1s XPS components, there is a considerable reduction in the fitted peak area of C-O and a slight reduction in C = O + COO (Fig. 7(b)). However, no significant changes are observed after 20 s of plasma reduction. Therefore, following Raman, the FTIR measurements were conducted to analyse plasma-induced changes in the functional groups of GO to understand more on the changes in functional entities (Fig. 7). In the case of short-time mild-plasma processing, it is expected the alterations should happen at the surface or between the layers neighbouring the surface. Thus, three samples were analysed using FTIR to investigate the aggressiveness of plasma on GO reduction: 'GO – 0 s', 'rGO – 10 s' and 'rGO – 240 s'; before and after being exposed to NH_3 gas (Fig. 7, (c-e)). The spectrum of the 'GO – 0 s' before ammonia detection exhibits the presence of broad asymmetric ν(O-H) stretching band centred between 3200 cm^{-1}, small ν(C = O) carboxyl band at 1730 cm^{-1}, C = C carbon stretching from unoxidized graphitic domains appearing at 1590 cm^{-1}, a complex mutual peak at 1410 cm^{-1} representing contribution from bending δ(C-H) or/and δ(O-H) bonds, C-OH at 1245 cm^{-1}, the strongest shouldered mode attributed to C–O stretching vibrations of C–O–C links [10,47,48]. The basal graphene plane FTIR features are also spotted at

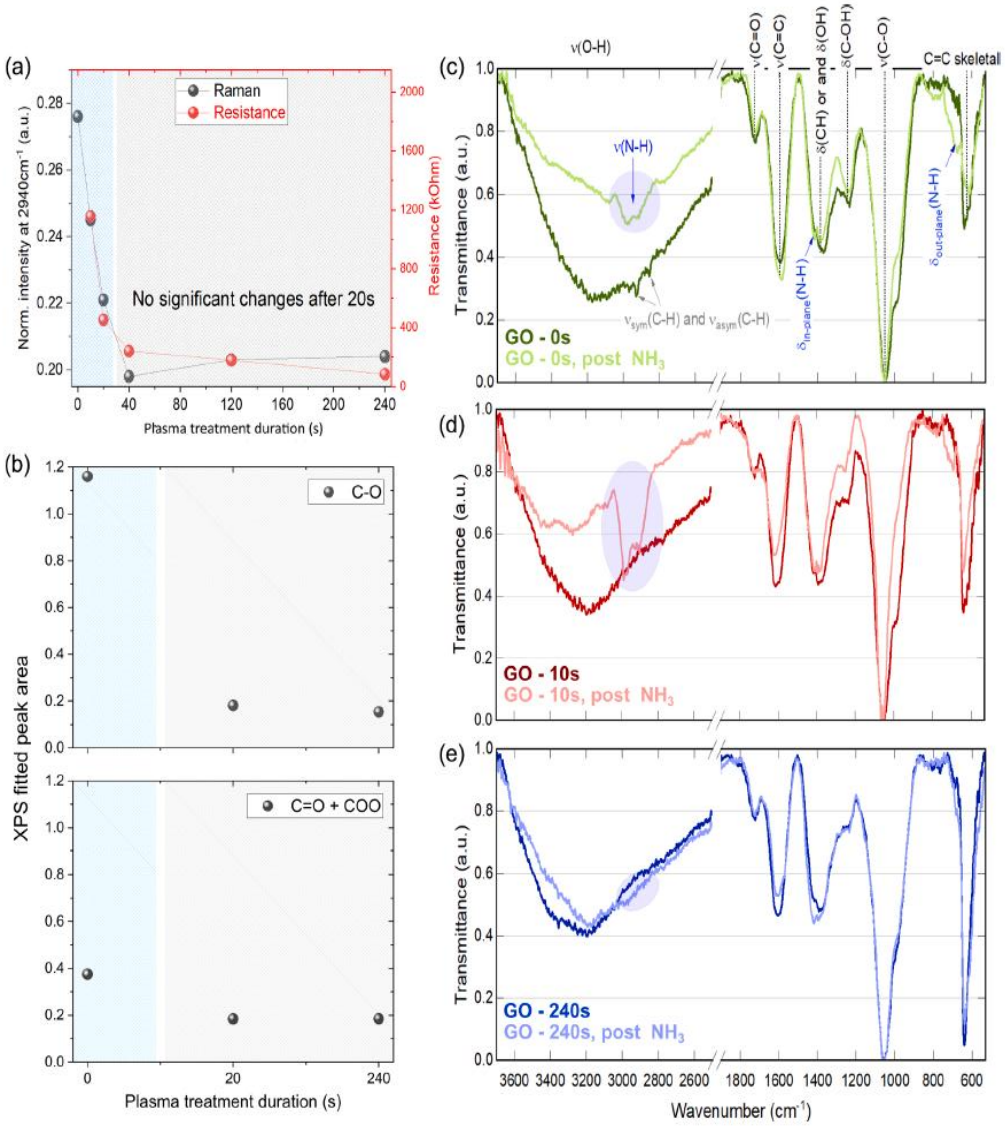

Fig. 7. (a) – Raman intensity of a selected mode at 2940 cm^{-1} and resistivity trend as a function of treatment time; (b) – Fitted peak area for C-O and C = O + COO extracted from C 1s XPS components; (c-e) - ATR-FTIR data of selected samples recorded before and after NH_3 sensing measurements.

about 630 cm^{-1}, which could be related to C = C skeletal vibrations that naturally gain intensity during reduction [49].

The samples were placed in the post-glow region to minimise surface damage due to the ion bombardment and surface temperature during the plasma treatment while using the tendency of hydrogen-plasma treatment to slightly etch the amorphous phases and impurities. In both treated samples, the most changes are seen in ν(O-H), C-OH and basal graphene regions, where OH-related bonds decrease and the C = C skeletal bond increases with plasma exposure time. This is evident from the interplay of peak ratios extracted from the transmittance data T (1245 cm^{-1})/T(630 cm^{-1}). This ratio reads as follows: 1.14 → 2.02 → 14.84 for control 'GO – 0 s', 'rGO – 10 s', and 'rGO – 240 s', respectively. Note that the value increases due to the C-OH peak tending towards '1' (lowering the absorption) and the δ(C-H) peak aiming towards '0' on the normalised transmittance scale (increasing the absorption). These observations agree with the changes in chemical composition observed in the XPS data and expand the understanding that reduction occurs not only at the surface but also within the few surface layers. However, the oxygen content in rGO is still detected since different O-related groups are still well detectable. This happens because of two factors: (i) the initial GO deposit layer is too thick to be reduced entirely (presence of OH-related bonds), and (ii) the insufficient energy to remove the C = O peak by mild plasma treatment, as it remains stable with a minor, almost negligible decrease in FTIR. These observations display similarities to the XPS data set, where the reduction of C = O is much smaller than that of C-O, suggesting an efficient removal of singly-bonded oxygen but not double-bonded oxygen (Fig. 7(b)). After H_2-plasma treatment, the oxygen content immediately decreases from an initial 30 a.t.% in the control sample to 20–23 a.t.%, depending on the treatment time. It can be referred to as the presence of C = O, as evident from XPS and FTIR.

As the FTIR results of plasma-reduced GO agree with the findings from XPS and Raman, FTIR spectra of the samples after exposure to NH_3 are also recorded to identify the changes in the chemical functionalities. All three sensors exhibit FTIR changes, in which the most significant changes are observed at around 3000 cm^{-1}, where new stretching ν(N-H) modes of different intensities appear [50]. Discussing the least treated and the most treated sensors, these peaks are more intense in 'rGO-10 s', indicating the out-of-plane δ(C-H) spectral interval are altered (see 'GO – 0 s' and 'rGO-10 s' samples in Fig. 7, (c), (d)). On the contrary, the 'rGO-240 s' sample demonstrates stability in the FTIR profile compared to the previous samples, with no significant modifications.

3.3. Double-play gas sensing mechanism

The physical and chemical composition changes observed from the surface and structural analysis suggest that oxygen-containing functional groups remain on the rGO surface. It is well known that the presence of oxygen-containing functional groups and lattice vacancies make rGO more sensitive towards ammonia, in contrast to the weakly interacting graphene, which lacks these trapping sites [7,48,51]. The reduction of GO is necessary as it increases its electrical conductivity and improves the response of rGO even towards low ammonia concentrations. Mild hydrogen plasma reduction allows for the tailoring of the material's conductivity, as confirmed by the significant decrease in resistance, from 1156 kΩ for the least treated ('rGO – 10 s') sensor to 83 kΩ for the most treated ('rGO – 240 s') sensor (Fig. 8(a)). These changes in material conductivity could be attributed to the partial restoration of the graphene structure by the plasma-assisted reduction/removal of oxygen groups and amorphous carbon phase from the surface of GO. This claim is supported by our XPS and FTIR analyses, where a decrease of oxygen content from 30a.t.% in the non-treated sample to 20a.t.% for the most treated sensor is recorded.

To detect ammonia, sensors based on rGO rely on electrical conductivity changes after gas molecule adsorption on the rGO surface. The electron transfer from NH_3 to rGO (a p-type material) reduces the number of holes in the conduction band due to electron-hole recombination (since NH_3 acts as a donor [34]) and thus increases electrical resistance [7]. The extent of this resistance change depends on the type of NH_3 adsorption in rGO, which, in turn, is greatly influenced by the presence of oxygen functional groups.

Ammonia interacts with rGO through two distinct mechanisms: physisorption and chemisorption. Physisorption primarily takes place on plain graphene regions, which could have been restored by the removal of oxygen atoms after plasma treatment, and it is driven by Van der Waals interactions [51]. This type of interaction can be easily reversed by pumping down and purging the system with an inert gas, such as N_2 in our case [10]. Chemisorption is due to the presence of oxygen groups and carbon vacancies in the lattice, which enable the surface reactions with NH_3. After these reactions, new chemically stable adsorbates are formed, which cannot be removed easily [51]. Earlier

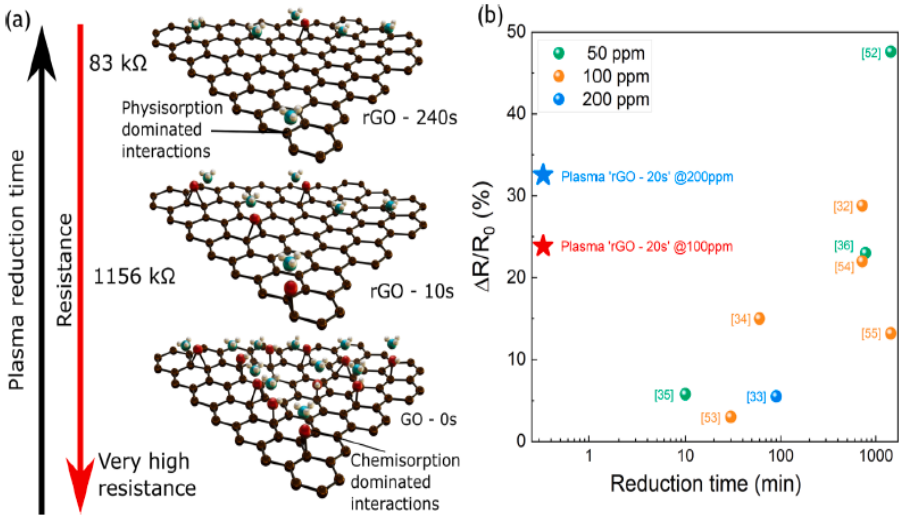

Fig. 8. (a) – A possible physisorption/chemisorption-assisted sensing mechanism towards ammonia in plasma reduced GO sensors; (b) – A comparison of this work's 'rGO – 20 s' sensor with the state-of-the-art rGO sensors.

studies based on the density-functional theory calculations [48] have confirmed that the charge transfer during the interaction between NH_3 and oxygen groups is more significant than compared to the weak NH_3 interactions with plain graphene.

Consequently, in cases where chemisorption dominates (i.e., for sensors reduced with lower plasma durations), the resistance changes in sensor response are more significant, making the sensor highly sensitive towards ammonia. However, because of the strong nature of the interaction, the sensor's recovery cannot be fully achieved in room temperature conditions. This is why nitrogen content was found on the shortest treated sensor after the sensing experiments, as observed in FTIR. Conversely, in instances of physisorption dominance (i.e., for sensors reduced with longer plasma durations), the sensor response towards ammonia is minimal. Nevertheless, because of the weak interaction, most of the NH_3 is desorbed from the surface during purging and pumping, promoting full and fast sensor recovery in room temperature conditions. This is in good agreement with the changes observed from the FTIR and XPS analyses, where the lowest nitrogen content after sensing experiments is found in the most treated sample.

To aid in visualisation, the possible interaction of ammonia with our plasma-reduced sensors is presented schematically in Fig. 8, (a). The least treated ('rGO – 10 s') and the most treated ('rGO – 240 s') sensors were compared to the non-treated GO ('GO – 0 s') to explain different sensing possibilities. Spectroscopic measurements reveal an immediate considerable reduction of weakly bounded surface oxygen just after 10 s of plasma treatment, which becomes even more prominent after 240 s of plasma reduction. Hence, due to the oxygen content level on the sensor's surface, there is a shift in interaction from chemisorption-dominated to physisorption-dominated as the plasma treatment duration increases. Because of the shift in the sensing mechanism, the sensitivity towards ammonia increases and the sensor's recovery ability decreases as we decrease the plasma treatment durations. Consequently, 'rGO – 240 s' exhibits the lowest sensitivity, while 'rGO – 20 s' displays the highest sensitivity. Interestingly, 'rGO – 10 s' departs from this pattern, showing a lower sensitivity compared to 'rGO – 20 s.'

As noted, the reduction for this sensor compared to others is the lowest, and the oxygen presence may hinder part of the ammonia from being physisorbed on plain graphene sites. The physisorption is not as present in 'rGO – 10 s' as in the more reduced sensors, considering the surface still contains a substantial amount of oxygen groups, as seen from spectroscopic analysis. However, when the sensor is further reduced for another 10 s, the highest sensitivity among the sensors is achieved. Though 20 s of plasma reduction does not eliminate the oxygen groups completely, it provides sufficient channels for the physisorption on graphene and chemisorption facilitated from oxygen groups. This leads us to conclude that achieving the optimal sensor sensitivity necessitates striking a balance between both chemisorption and physisorption, and this balance appears to be achieved at a plasma treatment duration of 20 s. To maximise the sensor's recovery, on the other hand, higher reduction times are favoured.

A comparison between the sensing performances of the 'rGO – 20 s' sensor in this work and the conventionally reduced GO sensors reported for room temperature NH_3 detection [32–36,52–55] is summarised in Fig. 8, (b). The results suggest that the plasma reduction is significantly faster than the other conventional techniques, and it provides sensors with comparable, if not higher, sensitivities to the conventionally prepared sensors. Apart from this, the potential of oxygen plasma functionalisation of graphene as a sensor for NH_3 has also been explored [29]. The sensing platform composed of a channel with oxygen plasma functionalized graphene on top and pristine graphene, demonstrated sensitivity of ~ 12 % to 100 ppm of NH_3. Such sensing response was achieved by 60 s plasma treatment duration. All the obtained results suggest the fast and effective nature of plasma-enabled surface engineering techniques to design efficient NH_3 gas sensors.

4. Conclusions

The environmental impact of ammonia has gained research attention over the years, and novel approaches have been identified to design advanced sensors for sufficient ammonia detection. In this work, we report the design of graphene oxide-based sensors for the efficient detection of ammonia. A fast low-pressure hydrogen plasma-assisted reduction mechanism was employed to overcome the insulating behaviour of GO, making it suitable for sensing applications. The plasma treatment time was varied between 10 and 240 s to investigate the efficiency and effectivity of plasma as a reduction method. The proposed method achieves a sufficient reduction of GO within 20 s, which is also tailored by varying H_2 plasma treatment time. Prolonged plasma reduction resulted in stability and good reversibility, albeit lower sensitivity ('rGO – 240 s' 4,4% for 100 ppm). Short plasma reduction resulted in the opposite, poor recovery, but higher sensitivity ('rGO – 20 s' 23,9% for 100 ppm). Such sensing behaviour was attributed to a physisorption/chemisorption-assisted mechanism. Our findings suggest that in an rGO sensor with a low remaining oxygen content after plasma reduction, a balanced contribution of both physisorption and chemisorption could improve sensitivity.

The plasma reduction approach proposed in this work is not only one of the fastest methods for the surface reduction of GO but it also delivers ammonia sensing performance comparable to other methods. This work, therefore, addresses the time constraints for GO reduction without compromising performance, aiming to aid in the design of next-generation sensor devices for hazardous gases.

CRediT authorship contribution statement

Ardita Kurtishaj Hamzaj: Writing – original draft, Methodology, Investigation, Formal analysis, Data curation. **Edoardo Donà:** Writing – original draft, Methodology, Investigation, Formal analysis, Data curation. **Neelakandan M Santhosh:** Writing – review & editing, Validation, Supervision, Formal analysis, Data curation. **Vasyl Shvalya:** Writing – review & editing, Validation, Supervision, Formal analysis, Data curation. **Martin Košiček:** Visualization, Investigation. **Uroš Cvelbar:** Writing – review & editing, Validation, Supervision, Resources, Project administration, Methodology, Funding acquisition, Conceptualization.

Declaration of competing interest

The authors declare that they have no known competing financial interests or personal relationships that could have appeared to influence the work reported in this paper.

Data availability

Data will be made available on request.

Acknowledgement

Authors would like to acknowledge Slovenian Research and Innovation Agency (ARIS) program P1-0417, and projects J2-4490, J2-50066, N2-0213, Z2-4467, and EU Graphene Flagship FLAG-ERA III JTC 2021 project "VEGA" (Funded by MIZS: PR-11938). E.D acknowledges a PhD fellowship funded by the EU Horizon 2020 research and innovation programme under the MSCA-FoodTraNet project (grant agreement no. 956265).

Appendix A. Supplementary data

Supplementary data to this article can be found online at https://doi.org/10.1016/j.apsusc.2024.160006.

References

[1] K.S. Novoselov, A.K. Geim, S.V. Morozov, D. Jiang, Y. Zhang, S.V. Dubonos, I. V. Grigorieva, A.A. Firsov, Electric field effect in atomically thin carbon films, Science 306 (2004) 666–669, https://doi.org/10.1126/science.1102896.

[2] C. Soldano, A. Mahmood, E. Dujardin, Production, properties and potential of graphene, Carbon N. Y. 48 (2010) 2127–2150, https://doi.org/10.1016/j.carbon.2010.01.058.

[3] M.F. Craciun, S. Russo, M. Yamamoto, S. Tarucha, Tuneable electronic properties in graphene, Nano Today 6 (2011) 42–60, https://doi.org/10.1016/J.NANTOD.2010.12.001.

[4] K.S. Novoselov, A.K. Geim, S.V. Morozov, D. Jiang, M.I. Katsnelson, I. V. Grigorieva, S.V. Dubonos, A.A. Firsov, Two-dimensional gas of massless Dirac fermions in graphene, Nature 438 (2005) 197–200, https://doi.org/10.1038/nature04233.

[5] T.J. Booth, P. Blake, R.R. Nair, D. Jiang, E.W. Hill, U. Bangert, A. Bleloch, M. Gass, K.S. Novoselov, M.I. Katsnelson, A.K. Geim, Macroscopic graphene membranes and their extraordinary stiffness, Nano Lett. 8 (2008) 2442–2446, https://doi.org/10.1021/nl801412y.

[6] E.W. Hill, A. Vijayaragahvan, K. Novoselov, Graphene sensors, IEEE Sens. J. 11 (2011) 3161–3170, https://doi.org/10.1109/JSEN.2011.2167608.

[7] S. Basu, P. Bhattacharyya, Recent developments on graphene and graphene oxide based solid state gas sensors, Sens. Actuators B Chem. 173 (2012) 1–21, https://doi.org/10.1016/J.SNB.2012.07.092.

[8] M. Pumera, A. Ambrosi, A. Bonanni, E.L.K. Chng, H.L. Poh, Graphene for electrochemical sensing and biosensing, TrAC Trends Anal. Chem. 29 (2010) 954–965, https://doi.org/10.1016/J.TRAC.2010.05.011.

[9] A. Eftekhari, H. Garcia, The necessity of structural irregularities for the chemical applications of graphene, Mater. Today Chem. 4 (2017) 1–16, https://doi.org/10.1016/J.MTCHEM.2017.02.003.

[10] C.R. Minitha, V.S. Anithaa, V. Subramaniam, R.T. Rajendra Kumar, Impact of oxygen functional groups on reduced graphene oxide-based sensors for ammonia and toluene detection at room temperature, ACS Omega 3 (2018) 4105–4112, https://doi.org/10.1021/acsomega.7b02085.

[11] W. Gao, The Chemistry of Graphene Oxide, in: Graphene Oxide, Springer International Publishing, Cham, 2015, pp. 61–95, https://doi.org/10.1007/978-3-319-15500-5_3.

[12] A.M. Dimiev, J.M. Tour, Mechanism of graphene oxide formation, ACS Nano 8 (2014) 3060–3068, https://doi.org/10.1021/nn500606a.

[13] I. Chowdhury, M.C. Duch, N.D. Mansukhani, M.C. Hersam, D. Bouchard, Colloidal properties and stability of graphene oxide nanomaterials in the aquatic environment, Environ. Sci. Technol. 47 (2013) 6288–6296, https://doi.org/10.1021/es400483k.

[14] S. Pei, H.-M. Cheng, The reduction of graphene oxide, Carbon N. Y. 50 (2012) 3210–3228, https://doi.org/10.1016/j.carbon.2011.11.010.

[15] H.A. Becerril, J. Mao, Z. Liu, R.M. Stoltenberg, Z. Bao, Y. Chen, Evaluation of solution-processed reduced graphene oxide films as transparent conductors, ACS Nano. 2 (2008) 463–470, https://doi.org/10.1021/nn700375n.

[16] H.C. Schniepp, J.-L. Li, M.J. McAllister, H. Sai, M. Herrera-Alonso, D.H. Adamson, R.K. Prud'homme, R. Car, D.A. Saville, I.A. Aksay, Functionalized single graphene sheets derived from splitting graphite oxide, J. Phys. Chem. B. 110 (2006) 8535–8539, https://doi.org/10.1021/jp060936f.

[17] C. Mattevi, G. Eda, S. Agnoli, S. Miller, K.A. Mkhoyan, O. Celik, D. Mastrogiovanni, G. Granozzi, E. Carfunkel, M. Chhowalla, Evolution of electrical, chemical, and structural properties of transparent and conducting chemically derived graphene thin films, Adv. Funct. Mater. 19 (2009) 2577–2583, https://doi.org/10.1002/ADFM.200900166.

[18] D. Yang, A. Velamakanni, G. Bozoklu, S. Park, M. Stoller, R.D. Piner, S. Stankovich, I. Jung, D.A. Field, C.A. Ventrice, R.S. Ruoff, Chemical analysis of graphene oxide films after heat and chemical treatments by X-ray photoelectron and Micro-Raman spectroscopy, Carbon N. Y. 47 (2009) 145–152, https://doi.org/10.1016/J.CARBON.2008.09.045.

[19] D. Li, M.B. Müller, S. Gilje, R.B. Kaner, G.G. Wallace, Processable aqueous dispersions of graphene nanosheets, Nat. Nanotechnol. 3 (2008) 101–105, https://doi.org/10.1038/nnano.2007.451.

[20] M.J. Fernández-Merino, L. Guardia, J.I. Paredes, S. Villar-Rodil, P. Solís-Fernández, A. Martínez-Alonso, J.M.D. Tascón, Vitamin C is an ideal substitute for hydrazine in the reduction of graphene oxide suspensions, J. Phys. Chem. C. 114 (2010) 6426–6432, https://doi.org/10.1021/jp100603h.

[21] S. Stankovich, R.D. Piner, X. Chen, N. Wu, S.T. Nguyen, R.S. Ruoff, Stable aqueous dispersions of graphitic nanoplatelets via the reduction of exfoliated graphite oxide in the presence of poly(sodium 4-styrenesulfonate), J. Mater. Chem. 16 (2006) 155–158, https://doi.org/10.1039/B512799H.

[22] J.T. Robinson, M. Zalalutdinov, J.W. Baldwin, E.S. Snow, Z. Wei, P. Sheehan, B. H. Houston, Wafer-scale reduced graphene oxide films for nanomechanical devices, Nano Lett. 8 (2008) 3441–3445, https://doi.org/10.1021/nl8023092.

[23] S.H.B. Vinoth Kumar, R. Muydinov, B. Szyszka, Plasma assisted reduction of graphene oxide films, Nanomaterials 11 (2021) 382, https://doi.org/10.3390/nano11020382.

[24] A. Dey, A. Chroneos, N.S.J. Braithwaite, R.P. Gandhiraman, S. Krishnamurthy, Plasma engineering of graphene, Appl. Phys. Rev. 3 (2016) 021301, https://doi.org/10.1063/1.4947188.

[25] H. Zhu, D. Ji, L. Jiang, H. Dong, W. Hu, Tuning electrical properties of graphite oxide by plasma, Philos. Trans. R. Soc. A Math. Phys. Eng. Sci. 371 (2013) 20120308, https://doi.org/10.1098/rsta.2012.0308.

[26] I. Levchenko, K.K. Ostrikov, J. Zheng, X. Li, M. Keidar, K.B.K. Teo, Scalable graphene production: perspectives and challenges of plasma applications, Nanoscale 8 (2016) 10511–10527, https://doi.org/10.1039/C5NR06537B.

[27] V.K. Abdelkader-Fernández, M. Melguizo, M. Domingo-García, F.J. López-Garzón, M. Pérez-Mendoza, Hydrogen cold plasma for the effective reduction of graphene oxide, Appl. Surf. Sci. 464 (2019) 673–681, https://doi.org/10.1016/j.apsusc.2018.09.121.

[28] F. Alotaibi, T.T. Tung, M.J. Nine, S. Kabiri, M. Moussa, D.N.H. Tran, D. Losic, Scanning atmospheric plasma for ultrafast reduction of graphene oxide and fabrication of highly conductive graphene films and patterns, Carbon N. Y. 127 (2018) 113–121, https://doi.org/10.1016/j.carbon.2017.10.075.

[29] H. Wu, X. Bu, M. Deng, G. Chen, G. Zhang, X. Li, X. Wang, W. Liu, A gas sensing channel composited with pristine and oxygen plasma-treated graphene, Sensors (Switzerland) 19 (2019), https://doi.org/10.3390/s19030625.

[30] Global ammonia annual production capacity | Statista, (n.d.). https://www.statista.com/statistics/1065865/ammonia-production-capacity-globally/ (accessed June 22, 2023).

[31] Y.K. Ip, S.F. Chew, D.J. Randall, Ammonia toxicity, tolerance, and excretion, Fish physiology 20 (2001) 109–148, https://doi.org/10.1016/S1546-5098(01)20005-3.

[32] D. Huang, X. Li, S. Wang, G. He, W. Jiang, J. Hu, Y. Wang, N. Hu, Y. Zhang, Z. Yang, Three-dimensional chemically reduced graphene oxide templated by silica spheres for ammonia sensing, Sens. Actuators B Chem. 252 (2017) 956–964, https://doi.org/10.1016/j.snb.2017.05.117.

[33] R. Ghosh, A. Midya, S. Santra, S.K. Ray, P.K. Guha, Chemically reduced graphene oxide for ammonia detection at room temperature, ACS Appl. Mater. Interfaces 5 (2013) 7599–7603, https://doi.org/10.1021/am4019109.

[34] Q.T. Tran, H.T.M. Hoa, D.-H. Yoo, T.V. Cuong, S.H. Hur, J.S. Chung, E.J. Kim, P. A. Kohl, Reduced graphene oxide as an over-coating layer on silver nanostructures for detecting NH3 gas at room temperature, Sens. Actuators B Chem. 194 (2014) 45–50, https://doi.org/10.1016/j.snb.2013.12.062.

[35] W. Li, X. Li, L. Cai, Y. Sun, M. Sun, D. Xie, Reduced graphene oxide for room temperature ammonia (NH_3) gas sensor, J. Nanosci. Nanotechnol. 18 (2018) 7927–7932, https://doi.org/10.1166/jnn.2018.15563.

[36] N. Hu, Z. Yang, Y. Wang, L. Zhang, Y. Wang, X. Huang, H. Wei, L. Wei, Y. Zhang, Ultrafast and sensitive room temperature NH_3 gas sensors based on chemically reduced graphene oxide, Nanotechnology. 25 (2014) 025502, https://doi.org/10.1088/0957-4484/25/2/025502.

[37] I. Jung, D. Dikin, S. Park, W. Cai, S.L. Mielke, R.S. Ruoff, Effect of water vapor on electrical properties of individual reduced graphene oxide sheets, J. Phys. Chem. C. 112 (2008) 20264–20268, https://doi.org/10.1021/jp807525d.

[38] J. Li, C. Chen, J. Wei, J. Li, X. Wang, Enhanced electrochemical performance of reduced graphene oxides by H_2/Ar plasma treatment, J. Phys. Chem. C. 118 (2014) 28440–28447, https://doi.org/10.1021/jp509182g.

[39] Y. Zhang, D. Zhang, L. Zhang, B. Yang, Z. Gan, The etching mechanisms of diamond, graphite, and amorphous carbon by hydrogen plasma: A reactive molecular dynamics study, Adv. Theory Simulations. (2023), https://doi.org/10.1002/adts.202300371.

[40] Z. Zhai, H. Shen, J. Chen, X. Li, Y. Jiang, Evolution of structural and electrical properties of carbon films from amorphous carbon to nanocrystalline graphene on quartz glass by HFCVD, ACS Appl. Mater. Interfaces 10 (2018) 17427–17436, https://doi.org/10.1021/acsami.8b01588.

[41] R. Al-Gaashani, A. Najjar, Y. Zakaria, S. Mansour, M.A. Atieh, XPS and structural studies of high quality graphene oxide and reduced graphene oxide prepared by different chemical oxidation methods, Ceram. Int. 45 (2019) 14439–14448, https://doi.org/10.1016/j.ceramint.2019.04.165.

[42] B. Yu, X. Wang, X. Qian, W. Xing, H. Yang, L. Ma, Y. Lin, S. Jiang, L. Song, Y. Hu, S. Lo, Functionalised graphene oxide/phosphoramide oligomer hybrids flame retardant prepared via in situ polymerisation for improving the fire safety of polypropylene, RSC Adv. 4 (2014) 31782, https://doi.org/10.1039/C3RA45945D.

[43] B. Ma, R.D. Rodriguez, A. Ruban, S. Pavlov, E. Sheremet, The correlation between electrical conductivity and second-order Raman modes of laser-reduced graphene oxide, Phys. Chem. Chem. Phys. 21 (2019) 10125–10134, https://doi.org/10.1039/C9CP00093C.

[44] A. Kaniyoor, S. Ramaprabhu, A Raman spectroscopic investigation of graphite oxide derived graphene, AIP Adv. 2 (2012), https://doi.org/10.1063/1.4756995.

[45] S. Claramunt, A. Varea, D. López-Díaz, M.M. Velázquez, A. Cornet, A. Cirera, The importance of interbands on the interpretation of the Raman spectrum of graphene oxide, J. Phys. Chem. C. 119 (2015) 10123–10129, https://doi.org/10.1021/acs.jpcc.5b01590.

[46] S. Muhammad Hafiz, R. Ritikos, T.J. Whitcher, N.M. Razib, D.C.S. Bien, N. Chanlek, H. Nakajima, T. Saisopa, P. Songsiriritthigul, N.M. Huang, S. A. Rahman, A practical carbon dioxide gas sensor using room-temperature hydrogen plasma reduced graphene oxide, Sensors Actuators B Chem. 193 (2014) 692–700, https://doi.org/10.1016/j.snb.2013.12.017.

[47] C. Zhang, D.M. Dabbs, L.-M. Liu, I.A. Aksay, R. Car, A. Selloni, Combined effects of functional groups, lattice defects, and edges in the infrared spectra of graphene oxide, J. Phys. Chem. C. 119 (2015) 18167–18176, https://doi.org/10.1021/acs.jpcc.5b02727.

[48] S. Tang, Z. Cao, Adsorption and dissociation of ammonia on graphene oxides: A first-principles study, J. Phys. Chem. C. 116 (2012) 8778–8791, https://doi.org/10.1021/jp212218w.

[49] I. Sengupta, S. Chakraborty, M. Talukdar, S.K. Pal, S. Chakraborty, Thermal reduction of graphene oxide: How temperature influences purity, J. Mater. Res. 33 (2018) 4113–4122, https://doi.org/10.1557/jmr.2018.338.

[50] S. Verma, R.K. Dutta, A facile method of synthesising ammonia modified graphene oxide for efficient removal of uranyl ions from aqueous medium, RSC Adv. 5 (2015) 77192–77203, https://doi.org/10.1039/C5RA10555B.
[51] E.C. Mattson, K. Pande, M. Unger, S. Cui, G. Lu, M. Gajdardziska-Josifovska, M. Weinert, J. Chen, C.J. Hirschmugl, Exploring adsorption and reactivity of NH_3 on reduced graphene oxide, J. Phys. Chem. C. 117 (2013) 10698–10707, https://doi.org/10.1021/jp3122853.
[52] X.L. Huang, N.T. Hu, Y.Y. Wang, Y.F. Zhang, Ammonia gas sensor based on aniline reduced graphene oxide, Adv. Mater. Res. 669 (2013) 79–84, https://doi.org/10.4028/www.scientific.net/AMR.669.79.
[53] R. Ghosh, A.K. Nayak, S. Santra, D. Pradhan, P.K. Guha, Enhanced ammonia sensing at room temperature with reduced graphene oxide/tin oxide hybrid films, RSC Adv. 5 (2015) 50165–50173, https://doi.org/10.1039/C5RA06696D.
[54] Y. Wang, L. Zhang, N. Hu, Y. Wang, Y. Zhang, Z. Zhou, Y. Liu, S. Shen, C. Peng, Ammonia gas sensors based on chemically reduced graphene oxide sheets self-assembled on Au electrodes, Nanoscale Res. Lett. 9 (2014) 251, https://doi.org/10.1186/1556-276X-9-251.
[55] D.C. Tiwari, P. Atri, R. Sharma, Sensitive detection of ammonia by reduced graphene oxide/polypyrrole nanocomposites, Synth. Met. 203 (2015) 228–234, https://doi.org/10.1016/j.synthmet.2015.02.026.

3.3 Organophosphates Detection

The detection of OP pesticides, such as dimethoate and chlorpyrifos, is crucial for ensuring food safety and environmental monitoring. Conventional analytical techniques, including GC-MS and HPLC-MS, provide high accuracy but are hindered by high costs, the requirement for specialized personnel, and limited portability, so their sampling capability is only a portion of the food that is produced. To overcome these limitations, fluorescence-based sensors have emerged as a promising alternative, offering simplicity, cost-effectiveness, and high sensitivity for trace-level detection of analytes. In this paragraph, two different methodologies for dimethoate and chlorpyrifos detection are presented.

3.3.1 Dimethoate detection through a fluorescent coumarin dye

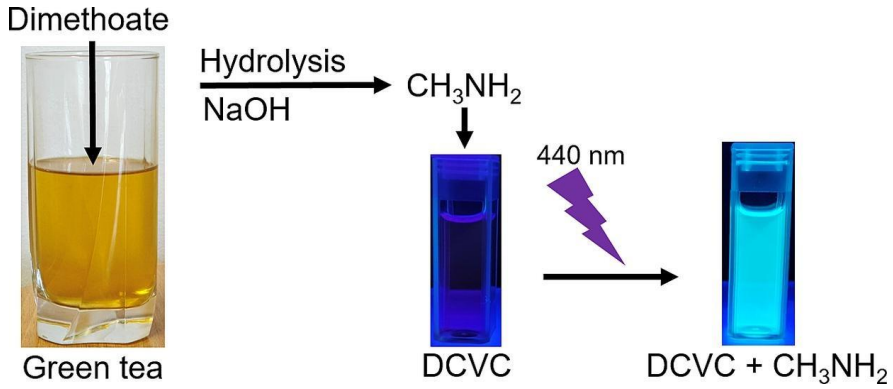

Figure 18: Graphical abstract of publication 2.

In this study, we developed a novel fluorescence-based probe using a coumarin dye for the selective detection of methylamine. Since OP pesticides break down in the environment and produce detectable byproducts, we focused on methylamine as a key hydrolysis product of dimethoate. Our approach relied on a reaction between methylamine and a custom-synthesized electrophilic coumarin dye, which generated a strong fluorescence signal.

By systematically studying the fluorescence response at different analyte concentrations, we determined a detection limit of 3.2 µg/L, well below internationally regulated limits. The reaction mechanism was based on TICT discussed in the introduction, where the nucleophilic addition of methylamine to the dicyanovinyl group significantly altered the dye's fluorescence properties. Selectivity studies further demonstrated the robustness of our method, showing no interference from other OPs, ensuring reliable pesticide detection even in complex matrices. To confirm its practical applicability, we tested dimethoate in green tea samples, achieving a recovery rate of 95.4%, which validated the method's effectiveness in real-world scenarios.

This study not only addresses gaps in current research by introducing a new fluorescence-based approach for dimethoate detection but also highlights the significance of monitoring pesticide hydrolysis products, as they can pose comparable risks to the parent compounds. Through this work, we confirmed hypotheses two and three, demonstrating the importance of studying pesticide degradation pathways.

In this article I contributed in: Writing - original draft, Visualization, Validation, Formal analysis, Data curation, Conceptualization.

Microchemical Journal 207 (2024) 112205

Contents lists available at ScienceDirect

Microchemical Journal

journal homepage: www.elsevier.com/locate/microc

Dimethoate detection through a fluorescent coumarin dye

Edoardo Donà [a,b,*], Gerhard J. Mohr [c], Aleksandra Lobnik [a,d]

[a] Institute for Environmental Protection and Sensors, Beloruska 7, Maribor SI-2000, Slovenia
[b] Jožef Stefan International Postgraduate School, Jamova cesta 39, Ljubljana SI-1000, Slovenia
[c] Joanneum Research Forschungsgesellschaft mbH—Materials, Franz-Pichler-Straße 30, A-8160 Weiz, Austria
[d] Faculty of Mechanical Engineering, University of Maribor, Smetanova 17, SI-2000 Maribor, Slovenia

ARTICLE INFO

Keywords:
Organophosphate pesticide
Methylamine
Coumarin
Fluorescence detection
Dimethoate
TICT

ABSTRACT

In this study, we present a straightforward and innovative approach utilizing a coumarin fluorescent dye for the detection of dimethoate in green tea. Initially, the pesticide undergoes hydrolysis in a NaOH solution, yielding our target analyte, methylamine. Following neutralization to pH 9, methylamine reacts with the dye in CH_3CN for 20 min. After a careful optimization, we achieved an outstanding linear correlation (R^2 = 0.999) for dimethoate, spanning concentrations from 7.8 to 292 μg/L and LOD of 3.2 μg/L. Moreover, we successfully detected dimethoate in green tea, with a recovery of 95.4% (σ = 5.7%). Organophosphates pesticides (OPs), which dimethoate is one of the most used, pose a significant threat due to their toxicity upon both high direct exposure and prolonged low-level exposure, which has been linked to cancer. Therefore, the development of a detection method that is both selective and sensitive is imperative for safeguarding both the population and the environment. This method effectively addresses the stability challenges encountered by enzyme-based fluorescent sensors, thereby opening new avenues for the detection of organophosphate pesticides.

1. Introduction

Pesticides are a category of chemical or biological compounds designed to destroy, prevent, and mitigate harmful organisms or their damage in the production, processing, storage, transport and marketing of crops, food and timber. Due to their pervasive use in agriculture, they have now contaminated the entire food chain through infiltration into groundwater, runoff to rivers, and their accumulation on the surface of plants, fruits and vegetables [1,2]. As the global population continues to grow, the environmental repercussions are expected to intensify. Organophosphates (OPs) pesticides appeared in the market in the early 70's, to replace organochlorine analogue (such as DDT), which had the problem of being persistent in the environment. Although OPs degrade by hydrolysis, making them more eco-friendly, they have a high acute toxicity. Nowadays OPs account for about 40 % of the worldwide use [3] of pesticides, and although less lethal than their gaseous counterparts, share the same mechanism of action, namely the inhibition of the acetylcholinesterase enzyme. Moreover, in 2007 they were responsible for more than 300 000 deaths [4] a year from acute exposure and are associated with cancer, and non-Hodgkin lymphoma [5–7]. Dimethoate in particular is well known to be used in crops such as fruit, vegetables, grain and ornamentals to control a wide variety of pests. Due to its high solubility (39 g/L) [8] it is easily found in groundwater and rivers and it is classified as possible human carcinogen by the US EPA. In the soil undergo degradation from 4-16 days [9], leading to toxic products [10]. Nowadays the gold-standard methodologies used to detect pesticides, HPLC and GC/MS, are very expensive instrumentation, require qualified personnel and are not portable. Therefore, it is clear that portable sensors, capable of providing results in a very short time, easy to use and cheap are the direction in which research is heading.

The main issue with pesticides sensors, is the limit of detection (LOD) that has to be reached. In EU dimethoate it is now banned [11], but in all other countries from which EU imported 172 billion of food in 2022 it is not [12]. The previous limit was 0.01 mg/kg that was challenging even for the aforementioned standard methodologies, which encounter serious issues with complex matrix or compound with similar molar weight. To overcome all these issues, academic research is very active in the field of optical sensors. Different types of spectroscopies are available, exploiting different principles to detect the pesticides, like surface enhance Raman scattering (SERS), surface plasmon resonance (SPR) and fluorescence. The latter has the advantage to be simple and cheap, allowing the detection of nM and even pM concentration of pesticides. In

* Corresponding author at: Institute for Environmental Protection and Sensors, Beloruska 7, Maribor SI-2000, Slovenia.
E-mail address: Edoardo.dona@ios.si (E. Donà).

https://doi.org/10.1016/j.microc.2024.112205
Received 23 April 2024; Received in revised form 24 October 2024; Accepted 14 November 2024
Available online 16 November 2024

literature, for the detection of dimethoate, fluorescence is always used in combination with other techniques: molecular imprinted polymers [13,14], quantum dots (QD) [15–17], Ag/Au nanoparticles [18,19], enzymes [20,21]. But all these methods present several drawbacks: they are expensive and/or dangerous materials, short stability and lack of selectivity. Instead, one simple approach is to hydrolyze the pesticide and utilize the product generated for a reaction with a fluorescent dye [22]. This method it is easy to use, do not require expensive or harmful materials, it is stable during time and the selectivity it is ensured by a chemical reaction. A comparison of all these methods is presented in Table 1.

In this study, we hypothesized and realized a method for determining dimethoate in green tea by monitoring changes in the fluorescence spectra of a coumarin-based dye functionalized with a dicyanovinyl group (DCVC, as shown in Fig. 1) synthesized by our team (according to [23]). This kind of scaffold presented already very good LOD and reversibility in literature towards thiols [24–27], and the dicyanovinyl group also towards amines [28–31]. After the hydrolysis and the neutralization, the dimethoate solution is added to DCVC in CH_3CN, where a fast and strong emission was captured by the fluorimeter. We tested dimethoate in solution at concentrations ranging from 7.8 to 292 μg/L with an LOD of 3.2 μg/L. We also measured a recovery of 95.4 % (σ = 5.7 %) in green tea. To the best of our knowledge, this is the first time that a coumarin dye detects dimethoate.

2. Materials and methods

2.1. Reagents

Hydrochloric acid, sodium hydroxide, acetonitrile, methylamine, thioglycolic acid, methanol, malonitrile, ethanol, piperidine, citric acid, sodium bicarbonate, lactic acid, tris buffer, acephate, malathion, demeton-S-methyl sulfone (demeton), dimethoate were purchased from Sigma-Aldrich. Acetic acid and glacial acetic acid were purchased from Merck, sodium hypochlorite, potassium dihydrogen phosphate from Gram-mol. 7-Diethylamino-3-formylcoumarin was kindly provided by Dyomics GmbH, Jena, Germany. All the reagents were used without any further purification. The reagents were all analytical grade unless otherwise stated.

2.2. Synthesis of DCVC

To synthesize 7-(diethylamino) coumarin-3-dicyanovinyl (DCVC) we followed the synthesis reported in literature [23] using 7-Diethylamino-3-formylcoumarin and malonitrile (for details see ESM and Fig. S3 and S4).

Table 1
State of the art of fluorescence sensors for detection of dimethoate.

Substrate	LOD (μg/L)	Reaction time (min)	Linear range (μg/L)	Reference
Co/N Graphene QD	64	20	10–800	[53]
CdSe QD	30	10	103–1835	[54]
CD with dithizone	15	15	34–1145	[15]
TPE dye with AChE	8	15	9–22500	[20]
ZnO QD MIP	6	7	20–3200	[55]
CdTe QD with dithizone	5	20	10–5000	[56]
Rhodamine B/ AuNPs	4	10	5–1000	[19]
MIP CdSe/ZnS QD	2.1	30	5–150	[57]
CuNPs in agarose hydrogel	1	10	5–1000	[21]
Coumarin dye	3.2	20	7.9–292	**This work**

2.3. Sensing measurements

The fluorescence (FL) intensity was measured at λ_{exc} = 440 nm (λ_{em} ≈ 475 nm), wavelength used in all the measurements here reported. We used a fluorescence spectrometer (PerkinElmer FL 8500) equipped with a Xenon Arc (150 W) lamp. The process can be divided in five main steps:

1. Hydrolysis of the pesticide in NaOH solution 1.8 M for 30 min at 50 °C;
2. Dilution of the hydrolysed solution 1/10 with Milli-Q water, to prevent the formation of a huge amount of NaCl (that disturbs the fluorescence measurement), since neutralization to pH 9 is required;
3. Neutralization with HCl to pH 9, to prevent the degradation of the dye at high pH;
4. Addition of 10 μL of the pH 9 solution with hydrolysed dimethoate to 2.5 mL of DCVC 20 μM in CH_3CN.
5. Measurement of the fluorescence after 20 min λ_{exc} = 440 nm (λ_{em} ≈ 475 nm).

2.4. Statistical analysis

2.4.1. Design of experiment methodology

The design of experiment methodology (DoE) is a well-known statistical technique used to optimize the number of experimental trials, to understand which the key factors are and to evaluate any significant cross interaction between them [32]. In the present work we used a full-factorial design for a total of 2^4 = 16 experiments (data in Table 1 ESM). We tested four different key parameters at two level each: temperature (T), time of hydrolysis, sodium hydroxide molarity and pH. The levels were:

- T: 22 and 50 °C
- Time: 20 and 45 min
- NaOH: 0.9 and 1.8 M
- pH: 9 and 10.

For the data analysis and visualization of the response surfaces we used R software.

2.4.2. Calibration curve

For the calculation of the calibration curve, we utilized the average of the data collected at each concentration. The LOD was calculated with the following formula present in ICH Q2(R2), that gives the LOD value with almost 99 % level of confidence:

$$LOD = \frac{3.3\sigma}{S}$$

where S is the slope of the calibration curve and σ is the standard deviation of the response without the analyte.

3. Results

3.1. Methylamine reaction

Following the literature on the hydrolysis of dimethoate depicted in Fig. 1, we were trying to understand which of the compounds reported was reacting. Methanol was not taken into account since was used as a possible solvent and the dye was stable in it (Fig. S2 in ESM). As we stated in the introduction, it is known that dicyanovinil group are reactive towards nucleophile [24], so we were focusing our attention on those hydrolysis products that were showing potential nucleophilicity. Methylamine and thioglycholic acid present this feature, so we focused our attention on those two compounds. We tested both of them (at pH 9) and we found out that both were reacting with the dye as shown in

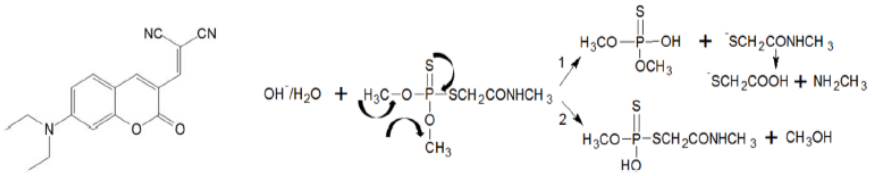

Fig. 1. On the left we can see the structure of DCVC. On the right two of the possible hydrolysis pathways of dimethoate (L. Wu et al., 2014).

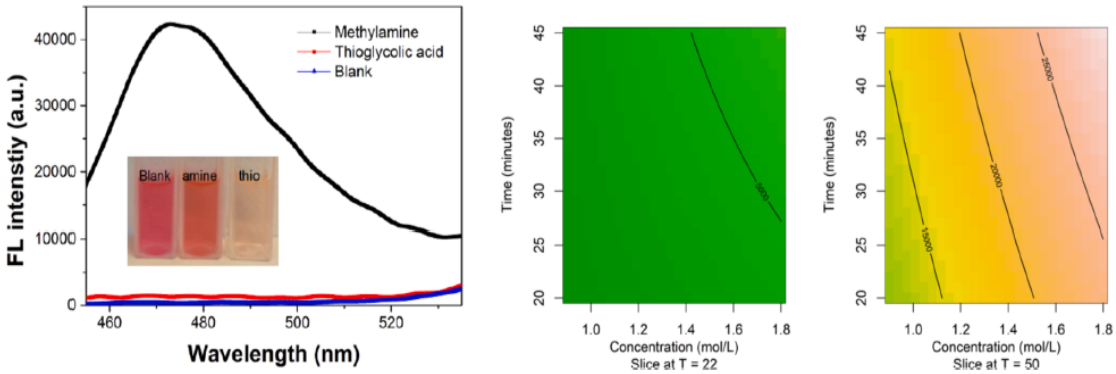

Fig. 2. On the left fluorescence intensity comparison (λ_{exc} = 440 nm) between methylamine and thioglycolic acid. On the right the response surfaces of fluorescence. Hydrolysis time (y) vs NaOH molarity (x), sliced at T = 22 °C and T = 50 °C.

Fig. 2. But the differences were significant, since methylamine shows a very high fluorescence peak and an orange colour, instead thioglycholic was not producing any fluorescence change and the color was pale orange. The changes observed with methylamine were identical to what we have seen with hydrolyzed dimethoate as shown in Fig. 3. So we were able to distinguish between the two compounds, ensuring the selectivitiy of the probe.

3.2. Response surfaces

Since detecting pesticides nM concentrations is a challenging task, optimization of the system is always a crucial step in the discovery of a new pesticide sensor. In order to maximize the fluorescence response of our dye, we studied, with DoE methodology, the hydrolysis condition of dimethoate and the pH of the final solution. In our case, this was even more important, since in literature are reported more than two pathways for the hydrolysis in basic media, with, as a consequence, multiple products [33–36]. We were actually looking in which conditions we had the maximum yield of methylamine and not only the fastest conditions to hydrolyse dimethoate. Since it is a hydrolysis and we are limited kinetically by the dimethoate solubility, to optimize it we can play with three factors: time, temperature and molar concentration of OH^-. In Fig. 2 we can see clearly that temperature is playing a pivotal role in maximizing the response, followed by the molarity of NaOH and by the time of hydrolysis. Since in general the nucleophilicity of a species (in our case methylamine) is higher when the charge is negative, it was clear that the pH was playing a fundamental role on our reaction. That is why after an initial screening in a separate experiment with pH from 6 to 9, where 9 was giving the highest response, we decided to compare in the DoE also pH 9 and 10, to see if there were any further improvement. From the outcome of the analysis, we come to the conclusion that pH did not further influence the fluorescence response. Another important consequence of the DoE was to find out that time was not playing the crucial role we were thinking at the beginning (an improvement of at least 30 %), the effect indeed is around 20 % (at 50 °C). Since time is always a key factor when monitoring pesticide, we tried to find a

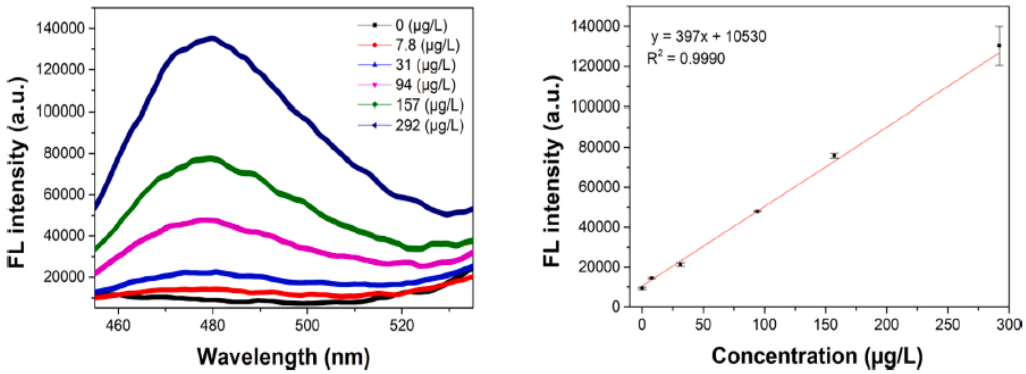

Fig. 3. Fluorescence spectra of DCVC with dimethoate at different concentration. On the right the calibration curve.

balance between sensitivity and hydrolysis time. Since we achieved a satisfactory LOD of 3.2 μg/L (below existing dimethoate limit worldwide) with a hydrolysis time of 30 min, we decided to use this hydrolysis time for our further investigation. For the same reason, we did not proceed with any further optimization [37].

3.3. Calibration curve

With the fundamental information extracted by the DoE analysis, we proceeded with the experiment for the calibration curve with the best hydrolysis condition. However, since the time was giving minor contribution and to accelerate the process, we decided to hydrolyse dimethoate for 30 min at 50 °C and NaOH 1.8 M. With these conditions we obtained the graph in Fig. 3 from which we obtained the calibration curve, with three measurements for each point (n = 3). As we can see in Fig. 3 the R^2 is 0.999, with a calculated LOD of 3.2 μg/L. As a comparison, in the countries we import from, such as Brazil, Australia, USA, Japan and India, the MRL is greater than or equal to the old EU limit of 10 μg/L, and often depends on the food.

4. Discussion

4.1. Sensing mechanism

In literature, aminocoumarins are known to have strong fluorescence emission. For instance, 7-Diethylamino-4-methylcoumarin (C1) has a Φ_{fl} = 0.63 in ethyl acetate (EtOAc) [38] that derives from the polar character of the low-lying excited states. But when to C1 is connected a dicyanovinyl group, this fluorescence is quenched (DCVC has a Φ_{fl} = 0.006 in EtOAc) [39]. The observed changes in the dye's photophysical properties can be rationalized in terms of the existing knowledge of the TICT (twisted intramolecular charge transfer) mechanism in 7-aminocoumarins (Fig. S1) [40–43] observed in the present case.

When we add methylamine coming from the hydrolysis of dimethoate in DCVC solution's it interacts with the electrophile C = C bound. The consequence is the disconnection of the π-cloud from the cyano group, so the TICT is less effective. Another consequence is the rise of the emission of the locally excited state (LE), that was previously absent (the peak in Fig. 3). The Φ_{fl} of the LE is also higher compared to the TICT state because the latter has a significant non-radiative component, (causing the low Φ_{fl} [44]), instead in the LE the non-radiative component is lower. At $\lambda_{em} \approx 475$ nm we can observe the above cited LE (λ_{exc} = 440 nm), that requires more energy to be excited compared to the TICT, since it is less stabilized (see Fig. S2 in ESM [45]). Another effect of the reaction is the colour change from red to orange (as we can see in Fig. 4), where the degree of colour change depends on the concentration of dimethoate and by the time given to the reaction to proceed (further discussed in section 4.2). The final colour is yellow, which is reached in few minutes with very high pesticide concentration (around 10^{-2} M). The understanding of the mechanism, namely that good nucleophiles are needed in order to react with our dye, give us another hint about the selectivity of our probe. Further discussion will be in section 4.3.

4.2. Kinetic

We conducted a kinetic experiment to better understand the behaviour of the reaction at λ_{exc} = 440 nm ($\lambda_{em} \approx 475$ nm). For the calibration curve we stopped the reaction after 20 min. This is the time required to almost complete the reaction for the lower concentration tested (7.8 μg/L).

At higher concentration (376 μg/L), as shown Fig. 4 the reaction continues during time, and even after 3 h the fluorescence is still increasing. The blank indeed, it is stable for at least 3 h. So, the decision to stop at 20 min is due to the compromise between time and sensitivity. Moreover, similar dyes with more rapid kinetics, can be promising for a fast recognition of dimethoate.

4.3. Interferences

To understand the potential real application of the system, we tested different interferences (3 repetition each), based on what is usually used to clean fruits and vegetables, or already present on the surface. All the tested interferences were measured at pH 9, at λ_{exc} = 440 nm ($\lambda_{em} \approx 475$ nm), with different concentrations based on the usual application of the chemical in the food industry [46–49]. The results are shown in Fig. 4, where we can see that, except Na_2SO_3 that we will discuss later, only NaClO might seriously interfere with the system. NaClO is frequently used as a food sanitizer in industry in concentration between 20–200 mg/L [47] but a rinsing process is always necessary. In a recent study [50] it was determined that lettuce has an intake of 10 % of the rinsing water, but after rinsing 1 min with tap water, the content went below the quantification limit (less than 0.5 mg/L). Regarding the use in potable water in Europe the limit in most country is below 0.1 mg/L. So overall we can say that NaClO will not be a particular issue to the applicability of the method, since at 1 mg/L was giving a fluorescence increase of 16 % compared to 100 % of dimethoate 7.8 μg/L. We were also interested if the interference was due to Na^+ or ClO^-. To clarify this aspect, it's useful to remember that NaCl is always present in all the solutions, since it's produced during the neutralization process explained in paragraph 2.3. To exclude NaCl as a possible interference we measured the fluorescence in comparison with Milli-Q water. Interestingly, no noticeable changes in fluorescence were observed. Consequently, NaCl 0.18 M was also excluded as a possible interference and used as a blank as shown in Figs. 2–4.

Finally, to understand if other OPs hydrolysed could interfere with our system, we tried to find OPs as much as similar to dimethoate as

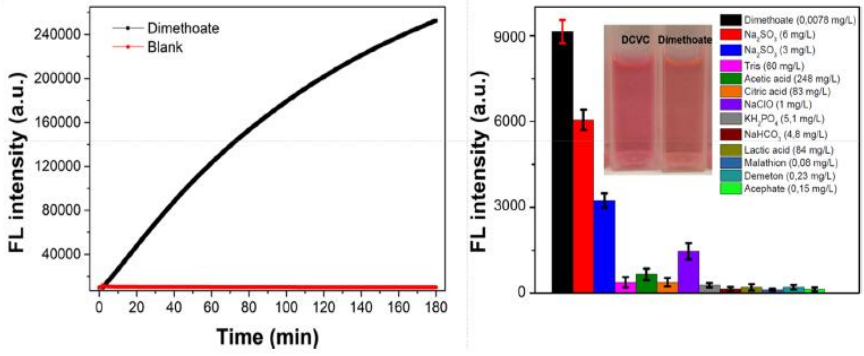

Fig. 4. Kinetic of DCVC + hydrolyzed dimethoate. On the right interference test and color change.

possible, and capable of releasing nucleophiles. Malathion, demeton-S-methylsulphon and acephate structurally fit this description. Malathion and demeton can release thiols [22] and acephate can potentially release a thiol and acetamide. They have been tested with the same method used for dimethoate and none of them present any response. We were expecting this result, since when thiols are produced, no fluorescence changes are observed. Moreover, we found the sulphite anion (SO_3^{2-}) as a major interference, as reported in literature [23]. We tested 3 and 6 mg/L, below and above the LOD cited in the article, and in both cases the anion was interfering severely with the system (Fig. 4), at least compared to the lowest concentration of dimethoate that we tested. So, in such cases where the sulphite anion is present, high inaccuracies can be encountered. The extent will depend on the concentration of dimethoate that has to be detected and to the concentration of Na_2SO_3. So particular attention must be taken in cases where this anion is present.

4.4. Green tea test

To comprehensively evaluate the practical viability of the method under real conditions, we tested our probe with dimethoate at 80 μg/L on green tea [51,52], as it is commonly sprayed on the leaves of tea plants. The green tea chosen for experimentation was sourced from the Lord Nelson brand, procured from a local supermarket. Preparation of the green tea adhered to manufacturer instructions, involving a 3-minute infusion period in 200 mL of freshly boiled tap water. After cooling to room temperature, the solution comprising dimethoate at a concentration of 243 mg/L in 10 mL of green tea was prepared, with the addition of NaOH pellets to attain a concentration of 1.8 M. Following these preparations, the experimental procedure reported in section 2.3 was replicated. The final concentration of dimethoate was 80 μg/L. To evaluate the efficacy of our methodology, the standard addition technique was employed utilizing a methylamine solution as a reference standard. Encouragingly, the results indicate a recovery of 95.4 %, with a σ of 5.7 %, which indicates the good accuracy of our system.

To frame our work in the state of the art of fluorescence sensors, in Table 1 we present a comparative analysis regarding various substrates utilized for the fluorescence-based detection of dimethoate. The majority of these substrates feature toxic quantum dots, enzymatic processes prone to instability, costly gold nanoparticles, intricate synthesis procedures, and challenges in both application and long-term stability. In contrast, our proposed methodology offers a stable solution with prolonged shelf-life, facile implementation, and compatibility with current literature standards in terms of performance. Given the aim of sensors scientific research to provide ideas to advance the state of the art and to improve the current technology on the market, the ease of use becomes a pivotal factor in the market acceptance of a product, alongside maintaining performance parity with existing methodologies.

5. Conclusions

In this study, we have integrated a novel coumarin fluorescent dye with a straightforward pre-treatment method for the detection of dimethoate in liquid samples. Through optimization, we successfully achieved dimethoate detection with high sensitivity and high selectivity. We also detected dimethoate in green tea with a recovery of 95.4% (σ = 5.7%). The hydrolysis of dimethoate, facilitate its detection and so we do believe that this methodology can be successfully extended to various other pesticides, not limited to OPs. Therefore, this work is not only a proof-of-concept, but offers a new strategy for detecting pesticides using fluorescent dyes.

CRediT authorship contribution statement

Edoardo Donà: Writing – original draft, Visualization, Validation, Formal analysis, Data curation, Conceptualization. Gerhard J. Mohr: Writing – review & editing, Validation, Supervision. Aleksandra Lobnik: Writing – review & editing, Validation, Supervision, Funding acquisition, Conceptualization.

Declaration of competing interest

The authors declare that they have no known competing financial interests or personal relationships that could have appeared to influence the work reported in this paper.

Acknowledgements

E.D and A.L acknowledge the EU Horizon 2020 research and innovation program under the MSCA-FoodTraNet project (grant agreement no. 956265). A.L acknoweldge the Slovenian Research Agency (Research Programmes P2-0424, P2-0438 "Optisens"). G.J.M was in part supported by the project NanoFlow (project number FO999899045) kindly funded by the Austrian Research Promotion Agency (FFG).

Appendix A. Supplementary data

Supplementary data to this article can be found online at https://doi.org/10.1016/j.microc.2024.112205.

Data availability

Data will be made available on request.

References

[1] M. Schleiffer, B. Speiser, Presence of pesticides in the environment, transition into organic food, and implications for quality assurance along the European organic food chain – A review, Environ. Pollut. 313 (2022) 120116, https://doi.org/10.1016/j.envpol.2022.120116.
[2] A. Wasim, S. Dwaipayan, C. Ashim, Impact of pesticides use in agriculture: their benefits and hazards, Interdiscip. Toxicol. 2 (1) (2009) 1, https://doi.org/10.2478/v10102-009-0001-7.
[3] J. Kaushal, M. Khatri, S.K. Arya, A treatise on Organophosphate pesticide pollution: Current strategies and advancements in their environmental degradation and elimination, Ecotoxicol. Environ. Saf. 207 (2021) 111483, https://doi.org/10.1016/j.ecoenv.2020.111483.
[4] E. L. Robb, M. B. Baker, Organophosphate toxicity, in: *StatPearls [Internet]*, StatPearls Publishing, Treasure Island (FL), 2023. [Online]. Available: http://europepmc.org/books/NBK470430.
[5] M. Bagchi, S. Zafra, D. Bagchi, DNA damage, gene expression, and carcinogenesis by organophosphates and carbamates, in: *Toxicology of Organophosphate & Carbamate Compounds*, R. C. Gupta, Ed., Burlington: Academic Press, 2006, pp. 533–548. doi: https://doi.org/10.1016/B978-012088523-7/50038-7.
[6] L. c. c,, et al., Organophosphate insecticide use and cancer incidence among spouses of pesticide applicators in the Agricultural Health Study, Occup. Environ. Med. 72 (10) (2015) 736–744, https://doi.org/10.1136/oemed-2014-102798.
[7] Y.K. June, L. Jennifer, P.H. Lui, Organophosphate pesticide exposure and breast cancer risk: a rapid review of human, animal, and cell-based studies, Int. J. Environ. Res. Public Health 17 (14) (2020) 5030, https://doi.org/10.3390/ijerph17145030.
[8] V.S. April, P. Ashley, Z. Xuyang, Environmental fate and toxicology of dimethoate, Rev. Environ. Contam. Toxicol. 237 (2016) 53–70, https://doi.org/10.1007/978-3-319-23573-8_3.
[9] M.F. Zaranyika, J. Mlilo, Speciation and persistence of dimethoate in the aquatic environment : characterization in terms of a rate model that takes into account hydrolysis, photolysis, microbial degradation and adsorption of the pesticide by colloidal and sediment particles : research article, S. Afr. J. Chem. 67 (1) (2014) 233–240, https://doi.org/10.10520/EJC164272.
[10] N.D. Forsberg, et al., Organophosphorus pesticide degradation product in vitro metabolic stability and time-course uptake and elimination in rats following oral and intravenous dosing, Xenobiotica 41 (5) (2011) 422–429, https://doi.org/10.3109/00498254.2010.550656.
[11] 'Pesticide residues Europe'. [Online]. Available: https://ec.europa.eu/food/plant/pesticides/eu-pesticides-database/start/screen/mrls/details?lg_code=EN&pest_res_id_list=76&product_id_list=.
[12] Directorate-General for Agriculture and Rural Development, 'Monitoring EU agri-food trade'. Accessed: Jan. 25, 2024. [Online]. Available: https://agriculture.ec.europa.eu/news/good-performance-eu-agri-food-trade-2022-despite-challenges-2023-04-13_en.
[13] V. Behrouz, Specific fluorescence probe for direct recognition of dimethoate using molecularly imprinting polymer on ZnO quantum dots, J. Fluoresc. 27 (2017) 1339–1347, https://doi.org/10.1007/s10895-017-2068-4.

[14] S. Li, et al., Selective determination of dimethoate via fluorescence resonance energy transfer between carbon dots and a dye-doped molecularly imprinted polymer, Sens. Actuators B Chem. 206 (2015) 14–21, https://doi.org/10.1016/j.snb.2014.09.038.

[15] H. Liu, J. Ding, L. Chen, L. Ding, A novel fluorescence assay based on self-doping biomass carbon dots for rapid detection of dimethoate, J. Photochem. Photobiol. A Chem. 400 (2020) 112724, https://doi.org/10.1016/j.jphotochem.2020.112724.

[16] Y. Xinpeng *et al.*, Rapid detection of dimethoate in soybean samples by microfluidic paper chips based on oil-soluble CdSe quantum dots, *Foods*, 10(11) (2021) doi: 10.3390/foods10112810.

[17] S. Zhen, Z. Jianfeng, L. Chenyu, C. Ligang, Fluorescent switching technology based on fluorescence resonance energy transfer for detecting dimethoate pesticides in environmental water, Anal. Methods 8 (48) (2016) 8506–8513, https://doi.org/10.1039/C6AY02803A.

[18] C.-W. Hsu, Z.-Y. Lin, T.-Y. Chan, T.-C. Chiu, C.-C. Hu, Oxidized multiwalled carbon nanotubes decorated with silver nanoparticles for fluorometric detection of dimethoate, Food Chem. 224 (2017) 353–358, https://doi.org/10.1016/j.foodchem.2016.12.095.

[19] S.-H. Hung, J.-Y. Lee, C.-C. Hu, T.-C. Chiu, Gold-nanoparticle-based fluorescent "turn-on" sensor for selective and sensitive detection of dimethoate, Food Chem. 260 (2018) 61–65, https://doi.org/10.1016/j.foodchem.2018.03.149.

[20] Y. Cai, J. Fang, B. Wang, F. Zhang, G. Shao, Y. Liu, A signal-on detection of organophosphorus pesticides by fluorescent probe based on aggregation-induced emission, Sens. Actuators B Chem. 292 (2019) 156–163, https://doi.org/10.1016/j.snb.2019.04.123.

[21] D. Kong, et al., Fluorescent hydrogel test kit coordination with smartphone: Robust performance for on-site dimethoate analysis, Biosens. Bioelectron. 145 (2019) 111706, https://doi.org/10.1016/j.bios.2019.111706.

[22] J. Zhe, et al., 3D-printed, portable, fluorescent-sensing platform for smartphone-capable detection of organophosphorus residue using reaction-based aggregation induced emission luminogens, ACS Sens. 6 (8) (2021) 2845–2850, https://doi.org/10.1021/acssensors.1c01178.

[23] M.-Y. Wu, T. He, K. Li, M.-B. Wu, Z. Huang, X.-Q. Yu, A real-time colorimetric and ratiometric fluorescent probe for sulfite, Analyst 138 (10) (2013) 3018–3025, https://doi.org/10.1039/C3AN00172E.

[24] K. Hyockman, K. Lee, K. Hae-Jo, Coumarin–malonitrile conjugate as a fluorescence turn-on probe for biothiols and its cellular expression, Chem. Commun. 47 (6) (2011) 1773–1775, https://doi.org/10.1039/C0CC04092D.

[25] Y. Long, L. Heyang, S. Lu, L. Liangliang, C. Zhang, X. Zhen, A highly sensitive fluorescence probe for fast thiol-quantification assay of glutathione reductase, Angew. Chem. Int. Ed. 48 (22) (2009) 4034–4037, https://doi.org/10.1002/anie.200805693.

[26] L. Weiying, Y. Lin, C. Zengmei, F. Yanming, L. Lingliang, A sensitive and selective fluorescent thiol probe in water based on the conjugate 1, 4-addition of thiols to α, β-unsaturated ketones, Chem. Eur. J. 15 (20) (2009) 5096–5103, https://doi.org/10.1002/chem.200802751.

[27] C.A. Young, C. Kihang, A coumarin-based fluorescence sensor for the reversible detection of thiols, Chem. Lett. 41 (12) (2012) 1611–1612, https://doi.org/10.1246/cl.2012.1611.

[28] L. Bu, et al., Sensitive 1,1-dicyanovinyl push-pull dye for primary amine sensing in solution by fluorescence, Dyes Pigm. 202 (2022) 110258, https://doi.org/10.1016/j.dyepig.2022.110258.

[29] T. Mastnak, A. Lobnik, G. J. Mohr, M. Finšgar, Indicator layers based on ethylene-vinyl acetate copolymer (EVA) and dicyanovinyl azobenzene dyes for fast and selective evaluation of vaporous biogenic amines, *Sensors*, 18(12) (2018), doi: 10.3390/s18124361.

[30] H. Ye, et al., Real-time fluorescence screening platform for meat freshness, Anal. Chem. 94 (44) (2022) 15423–15432, https://doi.org/10.1021/acs.analchem.2c03326.

[31] L. Zeng, X. Xiao, H. Ye, D. Ma, J. Zhou, Fast visual monitoring of the freshness of beef using a smart fluorescent sensor, Food Chem. 394 (2022) 133489, https://doi.org/10.1016/j.foodchem.2022.133489.

[32] L. Condra, Reliability Improvement with Design of Experiment, CRC Press (2018), https://doi.org/10.1201/9781482270846.

[33] L. Wu, J. Yao, P. Trebse, N. Zhang, H.H. Richnow, Compound specific isotope analysis of organophosphorus pesticides, Chemosphere 111 (2014) 458–463, https://doi.org/10.1016/j.chemosphere.2014.04.037.

[34] R. Farooq, F. Lin, Y. Wang, J. Huang, Z. Xu, S.F. Shaukat, Pressure hydrolysis for degradation of omethoate pesticide in water, J Shanghai Univ. (Engl. Ed.) 8 (2004) 221–226, https://doi.org/10.1007/s11741-004-0044-0.

[35] J.-J. Yao, M.R. Hoffmann, N.-Y. Gao, Z. Zhang, L. Li, Sonolytic degradation of dimethoate: Kinetics, mechanisms and toxic intermediates controlling, Water Res. 45 (18) (2011) 5886–5894, https://doi.org/10.1016/j.watres.2011.08.042.

[36] P. Giang, M. Schechter, Insecticide residues, colorimetric method for the estimation of dimethoate residues, J. Agric. Food Chem. 11 (1) (1963) 63–66, https://doi.org/10.1021/jf60125a019.

[37] S.A. Weissman, N.G. Anderson, Design of experiments (DoE) and process optimization. A review of recent publications, Org. Process Res. Dev. 19 (11) (2015) 1605–1633, https://doi.org/10.1021/op500169m.

[38] A. Barik, S. Nath, H. Pal, Effect of solvent polarity on the photophysical properties of coumarin-1 dye, J. Chem. Phys. 119 (19) (2003) 10202–10208, https://doi.org/10.1063/1.1619933.

[39] S.K. Lanke, N. Sekar, AIE based Coumarin chromophore-evaluation and correlation between Solvatochromism and solvent polarity parameters, J. Fluoresc. 26 (2016) 497–511, https://doi.org/10.1007/s10895-015-1735-6.

[40] C. Wang, W. Chi, Q. Qiao, D. Tan, Z. Xu, X. Liu, Twisted intramolecular charge transfer (TICT) and twists beyond TICT: from mechanisms to rational designs of bright and sensitive fluorophores, Chem. Soc. Rev. 50 (22) (2021) 12656–12678, https://doi.org/10.1039/D1CS00239B.

[41] A. Nag, K. Bhattacharyya, Role of twisted intramolecular charge transfer in the fluorescence sensitivity of biological probes: Diethylaminocoumarin laser dyes, Chem. Phys. Lett. 169 (1–2) (1990) 12–16, https://doi.org/10.1016/0009-2614(90)85156-7.

[42] W. Rettig, Charge separation in excited states of decoupled systems—TICT compounds and implications regarding the development of new laser dyes and the primary process of vision and photosynthesis, Angew. Chem. Int. Ed. Eng. 25 (11) (1986) 971–988, https://doi.org/10.1002/anie.198609711.

[43] B.B. Raju, T.S. Varadarajan, Spectroscopic studies of 7-diethylamino-3-styryl coumarins, J. Photochem. Photobiol. A Chem. 85 (3) (1995) 263–267, https://doi.org/10.1016/1010-6030(94)03905-A.

[44] C. Chen, C. Fang, Fluorescence modulation by amines: mechanistic insights into twisted intramolecular charge transfer (TICT) and beyond, Chemosensors 11 (2) (2023) 87, https://doi.org/10.3390/chemosensors11020087.

[45] J.L. Belmonte-Vázquez, Y.A. Amador-Sánchez, L.A. Rodr´iguez-Cortés, B. Rodr´iguez-Molina, Dual-state emission (DSE) in organic fluorophores: design and applications, Chem. Mater. 33 (18) (2021) 7160–7184, https://doi.org/10.1021/acs.chemmater.1c02460.

[46] T. Bhilwadikar, S. Pounraj, S. Manivannan, N.K. Rastogi, P.S. Negi, Decontamination of microorganisms and pesticides from fresh fruits and vegetables: a comprehensive review from common household processes to modern techniques, Compr. Rev. Food Sci. Food Saf. 18 (4) (2019) 1003–1038, https://doi.org/10.1111/1541-4337.12453.

[47] U. De Corato, Improving the shelf-life and quality of fresh and minimally-processed fruits and vegetables for a modern food industry: A comprehensive critical review from the traditional technologies into the most promising advancements, Crit. Rev. Food Sci. Nutr. 60 (6) (2020) 940–975, https://doi.org/10.1080/10408398.2018.1553025.

[48] N. Sumonsiri, S.A. Barringer, Fruits and vegetables – processing technologies and applications, in: Food Processing, Wiley & Sons, 2014, pp. 363–381, https://doi.org/10.1002/9781118846315.ch16.

[49] S.-J. Yang, et al., Effectiveness of different washing strategies on pesticide residue removal: the first comparative study on leafy vegetables, *Foods*, 11(18) (2022), doi: 10.3390/foods11182916.

[50] M.I. Gil, A. Marín, S. Andujar, A. Allende, Should chlorate residues be of concern in fresh-cut salads? Food Control 60 (2016) https://doi.org/10.1016/j.foodcont.2015.08.023.

[51] G. Ge, et al., Comparation study on the metabolism destination of neonicotinoid and organophosphate insecticides in tea plant (Camellia sinensis L.), Food Chem. 344 (May 2021) 128579, https://doi.org/10.1016/J.FOODCHEM.2020.128579.

[52] R. Pan, H.-P. Chen, M.-L. Zhang, Q.-H. Wang, Y. Jiang, X. Liu, Dissipation pattern, processing factors, and safety evaluation for dimethoate and its metabolite (Omethoate) in tea (Camellia Sinensis), PLoS One 10 (9) (2015) e0138309, https://doi.org/10.1371/journal.pone.0138309.

[53] M.R. Mahajan, P.O. Patil, One pot synthesis of cobalt and nitrogen co-doped graphene quantum dots based fluorescence "On-Off-On" probe for dimethoate sensing: A proof of concept, Inorg. Chem. Commun. 158 (2023) 111718, https://doi.org/10.1016/J.INOCHE.2023.111718.

[54] X. Yan, et al., Rapid detection of dimethoate in soybean samples by microfluidic paper chips based on oil-soluble CdSe quantum dots, Foods 10 (11) (2021) 2810, https://doi.org/10.3390/foods10112810.

[55] B. Vahid, Dimethoate using molecularly imprinting polymer on ZnO quantum dots, J. Fluoresc. 27 (2017) 1339–1347.

[56] Z. Sheng, J. Zhang, C. Li, L. Chen, Fluorescent switching technology based on fluorescence resonance energy transfer for detecting dimethoate pesticides in environmental water, Anal. Methods 8 (48) (2016) 8506–8513, https://doi.org/10.1039/C6AY02803A.

[57] Y. Yang, et al., Fluorometric microplate-based dimethoate assay using CdSe/ZnS quantum dots coated with a molecularly imprinted polymer, Microchim. Acta 186 (2019) 1–10.

3.3.2 Chlorpyrifos detection based on 9-fluorenone oxime

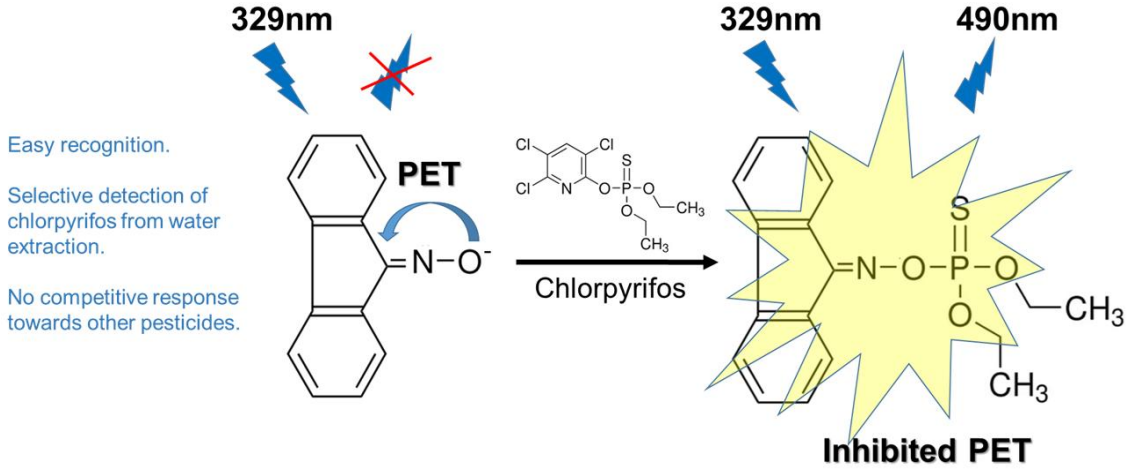

Figure 19: Graphical abstract of publication 3.

As highlighted in the introduction, oximes are well-known for their ability to reactivate AChE inhibited by OP pesticides. When deprotonated, oximes become highly nucleophilic, binding readily to phosphorus atoms. This makes them strong candidates for chemical sensing applications. However, despite their potential, little research has explored their integration into fluorescence-based detection systems, this knowledge gap motivated the development of our novel sensing strategy.

In this study, we designed a fluorescence-based probe using a fluorenone-derived oxime dye to detect chlorpyrifos. Deprotonation was necessary to enhance the dye's nucleophilicity, but direct deprotonation in water using a strong base was impractical since OP pesticides are prone to hydrolysis at high pH. Additionally, 9-fluorenone oxime would need to compete with hydroxide ions (OH^-), which are present in much higher concentrations. To overcome these challenges, we performed deprotonation in acetonitrile using a non-nucleophilic phosphazene base (P4), ensuring both selectivity and stability.

The fluorescence response was systematically analysed across varying analyte concentrations, resulting in a detection limit of 15.5 µg/L, in line with international regulatory standards. Selectivity was confirmed through minimal interference from other OPs, and the method's practical effectiveness was validated by successful chlorpyrifos detection in tap water, using a QuEChERS-based extraction process. The detection mechanism relied on a nucleophilic attack of the oxime on the pesticide's phosphate group, disrupting the PET mechanism and increasing the dye's fluorescence.

This study fills a significant gap in research by introducing an oxime-based fluorescent dye for direct OP pesticide detection. By capitalizing on the nucleophilic properties of oximes, it establishes a selective, efficient, and innovative approach for pesticide analysis, particularly in environmental water samples. The findings confirm our final hypothesis.

In this article I contributed in: conceptualization, methodology, validation, formal analysis, investigation, data curation, writing - original draft, visualization.

chemosensors

MDPI

Article

Chlorpyrifos Detection Based on 9-Fluorenone Oxime

Edoardo Donà [1,2] and Aleksandra Lobnik [1,3,*]

[1] Institute for Environmental Protection and Sensors, Beloruska 7, SI-2000 Maribor, Slovenia; edoardo.dona@ios.si
[2] Jožef Stefan International Postgraduate School, Jamova Cesta 39, SI-1000 Ljubljana, Slovenia
[3] Faculty of Mechanical Engineering, University of Maribor, Smetanova 17, SI-2000 Maribor, Slovenia
* Correspondence: aleksandra.lobnik@um.si

Abstract: Chlorpyrifos is one of the most toxic organophosphate pesticides, prompting its ban in Europe in 2020. Consequently, developing a detection method that is both selective and sensitive is essential for protecting human health and the environment. In this study, we report for the first time a fluorescent probe based on an oxime for the direct detection of chlorpyrifos. 9-fluorenone oxime, upon deprotonation with a phosphazene base, undergoes a nucleophilic attack on chlorpyrifos, resulting in a significant alteration of its fluorescence properties. Following careful optimization, the method demonstrated excellent linearity (R^2 = 0.98) over a concentration range of 350 to 6980 µg/L, with a limit of detection of 15.5 µg/L. Furthermore, the probe was successfully applied to chlorpyrifos detection in water samples, yielding satisfactory results. This approach effectively overcomes the stability limitations of enzyme-based fluorescent sensors, offering a robust and innovative solution for the detection of organophosphate pesticides.

Keywords: organophosphate pesticide; chlorpyrifos; fluorenone oxime; fluorescence; phosphazene

Received: 26 March 2025
Revised: 2 May 2025
Accepted: 2 May 2025
Published: 6 May 2025

Citation: Donà, E.; Lobnik, A. Chlorpyrifos Detection Based on 9-Fluorenone Oxime. *Chemosensors* **2025**, *13*, 170. https://doi.org/10.3390/chemosensors13050170

1. Introduction

Chlorpyrifos (CLP), patented in 1966 by the Dow Chemical Company, is a broad-spectrum chlorinated organophosphate (OP) pesticide widely used to control insect pests on various crops, particularly fruits and vegetables, thereby significantly contributing to agricultural yield [1,2]. It works by inhibiting acetylcholinesterase (AChE), an enzyme essential for the proper functioning of the nervous system [3,4]. This inhibition results in the accumulation of acetylcholine in synapses, leading to overstimulation of the nervous system, paralysis, and ultimately death in pests. A similar enzyme called butyrylcholinesterase is found in blood plasma and can be used as an antidote in the early stages of OP poisoning [5]. It binds nerve agents in the bloodstream before they can exert effects in the nervous system [6]. Until its ban in 2020, it was one of the most commonly used pesticides in food production within the European Union (EU) [7]. However, CLP is associated with reproductive toxicity, neurotoxicity, and genotoxicity, making it a frequent focus of scientific studies on OP pesticides in fruits and vegetables [8]. A major issue with CLP is its variable half-life, which, depending on soil conditions and application concentration, can range from a few days to as long as four years [9]. While its use is now prohibited within the EU, it remains widely employed in other regions, posing potential risks not only to local populations but also to Europe. For instance, in 2023, the EU imported 158 billion euros' worth of agri-food products, potentially exposing consumers to pesticides banned within its borders [10]. As the global population continues to grow, these environmental and

health risks are likely to intensify. To monitor pesticide residues, several analytical techniques are employed, with high-performance liquid chromatography (HPLC-MS/MS) and gas chromatography coupled with mass spectrometry (GC-MS/MS) considered the gold standards. While these methods ensure food safety, they are characterized by significant limitations, including high costs, time-consuming analyses, and lack of portability, which restrict the number of samples that can be tested daily. Ideally, all food products reaching consumers would be thoroughly monitored; however, achieving this requires alternative technologies. Consequently, research is increasingly focused on the development of sensors that are portable, rapid, user-friendly, and cost-effective, offering a promising solution to address these challenges of research.

Optical chemical sensors represent a promising approach due to their potential to offer several advantages. Various optical principles are currently under investigation, including surface-enhanced Raman scattering (SERS) [11], surface plasmon resonance (SPR) [12], and fluorescence. Among these, fluorescence is the most straightforward to implement, featuring a simple and cost-effective setup. Numerous studies have demonstrated its good selectivity and the capability to achieve limits of detection (LOD) at nanomolar (nM) [13] and even picomolar (pM) [14] concentrations of OPs. To contextualize this work within recent developments in fluorescence-based sensors for CLP detection, Table 1 presents a comparative analysis of different substrates employed for this purpose. The literature offers various approaches to fluorescence sensors for CLP, with only one reported example of direct detection using a fluorescent dye based on a europium coumarin complex [15]. Typically, biological methodologies [16–18] or hybrid techniques, such as nanoparticles (NPs) combined with dyes [19], quantum dots (QD) with molecularly imprinted polymers (MIPs) [20], or lanthanides with NPs [21], are good examples of very good sensors. However, these approaches often face significant drawbacks, including the use of expensive and/or hazardous materials, limited stability, or inadequate selectivity. In contrast, the method proposed in this work is straightforward, utilizes neither expensive nor hazardous materials, exhibits stability and easy repeatability, and ensures selectivity through a chemical reaction.

It is well established that oximes can reactivate the acetylcholinesterase enzyme [22] and protect it from phosphorylation by OP compounds [23]. Building on this knowledge, several studies have explored the development of fluorescent dyes suitable for OP detection [24–26]. However, most reports in the literature focus on OPs used as warfare agents rather than agricultural or environmental applications. In this study, we report for the first time the use of an oxime-based dye for the detection of CLP, marking only the second fluorophore [15] to directly detect this compound. We developed a novel method for determining CLP in water by monitoring changes in the fluorescence spectra of 9-fluorenone oxime (FLOX), as illustrated in Figure 1.

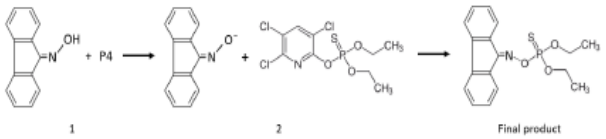

Figure 1. Proposed mechanism of reaction. FLOX is deprotonated by P4 (step 1) and then reacts with CLP (step 2) to give the proposed fluorescent product.

Although oximes are well-recognized as potent nucleophiles, their potential as scaffolds in sensors and probes applications remains largely unexplored. In our approach, FLOX was deprotonated using a phosphazene base and subsequently introduced into a solution of CLP in acetonitrile (CH_3CN) (see Figure 1). This interaction resulted in a rapid and strong fluorescence emission, which was captured by a fluorimeter. Chlorpyrifos

concentrations ranging from 350 to 6980 µg/L were successfully detected, with the method achieving a limit of detection (LOD) of 15.5 µg/L. Additionally, the probe was tested on water extracts, yielding satisfactory results, further demonstrating its applicability in real-world scenarios.

Table 1. State of the art of fluorescence sensors and probes for detection of chlorpyrifos.

Substrate	Reaction Time (min)	LOD (µg/L)	Linear Range (µg/L)	Reference
Eu (III)-TAN-1,10 phenanthroline naphthyl)-1,3-butanedione)	/	164	578–7713	[15]
Immunoassay-Rhodamine AuNPs	10	61	121–1250	[17]
Monoclonal antibody	10	15	15–64,000	[18]
CdS NPs–Eosin Y dye	20	10	10–100	[19]
QD–MIP flow cytometry	90	10	20–200	[20]
Tb^{3+} MOF–PDDA AuNPs	6	1.33	1.75–210	[21]
Polymer membrane with acryloyl-β-cyclodextrin	0.33	0.15	0.5–2.5	[27]
TEF-CDs	5	2.1	17–35,000	[28]
Nitrogen dots	5	2	10–500	[29]
Mn (II)-doped ZnS QD coated with MIP	10	6	105–21,000	[30]
Fluorenone oxime dye	20	15.5	350–6970	This work

2. Results

2.1. Response Surfaces

Detecting pesticides at micromolar concentrations presents a significant challenge, making system optimization a critical step in the development of new pesticide sensors. To maximize the fluorescence response of the dye, the optimal reaction conditions were investigated using the design of experiments (DoE) methodology. The analysis identified the optimal conditions as 20 min, FLOX at 60 µM, and P4 at 5 equivalents, as shown in Figure 2. No significant cross-interactions were observed; therefore, further optimization focused on the concentrations of FLOX and P4. Time optimization is addressed in Section 3.2. An attempt was made to increase the FLOX concentration to 100 µM; however, this led to suboptimal results due to self-quenching phenomena. For P4, comparisons were made between 5, 3, and 1.5 equivalents. It was determined that 3 equivalents provided the best results, as 1.5 equivalents were insufficient to fully deprotonate FLOX, and 5 equivalents resulted in diminished performance. Consequently, the optimized conditions used in subsequent sections of this study were as follows: 20 min, FLOX at 60 µM, and P4 at 3 equivalents (180 µM).

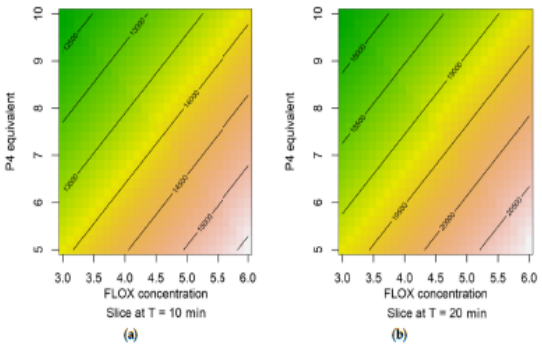

Figure 2. (**a**) Graph sliced at T = 10 min. (**b**) Graph sliced T = 20 min. On the y-axis we have the P4 equivalents added (from 5 to 10 times the FLOX concentration), on the x-axis the dye concentration (from 30 to 60 µM). The fluorescence intensity of the final product proposed in Figure 1 is our response variable that is graphically represented by the color change (from green to orange color). The fluorescence intensity increases from green to orange.

Chemosensors **2025**, *13*, 170

2.2. Calibration Curve

Building upon the fundamental insights obtained through the DoE methodology, the calibration curve experiment was conducted using the optimized parameters: FLOX at 60 µM, P4 at 180 µM, and a reaction time of 20 min. Under these conditions, the graph presented in Figure 3 was generated, from which the calibration curve was derived. Each data point represents the mean of three measurements (n = 3). As shown in Figure 3, the coefficient of determination (R^2) is 0.98. Further analysis revealed that this slight deviation from linearity is likely due to saturation effects or the inner filter effect, phenomena that commonly occur at elevated analyte concentrations and affect fluorescence-based systems. However, it is important to note that real-world CLP concentrations fall within the lower range of the calibration curve, where the relationship is strongly linear (removing the highest concentration point gives R^2 = 0.99). The calculated LOD is 15.5 µg/L. For comparison, the maximum residue limits (MRLs) for pesticides in drinking water in countries such as the United States (30 µg/L), Canada (90 µg/L), China (50 µg/L), and India (100 µg/L) are greater than or equal to the former EU limit of 10 µg/L.

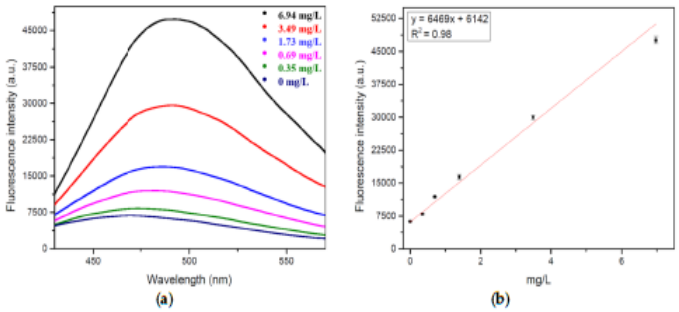

Figure 3. (**a**) Fluorescence spectra of the reaction in CH_3CN at CLP concentrations from 0 to 6.94 mg/L (λ_{exc}= 329 nm). (**b**) Associated calibration curve with the data reported in graph (**a**), λ_{em}= 490 nm.

2.3. Water Test

To thoroughly assess the practical viability of the method under real-world conditions, we tested our probe with CLP in the presence of a tap water extract. It is well established that CLP can contaminate groundwater due to its relatively long half-life in soil, which can ranges from few days to 126 or more days depending on environmental conditions [9,31]. Therefore, monitoring its presence in potable water is crucial. The water used in the experiment was sourced from the Maribor aqueduct. The preparation of the water extraction matrix followed the procedure outlined in Section 4.4 As shown in Figure S2 (see Supplementary Material) the LOD of the probe was significantly affected, increasing from 15.5 µg/L in pure CH_3CN to 114 µg/L in the presence of the water extract. This increase is expected due to matrix effects commonly observed in analytical chemistry. The observed LOD increase is attributed to fluorescence quenching caused by residual $MgSO_4$, acetic acid, and trace amounts of water retained in the matrix, even after extensive drying with $MgSO_4$ [32]. Additionally, the presence of organic compounds in water, combined with a λ_{exc} of 329 nm, can lead to background fluorescence interference, which can further explain the difference in the LOD. However, the limit of detection (LOD) remains significant in a global context, as regulatory limits for CLP in drinking water, vary widely as mentioned in Section 2.2. This demonstrates the method's suitability for pesticide monitoring. These findings emphasize the importance of matrix-specific calibration, a standard practice in analytical method development, and suggest that alternative extraction strategies could be explored to further optimize performance. Another possibility would be to identify suitable fluorescence oximes that deprotonate in low pH water.

3. Discussion

3.1. Sensing Mechanism

Oximes are commonly used as intermediates in the synthesis of their corresponding carbonyl compounds or as protective groups for these compounds. 9-Fluorenone oxime is typically synthesized through the reaction of hydroxylamine hydrochloride with fluorenone [33]. Super-nucleophiles are reactive species characterized by an atom with an unshared electron pair (commonly nitrogen or oxygen) adjacent to the nucleophilic site, a phenomenon referred to as the α-effect. Molecules exhibiting these features include oximes and hydrazones (R-NNH_2). Oximes, in particular, are widely employed as antidotes for OP poisoning, with pralidoxime being one of the most commonly available in the market. Additionally, the reactivity of oximes with OP warfare agents has been extensively studied in the literature [34–38]. OP warfare agents are significantly more reactive than their pesticide counterparts, primarily due to the presence of halogen atoms that serve as better leaving groups. In contrast, the reactivity of oximes with OP pesticides has been less extensively studied [24], as the nucleophilic attack is hindered by steric hindrance and the presence of poorer leaving groups. This challenge underscores the importance of maximizing the nucleophilicity of oximes, specifically through the deprotonation of the oxygen atom. Deprotonation can be achieved using strong bases such as NaOH or KOH. However, the hydroxide ion $(OH)^-$ is also a potent nucleophile and is well documented to promote the hydrolysis of OPs [39]. Consequently, competition arises between the deprotonated oxime and the hydroxide ion for nucleophilic attack on the phosphorus atom in CLP. To address this issue, a non-nucleophilic base, P4, was selected. This base effectively deprotonates the oxime without exhibiting nucleophilic behavior. The use of such bases requires an aprotic solvent to ensure efficient oxime deprotonation. Among the solvents tested, acetonitrile was identified as the most effective option.

To rationalize the photophysical properties of the dye that contribute to the sensing mechanism, it is essential to consider the well-established photoinduced electron transfer (PeT) mechanism. As shown in Figure 4, FLOX exhibits an absorbance peak at 309 nm and a fluorescence emission at 463 nm (λ_{exc} = 329 nm), which is partially quenched due to the presence of a PeT mechanism from the oxime group to the fluorene scaffold [40]. Upon the addition of P4, the fluorescence emission is significantly quenched (approximately five times, as shown by the dark blue line in Figure 4), due to proton removal (confirmed with ^{1}H-NMR spectra Figures S3 and S4) [41]. Simultaneously, the absorbance increases markedly in the region between 325 and 400 nm. After the addition of CLP, the fluorescence increases sharply after 20 min. We hypothesized that the final product is as shown in Figure 1, where the addition of the phosphate group would block the PeT quenching mechanism, thereby allowing the observed increase in fluorescence. The absorption between 325 and 400 nm instead decreases, since the concentration of the deprotonate oxime decreases due to the reaction. To understand better the possible outcome of the reaction proposed in Figure 1, we studied the reaction with ^{31}P-NMR. After we compared and confirmed P4 (Figure S6) [42] and CLP (Figure S5) [43] structures with the literature, we combined them to understand any possible product or adduct formed by the two compounds (Figure S7). Interestingly, the characteristic CLP peak at 60.48 ppm disappeared, while a multiplet at 62.32 ppm emerged, suggesting that CLP undergoes fragmentation or molecular rearrangement in the presence of P4. Additionally, we observed the appearance of a new singlet at 52.43 ppm, which we attribute to the formation of a stable P4-CLP species. When analyzing the full reaction mixture (FLOX + P4 + CLP), we observe the peaks of P4 (Figure S8), and the adduct P4-CLP at 52.43 ppm (Figure S9). Moreover, two new singlets appeared at 54.30 ppm and 67.88 ppm (Figure S9), suggesting the formation of the anticipated reaction product. Notably, the 67.88 ppm signal represents a significant

downfield shift (from P-O at 60.48 ppm), which is consistent with the formation of a P-O-N bond. This observation aligns with the expected deshielding effect in phosphorus environments where nitrogen exerts this effect more effectively compared to the P-O-C bonds in CLP. The 54.30 ppm peak may correspond to an alternative reaction pathway or an equilibrium species within the system.

To further corroborate our hypothesis proposed in Figure 1, we investigated potential alternatives, such as the Beckmann rearrangement and the reaction of FLOX with 3,5,6–trichloro-2-pyridinol (CPD), a known hydrolysis product of CLP [44,45]. The Beckmann rearrangement was quickly ruled out, as it typically occurs in the presence of an acid catalyst, whereas our environment is strongly basic. Nevertheless, to further confirm this, we reviewed the absorbance and fluorescence spectra of 6(5H)-phenanthridinone (a product of the potential Beckmann rearrangement) in the literature, which supported our initial hypothesis [46]. To better understand the interaction between CPD and FLOX, we tested various combinations, including the addition of P4. As shown in Figure 4, we first compared the spectra of pure CLP, CPD, and FLOX. CLP and CPD exhibit similar absorption, with a slight shift in the maximum absorbance below 300 nm. The fluorescence is negligible. Upon the addition of P4, the absorption increases around 338 nm for both CLP and CPD, while fluorescence does not show any significant peaks. When FLOX is added to CPD + P4 and CLP + P4, the absorption resembles that of FLOX + P4, but with CLP, it is reduced due to the consumption of $[FLOX]^-$, while with CPD, it increases due to the additive nature of absorbance. A significant difference is observed in the fluorescence spectra. It is evident that CPD does not react with FLOX + P4 (the emission is almost identical to that of FLOX + P4), while CLP does (the violet peak at 490 nm), confirming our initial hypothesis. Since the mechanism of reaction can be similar to that of other pesticides, we extensively discuss our interference testing in Section 3.2.

The main findings of this analysis can be summarized as follows:

- ^{1}H-NMR analysis confirmed the deprotonation of FLOX, a crucial step for its nucleophilic attack on CLP;
- ^{31}P-NMR revealed the disappearance of the CLP peak and the emergence of new phosphorus environments, supporting the occurrence of a reaction;
- The appearance of singlets at higher ppm values in ^{31}P-NMR suggests the formation of a P-O-N bond, consistent with the expected deshielding effect compared to the P-O-C bonds in CLP;
- Additional confirmation was provided by UV-Vis and fluorescence spectroscopy, further supporting the interaction between FLOX and the organophosphate;
- The known reactivity of deprotonated oximes with organophosphates further substantiates the proposed reaction mechanism.

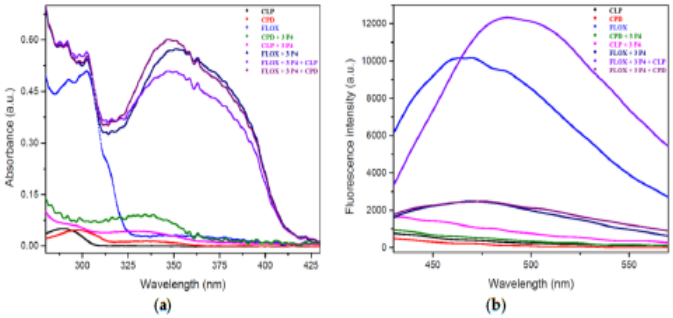

Figure 4. (**a**) UV-Vis and (**b**) fluorescence (λ_{exc}= 329 nm) of different combination of CLP, CPD, and FLOX with the addition of 3 equivalents of P4 (0.8 M in hexane) in CH_3CN. CPD and CLP are 8.3 µM, FLOX is 60 µM, and P4 is 180 µM.

3.2. Kinetic and Interferences

A kinetic experiment was conducted to better understand the behavior of the reaction at λ_{exc} = 329 nm (λ_{em} = 490 nm). As shown in Figure 5, the fluorescence peak is reached in 20 min, after which a gradual decrease begins, likely due to undesired side reactions. Therefore, further time optimization was not pursued, as it was clear that 20 min was the optimal duration. This time interval was used for all spectra presented in this work, unless otherwise stated. Additionally, similar dyes with faster kinetics may offer potential for the rapid detection of CLP. Once the mechanism of the reaction was understood, it became clear that other pesticides, particularly OPs, could potentially follow a similar pathway. To assess the potential real-world application of the system, we tested a range of pesticides (with three repetitions each), selected based on structural similarity and the presence of chlorine atoms, which we hypothesized could participate in similar reactions. The 13 pesticides tested included malathion (MALA), acephate (ACPH), dimethoate (DIME), ethion (ETHI), parathion (PARA), azamethiphos (AMT), azinphos methyl (AZOS), diazinon (DIA), trichlorfon (TCL), demeton-S-methyl sulfone (DEME), picloram (PCL), phorate (PHAE), and phosmet (PHET). All tested compounds, including CLP, were measured at a concentration of 1 µM, which is relatively high for pesticides. This concentration was chosen to clearly identify any potential interferences. As shown in Figure 5, four pesticides, AMT, ACPH, TCL, and PHET, emerged as potential concerns. Although such high concentrations are unlikely to occur in the same sample, we compared the fluorescence emission of CLP (1 µM) both with and without the presence of these four pesticides (also at 1 µM) (Figure S1 in Supplementary Material). The fluorescence of CLP was measured at 3656 (σ = 77), while the CLP–pesticide mixture gave a reading of 3788 (σ = 61). A two-tailed *t*-test was performed, and the calculated *p*-value was 0.23, indicating no statistically significant difference between the two measurements. Therefore, we demonstrated that, even in the presence of potential interferences, our fluorophore remains selective towards CLP.

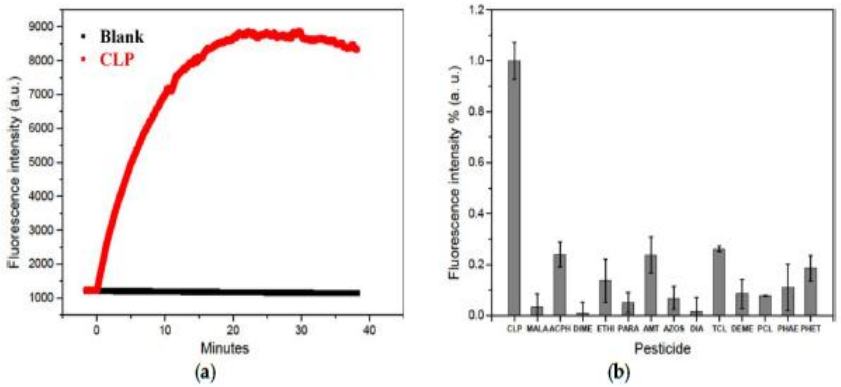

Figure 5. (**a**) Kinetic of FLOX + 3 P4 + CLP (5.82 mg/L), the blank, FLOX + 3P4 in CH_3CN at λ_{exc} = 329 nm and λ_{em} = 490 nm. (**b**) Interference test with 13 different organophosphate pesticides at a concentration of 1 µM in CH_3CN at λ_{exc} = 329 nm and λ_{em} = 490 nm.

4. Materials and Methods

4.1. Reagents

9-Fluorenone oxime acetonitrile, phosphazene base P4-t-Bu (P4) 0.8 M in hexane (CAS n°111324-04-0), picloram, trichlorfon, chlorpyrifos, diazinon, dimethoate, ethion, malathion, phorate, azametiphos, azinphos methyl, paraoxon ethyl, demeton-S-methyl sulfone (CAS n° 17040-19-6), acephate, phosmet, and 3,5,6-trichloro-2-pyridinol were brought from Sigma-Aldrich (St. Louis, MO, USA). Also, acetic acid, anhydrous $MgSO_4$, and NaCl were

bought from Sigma-Aldrich. All the reagents were used without any further purification. The reagents were all analytical grade unless otherwise stated.

4.2. Sensing Measurements

The fluorescence intensity was measured at λ_{exc} = 329 nm (λ_{em} = 490 nm), and wavelengths used in all the measurements are reported here. We used a fluorescence spectrometer (PerkinElmer FL 8500) equipped with a Xenon Arc (150 W) lamp and a UV-Vis spectrometer (PerkinElmer lambda 365+). The process can be divided into four main steps:

1. Preparation of FLOX solution at 60 µM in CH3CN;
2. Addition of P4 to a final concentration of 180 µM;
3. Addition of CLP;
4. Measurement of the fluorescence after 20 min at λ_{exc} = 329 nm (λ_{em} = 490 nm).

4.3. NMR Spectra

The ^{1}H-NMR spectra were recorded with a Magritek Spinsolve 60 NMR spectrometer, at 60 MHz. The ^{31}P-NMR spectra were recorded with a Bruker AVANCE NEO 600 MHz NMR spectrometer. The solvent was always d_6-DMSO with TMS as an internal standard.

4.4. Water Extraction Procedure

Tap water was collected from the sink of our laboratory. Then we followed the procedure based on the QuEChERS method in detail and well-established methods [47] were also validated according to the European Commission standards:

1. 35 g of tap water is measured into a 50 mL PTFE tube, and a concentrated solution of CLP is added to achieve the concentration specified in the calibration curve. This procedure is repeated for each concentration reported, with no CLP added to the blank.
2. 8.75 mL of CH_3CN containing 1% *v*/*v* of acetic acid is added.
3. 3.5 g of NaCl and 14 g of $MgSO_4$, are added, and the mixture is shaken for 1 min.
4. The mixture is centrifuged for 5 min at 4500 rpm.
5. 6.5 mL of the supernatant is extracted and transferred to another 50 mL PTFE tube.
6. 2.2 g of anhydrous $MgSO_4$ is added, and the mixture is shaken for 1 min.
7. The mixture is centrifuged for 2 min at 4500 rpm.
8. 4 mL of the solution is extracted and used as a solvent for the calibration curve.

4.5. Statistical Analysis

4.5.1. Design of Experiments Methodology

The design of experiments (DoE) methodology is a robust statistical technique employed to optimize parameters and achieve improved results. This approach is particularly valuable for identifying key factors and evaluating significant interactions between them [48]. In the present study, a full-factorial design comprising 2^4 = 16 experiments was utilized. Four parameters were tested at two levels each: time (T), P4 concentration, dye concentration, and an imaginary parameter (W) introduced to enhance model accuracy. The inclusion of W was justified by the high likelihood that all three primary parameters were significant (which in fact occurred), as well as the potential for cross-interactions. The levels tested were as follows:

- Time (T): 10 and 20 min;
- P4 concentration: 5 or 10 times the dye's concentration;
- FLOX concentration 30 or 60 µM;
- Imaginary parameter (W): levels 0 and 1.

Data analysis and visualization of the response surfaces were performed using R software version 4.3.3 for Windows.

4.5.2. Calibration Curve Calculation

The calibration curve was calculated using the average values of the data collected at each concentration. The LOD was determined at a 95% confidence level using the following formula: LOD = 3σ/S, where S represents the slope of the calibration curve and σ denotes the standard deviation of the response in the absence of the analyte.

5. Conclusions

In this study, we integrated a novel fluorene-based fluorescent dye with a simple method for the detection of CLP in liquid samples. Through optimization, we achieved CLP detection with high sensitivity (LOD = 15.5 µg/L) and selectivity among various pesticides. We also detected CLP in water with an LOD of 114 µg/L. We believe that this methodology, based on oxime fluorescent dyes, can be effectively extended to the detection of other OPs, where even better performance can be achieved improving the extraction method, or employing directly suitable deprotonated oximes in water systems. Thus, this work not only serves as a proof of concept, but also introduces a novel strategy for the direct detection of OPs pesticides using fluorescent dyes.

Supplementary Materials: The following supporting information can be downloaded at: https://www.mdpi.com/article/10.3390/chemosensors13050170/s1.

Author Contributions: Conceptualization, E.D. and A.L.; methodology, E.D. and A.L.; validation, E.D.; formal analysis, E.D.; investigation, E.D.; resources, A.L.; data curation, E.D.; writing—original draft preparation, E.D.; writing—review and editing, A.L.; visualization, E.D.; supervision, A.L.; project administration, A.L.; funding acquisition, A.L. All authors have read and agreed to the published version of the manuscript.

Funding: This research was funded by the EU Horizon 2020 research and innovation programme under the MSCA-FoodTraNet project (grant agreement no. 956265) and by the Slovenian Research Agency (Research Programmes P2-0424, P2-0438 "Optisens").

Institutional Review Board Statement: Not applicable.

Informed Consent Statement: Not applicable.

Data Availability Statement: No data are outside those reported in this article.

Conflicts of Interest: The authors declare no conflicts of interest.

Abbreviations

The following abbreviations are used in this manuscript:

AChE	Acetylcholinesterase enzyme
ACPH	Acephate
AMT	Azamethiphos
AZOS	Azinphos methyl
CLP	Chlorpyrifos
CPD	3,5,6-trichloro-2-pyridinol
DEME	Demeton-S-methyl sulfone
DIA	Diazinon
DIME	Dimethoate
EU	European union
ETHI	Ethion
FLOX	9-Fluorenone oxime

GC	Gas chromatography
HPLC	High performance liquid chromatography
LOD	Limit of detection
MALA	Malathion
MIP	Molecular imprinted polymers
MOF	Metal organic frameworks
MDPI	Multidisciplinary Digital Publishing Institute
MS	Mass spectrometry
OP	Organophosphate
P4	Phosphazene base P4-t-Bu
PARA	Parathion
PCL	Picloram
PDDA	Poly (diallyl-dimethylammonium chloride)
PHAE	Phorate
PHET	Phosmet
SERS	Surface enhance Raman scattering
SPR	Surface plasmon resonance
QD	Quantum dots
TCL	Trichlorfon

References

1. Itsoponpan, T.; Thanachayanont, C.; Hasin, P. Sponge-like CuInS2 microspheres on reduced graphene oxide as an electrocatalyst to construct an immobilized acetylcholinesterase electrochemical biosensor for chlorpyrifos detection in vegetables. *Sens. Actuators B Chem.* **2021**, *337*, 129775. [CrossRef]
2. Yuan, S.; Yang, F.; Yu, H.; Xie, Y.; Guo, Y.; Yao, W. Degradation mechanism and toxicity assessment of chlorpyrifos in milk by combined ultrasound and ultraviolet treatment. *Food Chem.* **2022**, *383*, 132550. [CrossRef] [PubMed]
3. Fournier, D.; Mutero, A. Modification of acetylcholinesterase as a mechanism of resistance to insecticides. *Comp. Biochem. Physiol. C Pharmacol. Toxicol. Endocrinol.* **1994**, *108*, 19–31. [CrossRef]
4. Colovic, M.B.; Krstic, D.Z.; Lazarevic-Pasti, T.D.; Bondzic, A.M.; Vasic, V.M. Acetylcholinesterase Inhibitors: Pharmacology and Toxicology. *Curr. Neuropharmacol.* **2013**, *11*, 315–335. [CrossRef]
5. Masson, P.; Lockridge, O. Butyrylcholinesterase for protection from organophosphorus poisons: Catalytic complexities and hysteretic behavior. *Arch. Biochem. Biophys.* **2010**, *494*, 107–120. [CrossRef]
6. Raveh, L.; Grunwald, J.; Marcus, D.; Papier, Y.; Cohen, E.; Ashani, Y. Human butyrylcholinesterase as a general prophylactic antidote for nerve agent toxicity. *Biochem. Pharmacol.* **1993**, *45*, 2465–2474. [CrossRef]
7. Wołejko, E.; Łozowicka, B.; Jabłońska-Trypuć, A.; Pietruszyńska, M.; Wydro, U. Chlorpyrifos Occurrence and Toxicological Risk Assessment: A Review. *Int. J. Environ. Res. Public Health* **2022**, *19*, 12209. [CrossRef]
8. Li, W.; Chen, J.; Linli, F.; Chen, X.; Huang, Y.; Yang, X. Organophosphorus pesticide contaminants in fruits and vegetables: A meta-analysis. *Food Chem. X* **2023**, *20*, 101014. [CrossRef]
9. John, E.M.; Shaike, J.M. Chlorpyrifos: Pollution and remediation. *Environ. Chem. Lett.* **2015**, *13*, 269–291. [CrossRef]
10. Directorate-General for Agriculture and Rural Development, "EU Agri-Food Exports Keep Growing Steadily in the First Quarter". Available online: https://agriculture.ec.europa.eu/news/eu-agri-food-exports-keep-growing-steadily-first-quarter-2024-06-25_en (accessed on 8 October 2024).
11. Xu, Q.; Guo, X.; Xu, L.; Ying, Y.; Wu, Y.; Wen, Y.; Yang, H. Template-free synthesis of SERS-active gold nanopopcorn for rapid detection of chlorpyrifos residues. *Sens. Actuators B Chem.* **2017**, *241*, 1008–1013. [CrossRef]
12. Li, Q.; Dou, X.; Zhang, L.; Zhao, X.; Luo, J.; Yang, M. Oriented assembly of surface plasmon resonance biosensor through staphylococcal protein A for the chlorpyrifos detection. *Anal. Bioanal. Chem.* **2019**, *411*, 6057–6066. [CrossRef] [PubMed]
13. Tao, X.; Mao, Y.; Alam, S.; Wang, A.; Qi, X.; Zheng, S.; Jiang, C.; Chen, S.-Y.; Lu, H. Sensitive fluorescence detection of glyphosate and glufosinate ammonium pesticides by purine-hydrazone-Cu2+ complex. *Spectrochim. Acta A Mol. Biomol. Spectrosc.* **2024**, *314*, 124226. [CrossRef]
14. Carullo, P.; Cetrangolo, G.; Mandrich, L.; Manco, G.; Febbraio, F. Fluorescence Spectroscopy Approaches for the Development of a Real-Time Organophosphate Detection System Using an Enzymatic Sensor. *Sensors* **2015**, *15*, 3932–3951. [CrossRef]

15. Azab, H.A.; Khairy, G.M.; Kamel, R.M. Time-resolved fluorescence sensing of pesticides chlorpyrifos, crotoxyphos and endosulfan by the luminescent Eu(III)–8-allyl-3-carboxycoumarin probe. *Spectrochim. Acta A Mol. Biomol. Spectrosc.* **2015**, *148*, 114–124. [CrossRef]
16. Zhang, M.; Chen, Z.; Liu, X.; Song, C.; Zeng, C.; Lv, T.; Xu, Z.; Chen, X.; Wang, L.; Liu, B.; et al. Dual-mode supramolecular fluorescent probe for rapid and on-site detection of chlorpyrifos in the environment. *J. Hazard. Mater.* **2023**, *452*, 131177. [CrossRef]
17. Dou, X.; Zhang, L.; Liu, C.; Li, Q.; Luo, J.; Yang, M. Fluorometric competitive immunoassay for chlorpyrifos using rhodamine-modified gold nanoparticles as a label. *Microchim. Acta* **2018**, *185*, 41. [CrossRef]
18. Xu, Z.-H.; Liu, J.; Li, B.; Wang, J.-K.; Zeng, X.; Chen, Z.-J.; Hongsibsong, S.; Huang, W.; Lei, H.-T.; Sun, Y.-M.; et al. The Simultaneous Determination of Chlorpyrifos–Ethyl and –Methyl with a New Format of Fluorescence-Based Immunochromatographic Assay. *Biosensors* **2022**, *12*, 1006. [CrossRef] [PubMed]
19. Dey, P.C.; Das, R. Ligand free surface of CdS nanoparticles enhances the energy transfer efficiency on interacting with Eosin Y dye – Helping in the sensing of very low level of chlorpyrifos in water. *Spectrochim. Acta A Mol. Biomol. Spectrosc.* **2019**, *207*, 156–163. [CrossRef]
20. Zhang, H.; Wang, P.; Zhou, Q.; Wang, Y. A Novel Method for the Detection of Chlorpyrifos by Combining Quantum Dot-labeled Molecularly Imprinted Polymer with Flow Cytometry. *Anal. Lett.* **2018**, *51*, 921–934. [CrossRef]
21. Liu, Q.; Wang, H.; Han, P.; Feng, X. Fluorescent aptasensing of chlorpyrifos based on the assembly of cationic conjugated polymer-aggregated gold nanoparticles and luminescent metal–organic frameworks. *Analyst* **2019**, *144*, 6025–6032. [CrossRef]
22. Kuznetsova, D.A.; Gaynanova, G.A.; Vasilieva, E.A.; Pavlov, R.V.; Zueva, I.V.; Babaev, V.M.; Kuznetsov, D.M.; Voloshina, A.D.; Petrov, K.A.; Zakharova, L.Y.; et al. Oxime Therapy for Brain AChE Reactivation and Neuroprotection after Organophosphate Poisoning. *Pharmaceutics* **2022**, *14*, 1950. [CrossRef] [PubMed]
23. Maynard, R.L.; Chilcott, R.P. Toxicology of Chemical Warfare Agents. In *General, Applied and Systems Toxicology*; Wiley: Hoboken, NJ, USA, 2009. [CrossRef]
24. Walton, I.; Davis, M.; Munro, L.; Catalano, V.J.; Cragg, P.J.; Huggins, M.T.; Wallace, K.J. A Fluorescent Dipyrrinone Oxime for the Detection of Pesticides and Other Organophosphates. *Org. Lett.* **2012**, *14*, 2686–2689. [CrossRef] [PubMed]
25. Lee, J.Y.; Lee, Y.H.; Byun, Y.G. Detection of Chemical Warfare Nerve Agents via a Beckmann Fragmentation of Aldoxime. *Phosphorus Sulfur. Silicon Relat. Elem.* **2012**, *187*, 641–649. [CrossRef]
26. Cai, Y.-C.; Li, C.; Song, Q.-H. Selective and visual detection of a nerve agent mimic by phosphorylation and protonation of quinolin oximes. *J. Mater. Chem. C Mater.* **2017**, *5*, 7337–7343. [CrossRef]
27. Çubuk, S.; Yetimoğlu, E.K.; Çalışkan, A.; Kahraman, M.V. A novel polymer based fluorimetric sensor for fast and selective determination of chlorpyrifos. *Microchem. J.* **2021**, *165*, 106098. [CrossRef]
28. Ghosh, S.; Gul, A.R.; Park, C.Y.; Kim, M.W.; Xu, P.; Baek, S.H.; Bhamore, J.R.; Kailasa, S.K.; Park, T.J. Facile synthesis of carbon dots from Tagetes erecta as a precursor for determination of chlorpyrifos via fluorescence turn-off and quinalphos via fluorescence turn-on mechanisms. *Chemosphere* **2021**, *279*, 130515. [CrossRef]
29. Tang, Z.; Chen, Z.; Li, G.; Hu, Y. Multicolor nitrogen dots for rapid detection of thiram and chlorpyrifos in fruit and vegetable samples. *Anal. Chim. Acta* **2020**, *1136*, 72–81. [CrossRef]
30. Ren, X.; Liu, H.; Chen, L. Fluorescent detection of chlorpyrifos using Mn(II)-doped ZnS quantum dots coated with a molecularly imprinted polymer. *Microchim. Acta* **2015**, *182*, 193–200. [CrossRef]
31. Liu, B.; McConnell, L.L.; Torrents, A. Hydrolysis of chlorpyrifos in natural waters of the Chesapeake Bay. *Chemosphere* **2001**, *44*, 1315–1323. [CrossRef]
32. Kalinke, N.; Stopper, P.; Völkl, L.; Diehl, F.; Huhn, C. SWIEET—A salt-free alternative to QuEChERS. *Anal. Bioanal. Chem.* **2024**, *416*, 6387–6403. [CrossRef]
33. Yoshihara, K.; Kearns, D.R. Spectroscopic Properties of the Lower-Lying Excited States of Fluorenone. *J. Chem. Phys.* **1966**, *45*, 1991–1999. [CrossRef]
34. Hewage, H.S.; Wallace, K.J.; Anslyn, E.V. Novel chemiluminescent detection of chemical warfare simulant. *Chem. Commun.* **2007**, 3909–3911. [CrossRef] [PubMed]
35. Wallace, K.J.; Fagbemi, R.I.; Folmer-Andersen, F.J.; Morey, J.; Lynth, V.M.; Anslyn, E.V. Detection of chemical warfare simulants by phosphorylation of a coumarin oximate. *Chem. Commun.* **2006**, 3886–3888. [CrossRef]
36. Qin, T.; Huang, Y.; Zhu, K.; Wang, J.; Pan, C.; Liu, B.; Wang, L. A flavonoid-based fluorescent test strip for sensitive and selective detection of a gaseous nerve agent simulant. *Anal. Chim. Acta* **2019**, *1076*, 125–130. [CrossRef]
37. Jang, Y.J.; Tsay, O.G.; Murale, D.P.; Jeong, J.A.; Segev, A.; Churchill, D.G. Novel and selective detection of Tabun mimics. *Chem. Commun.* **2014**, *50*, 7531–7534. [CrossRef]
38. Dale, T.J.; Rebek, J. Hydroxy Oximes as Organophosphorus Nerve Agent Sensors. *Angew. Chem. Int. Ed.* **2009**, *48*, 7850–7852. [CrossRef]
39. Donà, E.; Mohr, G.J.; Lobnik, A. Dimethoate detection through a fluorescent coumarin dye. *Microchem. J.* **2024**, *207*, 112205. [CrossRef]

40. Niu, H.; Liu, J.; O'Connor, H.M.; Gunnlaugsson, T.; James, T.D.; Zhang, H. Photoinduced electron transfer (PeT) based fluorescent probes for cellular imaging and disease therapy. *Chem. Soc. Rev.* **2023**, *52*, 2322–2357. [CrossRef]
41. Yu, J.; Lu, M. Copper(II)-promoted direct conversion of methylarenes into aromatic oximes. *Org. Biomol. Chem.* **2015**, *13*, 7397–7401. [CrossRef]
42. Schwesinger, R.; Kondo, Y. Phosphazene Base P4-t-Bu. In *Encyclopedia of Reagents for Organic Synthesis*; John Wiley & Sons, Ltd.: Chichester, UK, 2010. [CrossRef]
43. Shamsipur, M.; Sarkouhi, M.; Hassan, J. Selective Monitoring of Organophosphorus Pesticides by 31P-NMR Spectroscopy: Application to Purity Assay of Technical Products and Concentration Determination of Formulated Samples. *Appl. Magn. Reson.* **2012**, *42*, 227–237. [CrossRef]
44. Dahiya, V.; Chaubey, B.; Dhaharwal, A.K.; Pal, S. Solvent-dependent binding interactions of the organophosphate pesticide, chlorpyrifos (CPF), and its metabolite, 3,5,6-trichloro-2-pyridinol (TCPy), with Bovine Serum Albumin (BSA): A comparative fluorescence quenching analysis. *Pestic. Biochem. Physiol.* **2017**, *139*, 92–100. [CrossRef] [PubMed]
45. Žabar, R.; Sarakha, M.; Lebedev, A.T.; Polyakova, O.V.; Trebše, P. Photochemical fate and photocatalysis of 3,5,6-trichloro-2-pyridinol, degradation product of chlorpyrifos. *Chemosphere* **2016**, *144*, 615–620. [CrossRef] [PubMed]
46. Gentili, P.L.; Ortica, F.; Romani, A.; Favaro, G. Effects of Proximity on the Relaxation Dynamics of Flindersine and 6(5 *H*.)-Phenanthridinone. *J. Phys. Chem. A* **2007**, *111*, 193–200. [CrossRef] [PubMed]
47. Ghani, S.B.A.; Hanafi, A.H. QuEChERS method combined with GC-MS for pesticide residues determination in water. *J. Anal. Chem.* **2016**, *71*, 508–512. [CrossRef]
48. Condra, L.W. DoE in product design. In *Reliability Improvement with Design of Experiments*; CRC Press: Boca Raton, FL, USA, 2018; pp. 105–120. [CrossRef]

Chapter 4

Conclusions

Over the past 150 years since the Second Industrial Revolution, human activities have significantly altered our planet's natural balance. Industrialization, population growth, and intensive agriculture have led to pollution, biodiversity loss, and a growing crisis in food security. As we move toward a future where the global population is expected to reach 9.8 billion by 2050, the pressure on food production systems will intensify, necessitating innovative and sustainable solutions. While scientific progress continues to provide technological breakthroughs, real change requires the commitment of governments, industries, and consumers.

4.1 The Role of Sensors in Addressing Global Challenges

Among the many challenges, pesticide use and food waste represent two critical areas where innovative sensing technologies can contribute to a more sustainable and safer food system. Pesticides, essential for modern agriculture, have become both an asset and a threat. As OPs are increasingly replaced by pyrethroids (at least in the richest countries) due to their lower toxicity, the pursuit of truly sustainable, non-toxic, and cost-effective alternatives remains an ongoing challenge in the complex interaction between human needs and ecological balance. In the meantime, monitoring environmental pollution is crucial, not only to mitigate health risks, but also to sustain public awareness and drive political discourse toward long-term sustainable solutions.

This pattern is evident in the historical evolution of pesticide regulation. Initially, OC pesticides were widely used but were later banned due to their environmental and health risks. They were subsequently replaced by OPs, which are now slowly being replaced (at least in the richest countries) in favour of pyrethroids, following scientific assessments of their toxicity and growing public pressure. This ongoing cycle highlights the need for continuous monitoring and informed decision-making by policy makers, companies and the public opinion.

To support this process, data collection plays a vital role in keeping the public informed. Today, bio-chemical laboratories across Europe are making significant efforts to analyse pesticide residues in food. However, despite meticulous sampling focusing on products and sectors considered at risk, current testing covers only a small fraction of what is actually available on the market. This limitation underscores the potential of empowering consumers with accessible, real-time food quality monitoring tools. By integrating advanced sensing technologies, consumers could independently verify the safety of their food, fostering greater transparency and ultimately transforming the food industry into a more accountable and sustainable system.

4.2 Key Contributions of This Research

4.2.1 Organophosphate detection

In this thesis, I sought to advance the field of fluorescence-based pesticide detection by exploring novel sensing strategies for OPs. Fluorescent sensors offer a unique advantage due to their simplicity, affordability, and potential for consumer-friendly applications. I explored two different strategies tackling the problem from different perspectives. By leveraging the hydrolysis of dimethoate, it was developed a fluorescence-based detection method that successfully quantified the pesticide in green tea samples. Using a dicyanovinyl coumarin dye, achieving a detection limit of 3.2 µg/L and demonstrated successful application in green tea, with a recovery of 95.4% (σ = 5.7%). This work highlights an alternative approach to pesticide sensing, focusing on reaction-based fluorescence activation by a degradation product of dimethoate rather than the conventional direct detection used in other fluorescence applications.

The second study introduced a pharmacological approach to fluorescence sensing, utilizing 9-fluorenone oxime to directly detect chlorpyrifos. The reaction with the pesticide led to a significant fluorescence shift, achieving a limit of detection of 15.5 µg/L, with strong selectivity. The incorporation of oxime chemistry into fluorescence sensing offers a new avenue for selective OP detection, demonstrating how established pharmaceutical strategies can be applied to environmental monitoring.

These findings contribute to the broader field of environmental sensing, emphasizing the need for portable, cost-effective detection methods to empower both regulatory bodies and consumers. The detection mechanisms proposed in this thesis can be adapted to sense other OPs and also to other pesticides.

4.2.2 Ammonia sensing

Food waste is a multifaceted issue, with spoilage playing a key role. Currently, consumers rely primarily, beyond the expiry date, on visual and olfactory cues to assess food freshness, an approach that is often inaccurate and leads to excessive waste. My research explored a novel ammonia sensor based on rGO. Utilizing low pressure hydrogen plasma, it has been developed a rapid and efficient reduction method for GO, significantly improving its sensing performance. The optimized sensor demonstrated a sensitivity of 23.9% at 100 ppm and 47.1% at 1049 ppm, with the ability to function in air environments. Compared to conventional reduction techniques, within the experimental part it was demonstrated how this plasma treatment achieved similar or superior performance with only 20 seconds of processing time, an improvement of at least an order of magnitude in processing speed. It was also proved how plasma treatment time influence the reversibility (the longer the better), but already at 20 seconds the sensor was partially reversible, indicating it can be reused multiple times.

By optimizing both material properties and sensor response, this study paves the way for the integration of rGO-based ammonia sensors into food packaging or smart monitoring systems. Such advancements could enable real-time assessment of food freshness, reducing unnecessary waste and improving food security.

Chapter 5

Future Perspectives

The need for innovative food safety and environmental monitoring solutions has never been greater. Climate change, population growth, and industrial pollution have placed enormous strain on global food systems, requiring new strategies to ensure sustainability and security. The sensors developed in this research represent a step toward empowering individuals, industries, and policymakers with real-time data for safer, more sustainable decision-making.

The ammonia sensor could undergo further testing enhancing its selectivity towards ammonia, but also perform experiments in low-temperature environments and packaging conditions to evaluate its suitability for integration into smart refrigerators to forecast shelf-life and, potentially, in food packaging systems. The dimethoate probe could be adapted for use in a diagnostic kit aimed at early detection of the pesticide in tea leaves. Additionally, similar dye-based probes might be utilized to exploit hydrolysis reactions to detect other OP pesticides. To enhance the performance of the chlorpyrifos probe, alternative oximes could be synthesized and identified. To avoid the use of P4 and use the system directly in water, other oximes that deprotonate at lower pHs by mitigating competition with hydroxide ions (OH^-) might be promising. Such improvements could significantly reduce detection times, making the process more efficient and practical for real-world applications.

However, technological solutions alone are not enough. The broader challenge remains in bridging the gap between science, policy, and public engagement. Raising consumer awareness about pesticide contamination and food waste, promoting better agricultural practices, and fostering collaborations between researchers, governments, and private sectors will be critical to translating these innovations into real-world impact.

Looking forward, the true success of these technologies will be measured not just in laboratory performance but in their ability to drive meaningful change, whether by reducing food waste, enhancing supply chain transparency, or preventing toxic exposure in populations. By integrating scientific progress with social responsibility, we can move toward a future where food safety is not a privilege but a universal right.

While this thesis has explored fluorescence-based and rGO sensors as powerful tools for detection, their potential is far from fully realized. Further interdisciplinary efforts, including advances in material science, data analytics, and machine learning, could push these technologies beyond simple detection, but toward predictive and autonomous monitoring systems that proactively prevent contamination and waste. This journey is just beginning, and the responsibility of the scientific community is to continue driving innovation for all human beings.

References

[1] A. Beyin, "Upper Pleistocene Human Dispersals out of Africa: A Review of the Current State of the Debate," *Int J Evol Biol*, vol. 2011, pp. 1–17, May 2011, doi: 10.4061/2011/615094.

[2] S. López, L. Van Dorp, and G. Hellenthal, "Human Dispersal Out of Africa: A Lasting Debate," *Evolutionary Bioinformatics*, vol. 11s2, Jan. 2015, doi: 10.4137/EBO.S33489.

[3] K. Hawkes, J. O'Connell, and N. Blurton Jones, "Hunter-gatherer studies and human evolution: A very selective review," *Am J Phys Anthropol*, vol. 165, no. 4, pp. 777–800, Apr. 2018, doi: 10.1002/ajpa.23403.

[4] A. N. Crittenden and S. L. Schnorr, "Current views on hunter-gatherer nutrition and the evolution of the human diet," *Am J Phys Anthropol*, vol. 162, no. S63, pp. 84–109, Jan. 2017, doi: 10.1002/ajpa.23148.

[5] D. Q. Fuller, "Agricultural Origins and Frontiers in South Asia: A Working Synthesis," *J World Prehist*, vol. 20, no. 1, pp. 1–86, Dec. 2006, doi: 10.1007/s10963-006-9006-8.

[6] P. Bogucki, "Geography and Chronology of the Transition to Agriculture," in *Oxford Research Encyclopedia of Environmental Science*, Oxford University Press, 2019. doi: 10.1093/acrefore/9780199389414.013.165.

[7] W. M. Bowen and R. E. Gleeson, "The Advent of Permanent Human Settlements," in *The Evolution of Human Settlements*, Cham: Springer International Publishing, 2019, pp. 73–94. doi: 10.1007/978-3-319-95034-1_4.

[8] G. Larson and D. Q. Fuller, "The Evolution of Animal Domestication," *Annu Rev Ecol Evol Syst*, vol. 45, no. 1, pp. 115–136, Nov. 2014, doi: 10.1146/annurev-ecolsys-110512-135813.

[9] D. Q. Fuller, T. Denham, and R. Allaby, "Plant domestication and agricultural ecologies," *Current Biology*, vol. 33, no. 11, pp. R636–R649, Jun. 2023, doi: 10.1016/j.cub.2023.04.038.

[10] A. Fornasiero, R. A. Wing, and P. Ronald, "Rice domestication," *Current Biology*, vol. 32, no. 1, pp. R20–R24, Jan. 2022, doi: 10.1016/j.cub.2021.11.025.

[11] D. Tancredi and I. Cardinali, "Being a Dog: A Review of the Domestication Process," *Genes (Basel)*, vol. 14, no. 5, p. 992, Apr. 2023, doi: 10.3390/genes14050992.

[12] T. Cucchi and B. Arbuckle, "Animal domestication: from distant past to current development and issues," *Animal Frontiers*, vol. 11, no. 3, pp. 6–9, Jun. 2021, doi: 10.1093/af/vfab013.

[13] W. Albarracín, I. C. Sánchez, R. Grau, and J. M. Barat, "Salt in food processing; usage and reduction: a review," *Int J Food Sci Technol*, vol. 46, no. 7, pp. 1329–1336, Jul. 2011, doi: 10.1111/j.1365-2621.2010.02492.x.

[14] N. Nunn and N. Qian, "The Columbian Exchange: A History of Disease, Food, and Ideas," *Journal of Economic Perspectives*, vol. 24, no. 2, pp. 163–188, May 2010, doi: 10.1257/jep.24.2.163.

[15] P. de Zwart and D. O. Flynn, "The Significance of Early Globalization: Arguments and Evidence," 2021, pp. 35–67. doi: 10.1007/978-3-030-69666-5_2.

[16] R. Garcia and J. Adrian, "Nicolas Appert: Inventor and Manufacturer," *Food Reviews International*, vol. 25, no. 2, pp. 115–125, Apr. 2009, doi: 10.1080/87559120802682656.

[17] S. J. Risch, "Food Packaging History and Innovations," *J Agric Food Chem*, vol. 57, no. 18, pp. 8089–8092, Sep. 2009, doi: 10.1021/jf900040r.

[18] D. Knorr and M. A. Augustin, "Preserving the food preservation legacy," *Crit Rev Food Sci Nutr*, vol. 63, no. 28, pp. 9519–9538, Nov. 2023, doi: 10.1080/10408398.2022.2065459.

[19] P. Jacques and J. Jacques, "Monocropping Cultures into Ruin: The Loss of Food Varieties and Cultural Diversity," *Sustainability*, vol. 4, no. 11, pp. 2970–2997, Nov. 2012, doi: 10.3390/su4112970.

[20] L. Elizabeth, P. Machado, M. Zinöcker, P. Baker, and M. Lawrence, "Ultra-Processed Foods and Health Outcomes: A Narrative Review," *Nutrients*, vol. 12, no. 7, p. 1955, Jun. 2020, doi: 10.3390/nu12071955.

[21] M. J. Gibney, C. G. Forde, D. Mullally, and E. R. Gibney, "Ultra-processed foods in human health: a critical appraisal," *Am J Clin Nutr*, vol. 106, no. 3, pp. 717–724, Mar. 2017, doi: 10.3945/ajcn.117.160440.

[22] G. Pagliai, M. Dinu, M. P. Madarena, M. Bonaccio, L. Iacoviello, and F. Sofi, "Consumption of ultra-processed foods and health status: a systematic review and meta-analysis," *British Journal of Nutrition*, vol. 125, no. 3, pp. 308–318, Feb. 2021, doi: 10.1017/S0007114520002688.

[23] A. Roy, H. Moradkhani, M. Mekonnen, H. Moftakhari, and N. Magliocca, "Towards strategic interventions for global food security in 2050," *Science of The Total Environment*, vol. 954, p. 176811, Dec. 2024, doi: 10.1016/j.scitotenv.2024.176811.

[24] T. Searchinger, R. Waite, Hanson Craig, and Ranganathan Janet, "Creating a Sustainable Food Future." Accessed: Jan. 06, 2025. [Online]. Available: https://www.wri.org/research/creating-sustainable-food-future

[25] M. F. Bellemare, M. Çakir, H. H. Peterson, L. Novak, and J. Rudi, "On the Measurement of Food Waste," *Am J Agric Econ*, vol. 99, no. 5, pp. 1148–1158, Oct. 2017, doi: 10.1093/ajae/aax034.

[26] G. B. Zamri *et al.*, "Delivery, impact and approach of household food waste reduction campaigns," *J Clean Prod*, vol. 246, p. 118969, Feb. 2020, doi: 10.1016/j.jclepro.2019.118969.

[27] A. Rosi *et al.*, "Environmental impact of omnivorous, ovo-lacto-vegetarian, and vegan diet," *Sci Rep*, vol. 7, no. 1, p. 6105, Jul. 2017, doi: 10.1038/s41598-017-06466-8.

[28] A. C. Bunge, R. Mazac, M. Clark, A. Wood, and L. Gordon, "Sustainability benefits of transitioning from current diets to plant-based alternatives or whole-food diets in Sweden," *Nat Commun*, vol. 15, no. 1, p. 951, Feb. 2024, doi: 10.1038/s41467-024-45328-6.

[29] B. C. Chai, J. R. van der Voort, K. Grofelnik, H. G. Eliasdottir, I. Klöss, and F. J. A. Perez-Cueto, "Which Diet Has the Least Environmental Impact on Our Planet? A Systematic Review of Vegan, Vegetarian and Omnivorous Diets," *Sustainability*, vol. 11, no. 15, p. 4110, Jul. 2019, doi: 10.3390/su11154110.

[30] A. Aljaafari *et al.*, "Biodiesel Emissions: A State-of-the-Art Review on Health and Environmental Impacts," *Energies (Basel)*, vol. 15, no. 18, p. 6854, Sep. 2022, doi: 10.3390/en15186854.

[31] A. P. J. Mol, "Environmental authorities and biofuel controversies," *Env Polit*, vol. 19, no. 1, pp. 61–79, Feb. 2010, doi: 10.1080/09644010903396085.

[32] S. N. Gebremariam, "Biodiesel as a transport fuel, advantages and disadvantages: review," *Biofuels, Bioproducts and Biorefining*, vol. 17, no. 5, pp. 1445–1456, Sep. 2023, doi: 10.1002/bbb.2503.

[33] P. DeCicca and H. Krashinsky, "The effect of education on overall fertility," *J Popul Econ*, vol. 36, no. 1, pp. 471–503, Jan. 2023, doi: 10.1007/s00148-022-00897-y.

[34] F. Götmark and M. Andersson, "Human fertility in relation to education, economy, religion, contraception, and family planning programs," *BMC Public Health*, vol. 20, no. 1, p. 265, Dec. 2020, doi: 10.1186/s12889-020-8331-7.

[35] J. Kim, "Female education and its impact on fertility," *IZA World of Labor*, 2023, doi: 10.15185/izawol.228.v2.

[36] N. Heslot, J. Jannink, and M. E. Sorrells, "Perspectives for Genomic Selection Applications and Research in Plants," *Crop Sci*, vol. 55, no. 1, pp. 1–12, Jan. 2015, doi: 10.2135/cropsci2014.03.0249.

[37] M. K. Rakkar and H. Blanco-Canqui, "Grazing of crop residues: Impacts on soils and crop production," *Agric Ecosyst Environ*, vol. 258, pp. 71–90, Apr. 2018, doi: 10.1016/j.agee.2017.11.018.

[38] M. Abdalla *et al.*, "Critical review of the impacts of grazing intensity on soil organic carbon storage and other soil quality indicators in extensively managed grasslands," *Agric Ecosyst Environ*, vol. 253, pp. 62–81, Feb. 2018, doi: 10.1016/j.agee.2017.10.023.

[39] F. S. Galindo, K. Delate, B. Heins, H. Phillips, A. Smith, and P. H. Pagliari, "Cropping System and Rotational Grazing Effects on Soil Fertility and Enzymatic Activity in an Integrated Organic Crop-Livestock System," *Agronomy*, vol. 10, no. 6, p. 803, Jun. 2020, doi: 10.3390/agronomy10060803.

[40] M. Tudi *et al.*, "Agriculture Development, Pesticide Application and Its Impact on the Environment," *Int J Environ Res Public Health*, vol. 18, no. 3, p. 1112, Jan. 2021, doi: 10.3390/ijerph18031112.

[41] A. J. Lorenz *et al.*, "Genomic Selection in Plant Breeding," 2011, pp. 77–123. doi: 10.1016/B978-0-12-385531-2.00002-5.

[42] J. Crossa *et al.*, "Genomic Selection in Plant Breeding: Methods, Models, and Perspectives," *Trends Plant Sci*, vol. 22, no. 11, pp. 961–975, Nov. 2017, doi: 10.1016/j.tplants.2017.08.011.

[43] A. Pantera, M. R. Mosquera-Losada, F. Herzog, and M. den Herder, "Agroforestry and the environment," *Agroforestry Systems*, vol. 95, no. 5, pp. 767–774, Jun. 2021, doi: 10.1007/s10457-021-00640-8.

[44] M. Sollen-Norrlin, B. B. Ghaley, and N. L. J. Rintoul, "Agroforestry Benefits and Challenges for Adoption in Europe and Beyond," *Sustainability*, vol. 12, no. 17, p. 7001, Aug. 2020, doi: 10.3390/su12177001.

[45] F. Humpenöder *et al.*, "Peatland protection and restoration are key for climate change mitigation," *Environmental Research Letters*, vol. 15, no. 10, p. 104093, Oct. 2020, doi: 10.1088/1748-9326/abae2a.

[46] J. Loisel and A. Gallego-Sala, "Ecological resilience of restored peatlands to climate change," *Commun Earth Environ*, vol. 3, no. 1, p. 208, Sep. 2022, doi: 10.1038/s43247-022-00547-x.

[47] U. R. Sumaila, C. Bellmann, and A. Tipping, "Fishing for the future: An overview of challenges and opportunities," *Mar Policy*, vol. 69, pp. 173–180, Jul. 2016, doi: 10.1016/j.marpol.2016.01.003.

[48] U. R. Sumaila and T. C. Tai, "End Overfishing and Increase the Resilience of the Ocean to Climate Change," *Front Mar Sci*, vol. 7, Jul. 2020, doi: 10.3389/fmars.2020.00523.

[49] H. I. A. Clovis and A. M. Simon, "Understanding Overfishing: A Literature Review," *Asian Journal of Fisheries and Aquatic Research*, vol. 26, no. 1, pp. 61–71, Jan. 2024, doi: 10.9734/ajfar/2024/v26i1727.

[50] S. Maulu *et al.*, "Climate Change Effects on Aquaculture Production: Sustainability Implications, Mitigation, and Adaptations," *Front Sustain Food Syst*, vol. 5, Mar. 2021, doi: 10.3389/fsufs.2021.609097.

[51] M. Føre *et al.*, "Precision fish farming: A new framework to improve production in aquaculture," *Biosyst Eng*, vol. 173, pp. 176–193, Sep. 2018, doi: 10.1016/j.biosystemseng.2017.10.014.

[52] A. B. M. M. Haque, Md. A. Khan, M. M. Hossain, Md. E. Hossain, Md. Nahiduzzaman, and M. S. Islam, "Improved aquaculture management practices and its impact on small-scale rural aquaculture farmers in Bangladesh," *Aquaculture*, vol. 594, p. 741459, Jan. 2025, doi: 10.1016/j.aquaculture.2024.741459.

[53] K. Yue and Y. Shen, "An overview of disruptive technologies for aquaculture," *Aquac Fish*, vol. 7, no. 2, pp. 111–120, Mar. 2022, doi: 10.1016/j.aaf.2021.04.009.

[54] H. Ritchie, "Food production is responsible for one-quarter of the world's greenhouse gas emissions," *Our World in Data*, 2021, Accessed: Jan. 08, 2025. [Online]. Available: https://ourworldindata.org/greenhouse-gas-emissions-food

[55] A. Moumen, G. Azizi, K. Ben Chekroun, and M. Baghour, "The effects of livestock methane emission on the global warming: a review," *International Journal of Global Warming*, vol. 9, no. 2, p. 229, 2016, doi: 10.1504/IJGW.2016.074956.

[56] M. Herrero *et al.*, "Greenhouse gas mitigation potentials in the livestock sector," *Nat Clim Chang*, vol. 6, no. 5, pp. 452–461, May 2016, doi: 10.1038/nclimate2925.

[57] R. D. Kinley, G. Martinez-Fernandez, M. K. Matthews, R. de Nys, M. Magnusson, and N. W. Tomkins, "Mitigating the carbon footprint and improving productivity of ruminant livestock agriculture using a red seaweed," *J Clean Prod*, vol. 259, p. 120836, Jun. 2020, doi: 10.1016/j.jclepro.2020.120836.

[58] L. O. Tedeschi, J. P. Muir, D. G. Riley, and D. G. Fox, "The role of ruminant animals in sustainable livestock intensification programs," *International Journal of Sustainable Development & World Ecology*, pp. 1–14, Aug. 2015, doi: 10.1080/13504509.2015.1075441.

[59] M. Eugène, K. Klumpp, and D. Sauvant, "Methane mitigating options with forages fed to ruminants," *Grass and Forage Science*, vol. 76, no. 2, pp. 196–204, Jun. 2021, doi: 10.1111/gfs.12540.

[60] J. Guyader, H. H. Janzen, R. Kroebel, and K. A. Beauchemin, "Forage use to improve environmental sustainability of ruminant production12," *J Anim Sci*, vol. 94, no. 8, pp. 3147–3158, Aug. 2016, doi: 10.2527/jas.2015-0141.

[61] L. Kelly and E. Kebreab, "Recent advances in feed additives with the potential to mitigate enteric methane emissions from ruminant livestock," *J Soil Water Conserv*, vol. 78, no. 2, pp. 111–123, Mar. 2023, doi: 10.2489/jswc.2023.00070.

[62] A. Melgar *et al.*, "Effects of 3-nitrooxypropanol on rumen fermentation, lactational performance, and resumption of ovarian cyclicity in dairy cows," *J Dairy Sci*, vol. 103, no. 1, pp. 410–432, Jan. 2020, doi: 10.3168/jds.2019-17085.

[63] D. Chadwick *et al.*, "Manure management: Implications for greenhouse gas emissions," *Anim Feed Sci Technol*, vol. 166–167, pp. 514–531, Jun. 2011, doi: 10.1016/j.anifeedsci.2011.04.036.

[64] C. Pratt, M. Redding, J. Hill, and P. D. Jensen, "Does manure management affect the latent greenhouse gas emitting potential of livestock manures?," *Waste Management*, vol. 46, pp. 568–576, Dec. 2015, doi: 10.1016/j.wasman.2015.08.019.

[65] M. Anas *et al.*, "Fate of nitrogen in agriculture and environment: agronomic, eco-physiological and molecular approaches to improve nitrogen use efficiency," *Biol Res*, vol. 53, no. 1, p. 47, Dec. 2020, doi: 10.1186/s40659-020-00312-4.

[66] C. O. Dimkpa, J. Fugice, U. Singh, and T. D. Lewis, "Development of fertilizers for enhanced nitrogen use efficiency – Trends and perspectives," *Science of The Total Environment*, vol. 731, p. 139113, Aug. 2020, doi: 10.1016/j.scitotenv.2020.139113.

[67] S. Hussain *et al.*, "Rice management interventions to mitigate greenhouse gas emissions: a review," *Environmental Science and Pollution Research*, vol. 22, no. 5, pp. 3342–3360, Mar. 2015, doi: 10.1007/s11356-014-3760-4.

[68] T. N. Maraseni, R. C. Deo, J. Qu, P. Gentle, and P. R. Neupane, "An international comparison of rice consumption behaviours and greenhouse gas emissions from rice production," *J Clean Prod*, vol. 172, pp. 2288–2300, Jan. 2018, doi: 10.1016/j.jclepro.2017.11.182.

[69] A. Chel and G. Kaushik, "Renewable energy for sustainable agriculture," *Agron Sustain Dev*, vol. 31, no. 1, pp. 91–118, Jan. 2011, doi: 10.1051/agro/2010029.

[70] A. T. Balafoutis, M. Borzecka, S. Rozakis, K. Troullaki, F. Vandorou, and M. Wydra, "Investigating Published Research towards a Fossil-Energy-Free Agriculture Transformation," *Energies (Basel)*, vol. 17, no. 17, p. 4409, Sep. 2024, doi: 10.3390/en17174409.

[71] M. Hebrok and C. Boks, "Household food waste: Drivers and potential intervention points for design – An extensive review," *J Clean Prod*, vol. 151, pp. 380–392, May 2017, doi: 10.1016/j.jclepro.2017.03.069.

[72] E. Di Talia, M. Simeone, and D. Scarpato, "Consumer behaviour types in household food waste," *J Clean Prod*, vol. 214, pp. 166–172, Mar. 2019, doi: 10.1016/j.jclepro.2018.12.216.

[73] L. van Geffen, E. van Herpen, and H. van Trijp, "Household Food Waste—How to Avoid It? An Integrative Review," in *Food Waste Management*, Cham: Springer International Publishing, 2020, pp. 27–55. doi: 10.1007/978-3-030-20561-4_2.

[74] R. N. Zuñiga and E. Troncoso, "Shelf-life calculation and temperature-time indicators: importance in food safety," in *Chemical Food Safety and Health*, Franco Pedreschi Plasencia and Zuzana Ciesarová, Eds., Nova Science Publishers, Inc., 2013, pp. 131–148.

[75] P. C. Wanniarachchi, K. G. Upul Kumarasinghe, and C. Jayathilake, "Recent advancements in chemosensors for the detection of food spoilage," *Food Chem*, vol. 436, p. 137733, Mar. 2024, doi: 10.1016/j.foodchem.2023.137733.

[76] S. Huh, H.-J. Kim, S. Lee, J. Cho, A. Jang, and J. Bae, "Utilization of Electrical Impedance Spectroscopy and Image Classification for Non-Invasive Early Assessment of Meat Freshness," *Sensors*, vol. 21, no. 3, p. 1001, Feb. 2021, doi: 10.3390/s21031001.

[77] "Related titles from Woodhead's food science, technology and nutrition list," in *Understanding and Measuring the Shelf-Life of Food*, Elsevier, 2004, p. ii. doi: 10.1016/B978-1-85573-732-7.50001-9.

[78] W. Heo and S. Lim, "A Review on Gas Indicators and Sensors for Smart Food Packaging," *Foods*, vol. 13, no. 19, p. 3047, Sep. 2024, doi: 10.3390/foods13193047.

[79] C. S. Barry and J. J. Giovannoni, "Ethylene and Fruit Ripening," *J Plant Growth Regul*, vol. 26, no. 2, p. 143, Jun. 2007, doi: 10.1007/s00344-007-9002-y.

[80] X. Kou *et al.*, "Different regulatory mechanisms of plant hormones in the ripening of climacteric and non-climacteric fruits: a review," *Plant Mol Biol*, vol. 107, no. 6, pp. 477–497, Dec. 2021, doi: 10.1007/s11103-021-01199-9.

[81] V. Paul, R. Pandey, and G. C. Srivastava, "The fading distinctions between classical patterns of ripening in climacteric and non-climacteric fruit and the ubiquity of ethylene—An overview," *J Food Sci Technol*, vol. 49, no. 1, pp. 1–21, Feb. 2012, doi: 10.1007/s13197-011-0293-4.

[82] J. Yan, Z. Zhao, X. Wang, and J. Xie, "Hydrogen sulfide in seafood: Formation, hazards, and control," *Trends Food Sci Technol*, vol. 148, p. 104512, Jun. 2024, doi: 10.1016/j.tifs.2024.104512.

[83] F. Saliu and R. Della Pergola, "Carbon dioxide colorimetric indicators for food packaging application: Applicability of anthocyanin and poly-lysine mixtures," *Sens Actuators B Chem*, vol. 258, pp. 1117–1124, Apr. 2018, doi: 10.1016/j.snb.2017.12.007.

[84] C. Rukchon, A. Nopwinyuwong, S. Trevanich, T. Jinkarn, and P. Suppakul, "Development of a food spoilage indicator for monitoring freshness of skinless chicken breast," *Talanta*, vol. 130, pp. 547–554, Dec. 2014, doi: 10.1016/j.talanta.2014.07.048.

[85] P. Puligundla, J. Jung, and S. Ko, "Carbon dioxide sensors for intelligent food packaging applications," *Food Control*, vol. 25, no. 1, pp. 328–333, May 2012, doi: 10.1016/j.foodcont.2011.10.043.

[86] A. J. Pellissery, P. G. Vinayamohan, M. A. R. Amalaradjou, and K. Venkitanarayanan, "Spoilage bacteria and meat quality," in *Meat Quality Analysis*, Elsevier, 2020, pp. 307–334. doi: 10.1016/B978-0-12-819233-7.00017-3.

[87] D. Doeun, M. Davaatseren, and M.-S. Chung, "Biogenic amines in foods," *Food Sci Biotechnol*, vol. 26, no. 6, pp. 1463–1474, Dec. 2017, doi: 10.1007/s10068-017-0239-3.

[88] S. Ghavam, M. Vahdati, I. A. G. Wilson, and P. Styring, "Sustainable Ammonia Production Processes," *Front Energy Res*, vol. 9, Mar. 2021, doi: 10.3389/fenrg.2021.580808.

[89] J. Guo and P. Chen, "Ammonia history in the making," *Nat Catal*, vol. 4, no. 9, pp. 734–735, Sep. 2021, doi: 10.1038/s41929-021-00676-0.

[90] M. A. Sutton, J. W. Erisman, F. Dentener, and D. Möller, "Ammonia in the environment: From ancient times to the present," *Environmental Pollution*, vol. 156, no. 3, pp. 583–604, Dec. 2008, doi: 10.1016/j.envpol.2008.03.013.

[91] Y. Watanabe, W. Aoki, and M. Ueda, "Ammonia Production Using Bacteria and Yeast toward a Sustainable Society," *Bioengineering*, vol. 10, no. 1, p. 82, Jan. 2023, doi: 10.3390/bioengineering10010082.

[92] Ghaly, "Fish Spoilage Mechanisms and Preservation Techniques: Review," *Am J Appl Sci*, vol. 7, no. 7, pp. 859–877, Jul. 2010, doi: 10.3844/ajassp.2010.859.877.

[93] C. A. Damalas and I. G. Eleftherohorinos, "Pesticide Exposure, Safety Issues, and Risk Assessment Indicators," *Int J Environ Res Public Health*, vol. 8, no. 5, pp. 1402–1419, May 2011, doi: 10.3390/ijerph8051402.

[94] S. Anderson, "No Flies on Me Thanks to DDT - Black Flag," CC BY-NC-SA 2.0, https://www.flickr.com/photos/swanksalot/46978564681/in/photostream/.

[95] J. BEARD, "DDT and human health," *Science of The Total Environment*, vol. 355, no. 1–3, pp. 78–89, Feb. 2006, doi: 10.1016/j.scitotenv.2005.02.022.

[96] J. W. Grier, "Ban of DDT and Subsequent Recovery of Reproduction in Bald Eagles," *Science (1979)*, vol. 218, no. 4578, pp. 1232–1235, Dec. 1982, doi: 10.1126/science.7146905.

[97] W. W. Walker and B. J. Stojanovic, "Acetylcholinesterase Toxicity of Malathion and Its Metabolites," *J Environ Qual*, vol. 2, no. 4, pp. 474–475, Oct. 1973, doi: 10.2134/jeq1973.00472425000200040015x.

[98] H. W. Chambers, "Organophosphorus Compounds: An Overview," in *Organophosphates Chemistry, Fate, and Effects*, Elsevier, 1992, pp. 3–17. doi: 10.1016/B978-0-08-091726-9.50005-7.

[99] J. Kaushal, M. Khatri, and S. K. Arya, "A treatise on Organophosphate pesticide pollution: Current strategies and advancements in their environmental degradation and elimination," *Ecotoxicol Environ Saf*, vol. 207, p. 111483, 2021, doi: https://doi.org/10.1016/j.ecoenv.2020.111483.

[100] S. I. Mulla *et al.*, "Organophosphate Pesticides: Impact on Environment, Toxicity, and Their Degradation," in *Bioremediation of Industrial Waste for Environmental Safety*, Singapore: Springer Singapore, 2020, pp. 265–290. doi: 10.1007/978-981-13-1891-7_13.

[101] K. V. RAGNARSDOTTIR, "Environmental fate and toxicology of organophosphate pesticides," *J Geol Soc London*, vol. 157, no. 4, pp. 859–876, Jul. 2000, doi: 10.1144/jgs.157.4.859.

[102] S. W. Zhang, R. Wang, F. Wang, and M. Cai, "Assessment of currently used and restricted organophosphorus pesticides and their degradation products in urban drinking water: An investigation of eight cities in Yangtze River Delta urban agglomeration, East China," *Journal of Hazardous Materials Advances*, vol. 9, p. 100211, Feb. 2023, doi: 10.1016/j.hazadv.2022.100211.

[103] M. A. Dar, G. Kaushik, and J. F. Villareal Chiu, "Pollution status and biodegradation of organophosphate pesticides in the environment," in *Abatement of Environmental Pollutants*, Elsevier, 2020, pp. 25–66. doi: 10.1016/B978-0-12-818095-2.00002-3.

[104] J. Kaushal, M. Khatri, and S. K. Arya, "A treatise on Organophosphate pesticide pollution: Current strategies and advancements in their environmental degradation and elimination," *Ecotoxicol Environ Saf*, vol. 207, p. 111483, Jan. 2021, doi: 10.1016/j.ecoenv.2020.111483.

[105] A. R. Nandhini, M. Harshiny, and S. N. Gummadi, "Chlorpyrifos in environment and food: a critical review of detection methods and degradation pathways," *Environ Sci Process Impacts*, vol. 23, no. 9, pp. 1255–1277, 2021, doi: 10.1039/D1EM00178G.

[106] S. O. Duke, "Glyphosate: environmental fate and impact," *Weed Sci*, vol. 68, no. 3, pp. 201–207, May 2020, doi: 10.1017/wsc.2019.28.

[107] A. Van Scoy, A. Pennell, and X. Zhang, "Environmental Fate and Toxicology of Dimethoate," 2016, pp. 53–70. doi: 10.1007/978-3-319-23573-8_3.

[108] L. Gorecki *et al.*, "Oxime K203: a drug candidate for the treatment of tabun intoxication," *Arch Toxicol*, vol. 93, no. 3, pp. 673–691, Mar. 2019, doi: 10.1007/s00204-018-2377-7.

[109] L. Carrasco Cabrera, G. Di Piazza, B. Dujardin, E. Marchese, and P. Medina Pastor, "The 2022 European Union report on pesticide residues in food," *EFSA Journal*, vol. 22, no. 4, Apr. 2024, doi: 10.2903/j.efsa.2024.8753.

[110] R. A. Hites, "The Rise and Fall of Chlorpyrifos in the United States," *Environ Sci Technol*, vol. 55, no. 3, pp. 1354–1358, Feb. 2021, doi: 10.1021/acs.est.0c06579.

[111] D. L. Eaton *et al.*, "Review of the Toxicology of Chlorpyrifos With an Emphasis on Human Exposure and Neurodevelopment," *Crit Rev Toxicol*, vol. 38, no. sup2, pp. 1–125, Jan. 2008, doi: 10.1080/10408440802272158.

[112] E. D. Levin, N. Addy, A. Nakajima, N. C. Christopher, F. J. Seidler, and T. A. Slotkin, "Persistent behavioral consequences of neonatal chlorpyrifos exposure in

rats," *Developmental Brain Research*, vol. 130, no. 1, pp. 83–89, Sep. 2001, doi: 10.1016/S0165-3806(01)00215-2.

[113] H. Ubaid ur Rahman, W. Asghar, W. Nazir, M. A. Sandhu, A. Ahmed, and N. Khalid, "A comprehensive review on chlorpyrifos toxicity with special reference to endocrine disruption: Evidence of mechanisms, exposures and mitigation strategies," *Science of The Total Environment*, vol. 755, p. 142649, Feb. 2021, doi: 10.1016/j.scitotenv.2020.142649.

[114] E. M. John and J. M. Shaike, "Chlorpyrifos: pollution and remediation," *Environ Chem Lett*, vol. 13, no. 3, pp. 269–291, Sep. 2015, doi: 10.1007/s10311-015-0513-7.

[115] X. Huang, H. Cui, and W. Duan, "Ecotoxicity of chlorpyrifos to aquatic organisms: A review," *Ecotoxicol Environ Saf*, vol. 200, p. 110731, Sep. 2020, doi: 10.1016/j.ecoenv.2020.110731.

[116] M. Z. Ahmad, A. Khan, M. T. Javed, and I. Hussain, "Impact of chlorpyrifos on health biomarkers of broiler chicks," *Pestic Biochem Physiol*, vol. 122, pp. 50–58, Jul. 2015, doi: 10.1016/j.pestbp.2014.12.024.

[117] A. Villalba, M. Maggi, P. M. Ondarza, N. Szawarski, and K. S. B. Miglioranza, "Influence of land use on chlorpyrifos and persistent organic pollutant levels in honey bees, bee bread and honey: Beehive exposure assessment," *Science of The Total Environment*, vol. 713, p. 136554, Apr. 2020, doi: 10.1016/j.scitotenv.2020.136554.

[118] Directorate-General for Agriculture and Rural Development, "EU agri-food exports keep growing steadily in the first quarter." Accessed: Oct. 08, 2024. [Online]. Available: https://agriculture.ec.europa.eu/news/eu-agri-food-exports-keep-growing-steadily-first-quarter-2024-06-25_en

[119] G. W. Lucier and R. E. Menzer, "Metabolism of dimethoate in bean plants in relation to its mode of application," *J Agric Food Chem*, vol. 16, no. 6, pp. 936–945, Nov. 1968, doi: 10.1021/jf60160a020.

[120] D. A. Lindquist, J. Hacskaylo, J. C. Clark, and T. B. Davich, "Systemic Activity of Dimethoate Applied to Cotton Seeds1," *J Econ Entomol*, vol. 54, no. 6, pp. 1132–1135, Dec. 1961, doi: 10.1093/jee/54.6.1132.

[121] A. Van Scoy, A. Pennell, and X. Zhang, "Environmental Fate and Toxicology of Dimethoate," 2016, pp. 53–70. doi: 10.1007/978-3-319-23573-8_3.

[122] A. Eken, "Dimethoate organophosphate insecticide toxicity and the role of oxidative stress," in *Toxicology*, Elsevier, 2021, pp. 59–68. doi: 10.1016/B978-0-12-819092-0.00007-8.

[123] P. Giang and M. Schechter, "Insecticide Residues, Colorimetric Method for the Estimation of Dimethoate Residues," *J Agric Food Chem*, vol. 11, no. 1, pp. 63–66, Jan. 1963, doi: 10.1021/jf60125a019.

[124] B. Jaselskis, C. E. Moore, and A. von Smolinski, "Development of the pH Meter," 1989, pp. 254–271. doi: 10.1021/bk-1989-0390.ch018.

[125] C. Corsi, "History highlights and future trends of infrared sensors," *J Mod Opt*, vol. 57, no. 18, pp. 1663–1686, Oct. 2010, doi: 10.1080/09500341003693011.

[126] M. F. S. Ferreira *et al.*, "Roadmap on optical sensors," *Journal of Optics*, vol. 19, no. 8, p. 083001, Aug. 2017, doi: 10.1088/2040-8986/aa7419.

[127] N. Sharma, M. Shamkuwar, and I. Singh, "The History, Present and Future with IoT," 2019, pp. 27–51. doi: 10.1007/978-3-030-04203-5_3.

[128] N. C. Thomas, "The early history of spectroscopy," *J Chem Educ*, vol. 68, no. 8, p. 631, Aug. 1991, doi: 10.1021/ed068p631.

[129] Philip and T. Sadtler, "History of 'Sadtler' Spectroscopy," *Appl Spectrosc*, vol. 39, no. 6, pp. xix–xxii, Nov. 1985, doi: 10.1366/0003702854249448.

[130] J. Hecht, "Short history of laser development," *Optical Engineering*, vol. 49, no. 9, p. 091002, Sep. 2010, doi: 10.1117/1.3483597.

[131] J. Ballato and P. Dragic, "Glass: The Carrier of Light - A Brief History of Optical Fiber," *Int J Appl Glass Sci*, vol. 7, no. 4, pp. 413–422, Dec. 2016, doi: 10.1111/ijag.12239.

[132] J. Haus, *Optical Sensors*. Wiley, 2010. doi: 10.1002/9783527629435.

[133] G. Gauglitz, "Direct optical sensors: principles and selected applications," *Anal Bioanal Chem*, vol. 381, no. 1, pp. 141–155, Jan. 2005, doi: 10.1007/s00216-004-2895-4.

[134] L. Basabe-Desmonts, D. N. Reinhoudt, and M. Crego-Calama, "Design of fluorescent materials for chemical sensing," *Chem Soc Rev*, vol. 36, no. 6, p. 993, 2007, doi: 10.1039/b609548h.

[135] Y. Xu *et al.*, "Optical Refractive Index Sensors with Plasmonic and Photonic Structures: Promising and Inconvenient Truth," *Adv Opt Mater*, vol. 7, no. 9, May 2019, doi: 10.1002/adom.201801433.

[136] B. R. Masters, "Molecular Fluorescence: Principles and Applications, Second Edition," *J Biomed Opt*, vol. 18, no. 3, p. 039901, Mar. 2013, doi: 10.1117/1.JBO.18.3.039901.

[137] J. R. Lakowicz, "Introduction to Fluorescence," in *Principles of Fluorescence Spectroscopy*, Boston, MA: Springer US, 1999, pp. 1–23. doi: 10.1007/978-1-4757-3061-6_1.

[138] CactiStaccingCrane, "Stokes shift diagram," CC BY 4.0, https://en.wikipedia.org/wiki/File:Stokes_shift_diagram.svg.

[139] B. Bagchi, D. W. Oxtoby, and G. R. Fleming, "Theory of the time development of the stokes shift in polar media," *Chem Phys*, vol. 86, no. 3, pp. 257–267, 1984, doi: 10.1016/0301-0104(84)80014-2.

[140] W. McCall *et al.*, "Evaluation and application of the optical image profiler (OIP) a direct push probe for photo-logging UV-induced fluorescence of petroleum hydrocarbons," *Environ Earth Sci*, vol. 77, no. 10, p. 374, May 2018, doi: 10.1007/s12665-018-7442-2.

[141] M. M. Somoza, "Vibration-fluor-abs," CC-BY-SA 2.5, https://commons.wikimedia.org/wiki/File:Vibration-fluor-abs.png.

[142] A. Bączyński and D. Radomska, "Electronic spectra of dye solutions. I. The mirror image rule," *J Fluoresc*, vol. 2, no. 3, pp. 175–180, Sep. 1992, doi: 10.1007/BF00866932.

[143] R. F. Chen, "Some characteristics of the fluorescence of quinine," *Anal Biochem*, vol. 19, no. 2, pp. 374–387, May 1967, doi: 10.1016/0003-2697(67)90174-1.

[144] J. C. del Valle and J. Catalán, "Kasha's rule: a reappraisal," *Physical Chemistry Chemical Physics*, vol. 21, no. 19, pp. 10061–10069, 2019, doi: 10.1039/C9CP00739C.

[145] J. L. Abernethy, "The historical and current interest in coumarin," *J Chem Educ*, vol. 46, no. 9, p. 561, Sep. 1969, doi: 10.1021/ed046p561.

[146] P.-S. Song and W. H. Gordon, "Spectroscopic study of the excited states of coumarin," *J Phys Chem*, vol. 74, no. 24, pp. 4234–4240, Nov. 1970, doi: 10.1021/j100718a010.

[147] D. Cao *et al.*, "Coumarin-Based Small-Molecule Fluorescent Chemosensors," *Chem Rev*, vol. 119, no. 18, pp. 10403–10519, Sep. 2019, doi: 10.1021/acs.chemrev.9b00145.

[148] Pooja, H. Pandey, S. Aggarwal, M. Vats, V. Rawat, and S. R. Pathak, "Coumarin-based Chemosensors for Metal Ions Detection," *Asian J Org Chem*, vol. 11, no. 12, Dec. 2022, doi: 10.1002/ajoc.202200455.

[149] M.-Y. Wu, T. He, K. Li, M.-B. Wu, Z. Huang, and X.-Q. Yu, "A real-time colorimetric and ratiometric fluorescent probe for sulfite," *Analyst*, vol. 138, no. 10, p. 3018, 2013, doi: 10.1039/c3an00172e.

[150] H. Zhang, X. Liu, Y. Gong, T. Yu, and Y. Zhao, "Synthesis and characterization of SFX-based coumarin derivatives for OLEDs," *Dyes and Pigments*, vol. 185, p. 108969, Feb. 2021, doi: 10.1016/j.dyepig.2020.108969.

[151] X. Liu, J. M. Cole, P. G. Waddell, T.-C. Lin, J. Radia, and A. Zeidler, "Molecular Origins of Optoelectronic Properties in Coumarin Dyes: Toward Designer Solar Cell and Laser Applications," *J Phys Chem A*, vol. 116, no. 1, pp. 727–737, Jan. 2012, doi: 10.1021/jp209925y.

[152] B. B. Raju and T. S. Varadarajan, "Spectroscopic studies of 7-diethylamino-3-styryl coumarins," *J Photochem Photobiol A Chem*, vol. 85, no. 3, pp. 263–267, Jan. 1995, doi: 10.1016/1010-6030(94)03905-A.

[153] S. M. Hossain, K. Singh, A. Lakma, R. N. Pradhan, and A. K. Singh, "A schiff base ligand of coumarin derivative as an ICT-Based fluorescence chemosensor for Al 3+," *Sens Actuators B Chem*, vol. 239, pp. 1109–1117, Feb. 2017, doi: 10.1016/j.snb.2016.08.093.

[154] J. L. Belmonte-Vázquez, Y. A. Amador-Sánchez, L. A. Rodríguez-Cortés, and B. Rodríguez-Molina, "Dual-State Emission (DSE) in Organic Fluorophores: Design and Applications," *Chemistry of Materials*, vol. 33, no. 18, pp. 7160–7184, Sep. 2021, doi: 10.1021/acs.chemmater.1c02460.

[155] C. Chen and C. Fang, "Fluorescence Modulation by Amines: Mechanistic Insights into Twisted Intramolecular Charge Transfer (TICT) and Beyond," *Chemosensors*, vol. 11, no. 2, p. 87, Jan. 2023, doi: 10.3390/chemosensors11020087.

[156] G. Chu and F. Yangbo, "Solvent and substituent effects on intramolecular charge transfer of selected derivatives of 4-trifluoromethyl-7-aminocoumarin," *Journal of the Chemical Society, Faraday Transactions 1: Physical Chemistry in Condensed Phases*, vol. 83, no. 8, p. 2533, 1987, doi: 10.1039/f19878302533.

[157] A. Tarai and B. Nath, "A review on oxime functionality: an ordinary functional group with significant impacts in supramolecular chemistry," *Chemical Communications*, vol. 60, no. 57, pp. 7266–7287, 2024, doi: 10.1039/D4CC01397B.

[158] F. Worek, H. Thiermann, and T. Wille, "Oximes in organophosphate poisoning: 60 years of hope and despair," *Chem Biol Interact*, vol. 259, pp. 93–98, Nov. 2016, doi: 10.1016/j.cbi.2016.04.032.

[159] J. Collins, Z. Xiao, M. Müllner, and L. A. Connal, "The emergence of oxime click chemistry and its utility in polymer science," *Polym Chem*, vol. 7, no. 23, pp. 3812–3826, 2016, doi: 10.1039/C6PY00635C.

[160] V. Yu. Kukushkin and A. J. L. Pombeiro, "Oxime and oximate metal complexes: unconventional synthesis and reactivity," *Coord Chem Rev*, vol. 181, no. 1, pp. 147–175, Jan. 1999, doi: 10.1016/S0010-8545(98)00215-X.

[161] F. Worek, H. Thiermann, and T. Wille, "Organophosphorus compounds and oximes: a critical review," *Arch Toxicol*, vol. 94, no. 7, pp. 2275–2292, Jul. 2020, doi: 10.1007/s00204-020-02797-0.

[162] I. Oh and R. I. Masel, "Electrochemical Organophosphate Sensor Based on Oxime Chemistry," *Electrochemical and Solid-State Letters*, vol. 10, no. 2, p. J19, 2007, doi: 10.1149/1.2400206.

[163] M. Dolai, R. Alam, A. Katarkar, K. Chaudhuri, and M. Ali, "Oxime Based Selective Fluorescent Sensor for Arsenate Ion in a Greener Way with Bio-Imaging Application," *Analytical Sciences*, vol. 32, no. 12, pp. 1295–1300, Dec. 2016, doi: 10.2116/analsci.32.1295.

[164] I. Walton *et al.*, "A Fluorescent Dipyrrinone Oxime for the Detection of Pesticides and Other Organophosphates," *Org Lett*, vol. 14, no. 11, pp. 2686–2689, Jun. 2012, doi: 10.1021/ol300799f.

[165] T. J. Dale and J. Rebek, "Hydroxy Oximes as Organophosphorus Nerve Agent Sensors," *Angewandte Chemie International Edition*, vol. 48, no. 42, pp. 7850–7852, Oct. 2009, doi: 10.1002/anie.200902820.

[166] S.-W. Zhang and T. M. Swager, "Fluorescent Detection of Chemical Warfare Agents: Functional Group Specific Ratiometric Chemosensors," *J Am Chem Soc*, vol. 125, no. 12, pp. 3420–3421, Mar. 2003, doi: 10.1021/ja029265z.

[167] J. Y. Lee, Y. H. Lee, and Y. G. Byun, "Detection of Chemical Warfare Nerve Agents via a Beckmann Fragmentation of Aldoxime," *Phosphorus Sulfur Silicon Relat Elem*, vol. 187, no. 5, pp. 641–649, May 2012, doi: 10.1080/10426507.2011.636110.

[168] L. D. Landau, "On the theory of phase transitions," *Zh. Eksp. Teor. Fiz.*, vol. 7, pp. 19–32, 1937, doi: 10.1016/B978-0-08-010586-4.50034-1.

[169] R. Peierls, "Quelques propriétés typiques des corps solides," *Annales de l'institut Henri Poincaré*, vol. 5, no. 3, pp. 177–222, 1935, [Online]. Available: http://www.numdam.org/item/AIHP_1935___5_3_177_0/

[170] K. S. Novoselov *et al.*, "Electric Field Effect in Atomically Thin Carbon Films," *Science (1979)*, vol. 306, no. 5696, pp. 666–669, Oct. 2004, doi: 10.1126/science.1102896.

[171] N. Bellier, P. Baipaywad, N. Ryu, J. Y. Lee, and H. Park, "Recent biomedical advancements in graphene oxide- and reduced graphene oxide-based nanocomposite nanocarriers," *Biomater Res*, vol. 26, no. 1, Sep. 2022, doi: 10.1186/s40824-022-00313-2.

[172] A. R. Urade, I. Lahiri, and K. S. Suresh, "Graphene Properties, Synthesis and Applications: A Review," *JOM*, vol. 75, no. 3, pp. 614–630, Mar. 2023, doi: 10.1007/s11837-022-05505-8.

[173] F. Farjadian *et al.*, "Recent Developments in Graphene and Graphene Oxide: Properties, Synthesis, and Modifications: A Review," *ChemistrySelect*, vol. 5, no. 33, pp. 10200–10219, Sep. 2020, doi: 10.1002/slct.202002501.

[174] T. H. Banglani *et al.*, "Graphene-based nanocomposites for gas sensors: challenges and opportunities," *Reviews in Inorganic Chemistry*, vol. 44, no. 3, pp. 385–408, Sep. 2024, doi: 10.1515/revic-2023-0033.

[175] G. Ji, J. Tian, F. Xing, and Y. Feng, "Optical Biosensor Based on Graphene and Its Derivatives for Detecting Biomolecules," *Int J Mol Sci*, vol. 23, no. 18, p. 10838, Sep. 2022, doi: 10.3390/ijms231810838.

[176] T. Schmaltz, L. Wormer, U. Schmoch, and H. Döscher, "Graphene Roadmap Briefs (No. 3): meta-market analysis 2023," *2d Mater*, vol. 11, no. 2, p. 022002, Apr. 2024, doi: 10.1088/2053-1583/ad1e78.

[177] W. Gao, "The Chemistry of Graphene Oxide," in *Graphene Oxide*, Cham: Springer International Publishing, 2015, pp. 61–95. doi: 10.1007/978-3-319-15500-5_3.

[178] F. Farjadian *et al.*, "Recent Developments in Graphene and Graphene Oxide: Properties, Synthesis, and Modifications: A Review," *ChemistrySelect*, vol. 5, no. 33, pp. 10200–10219, Sep. 2020, doi: 10.1002/slct.202002501.

[179] W. Yu, L. Sisi, Y. Haiyan, and L. Jie, "Progress in the functional modification of graphene/graphene oxide: a review," *RSC Adv*, vol. 10, no. 26, pp. 15328–15345, 2020, doi: 10.1039/D0RA01068E.

[180] K. Toda, R. Furue, and S. Hayami, "Recent progress in applications of graphene oxide for gas sensing: A review," *Anal Chim Acta*, vol. 878, pp. 43–53, Jun. 2015, doi: 10.1016/j.aca.2015.02.002.

[181] C. R. Minitha, V. S. Anithaa, V. Subramaniam, and R. T. Rajendra Kumar, "Impact of Oxygen Functional Groups on Reduced Graphene Oxide-Based Sensors for Ammonia and Toluene Detection at Room Temperature," *ACS Omega*, vol. 3, no. 4, pp. 4105–4112, Apr. 2018, doi: 10.1021/acsomega.7b02085.

[182] Y. Peng and J. Li, "Ammonia adsorption on graphene and graphene oxide: a first-principles study," *Front Environ Sci Eng*, vol. 7, no. 3, pp. 403–411, Jun. 2013, doi: 10.1007/s11783-013-0491-6.

[183] R. Tarcan, O. Todor-Boer, I. Petrovai, C. Leordean, S. Astilean, and I. Botiz, "Reduced graphene oxide today," *J Mater Chem C Mater*, vol. 8, no. 4, pp. 1198–1224, 2020, doi: 10.1039/C9TC04916A.

[184] S. Pei and H.-M. Cheng, "The reduction of graphene oxide," *Carbon N Y*, vol. 50, no. 9, pp. 3210–3228, Aug. 2012, doi: 10.1016/j.carbon.2011.11.010.

[185] R. Larciprete, S. Fabris, T. Sun, P. Lacovig, A. Baraldi, and S. Lizzit, "Dual Path Mechanism in the Thermal Reduction of Graphene Oxide," *J Am Chem Soc*, vol. 133, no. 43, pp. 17315–17321, Nov. 2011, doi: 10.1021/ja205168x.

[186] Q. T. Tran *et al.*, "Reduced graphene oxide as an over-coating layer on silver nanostructures for detecting NH3 gas at room temperature," *Sens Actuators B Chem*, vol. 194, pp. 45–50, Apr. 2014, doi: 10.1016/j.snb.2013.12.062.

[187] W. Li, X. Li, L. Cai, Y. Sun, M. Sun, and D. Xie, "Reduced Graphene Oxide for Room Temperature Ammonia (NH_3) Gas Sensor," *J Nanosci Nanotechnol*, vol. 18, no. 11, pp. 7927–7932, Nov. 2018, doi: 10.1166/jnn.2018.15563.

[188] V. Agarwal and P. B. Zetterlund, "Strategies for reduction of graphene oxide – A comprehensive review," *Chemical Engineering Journal*, vol. 405, p. 127018, Feb. 2021, doi: 10.1016/j.cej.2020.127018.

[189] C. K. Chua and M. Pumera, "Chemical reduction of graphene oxide: a synthetic chemistry viewpoint," *Chem. Soc. Rev.*, vol. 43, no. 1, pp. 291–312, 2014, doi: 10.1039/C3CS60303B.

[190] A. E. F. Oliveira, G. B. Braga, C. R. T. Tarley, and A. C. Pereira, "Thermally reduced graphene oxide: synthesis, studies and characterization," *J Mater Sci*, vol. 53, no. 17, pp. 12005–12015, Sep. 2018, doi: 10.1007/s10853-018-2473-3.

[191] A. E. F. Oliveira, G. B. Braga, C. R. T. Tarley, and A. C. Pereira, "Thermally reduced graphene oxide: synthesis, studies and characterization," *J Mater Sci*, vol. 53, no. 17, pp. 12005–12015, Sep. 2018, doi: 10.1007/s10853-018-2473-3.

[192] S. H. B. Vinoth Kumar, R. Muydinov, and B. Szyszka, "Plasma Assisted Reduction of Graphene Oxide Films," *Nanomaterials*, vol. 11, no. 2, p. 382, Feb. 2021, doi: 10.3390/nano11020382.

[193] L. Guardia, S. Villar-Rodil, J. I. Paredes, R. Rozada, A. Martínez-Alonso, and J. M. D. Tascón, "UV light exposure of aqueous graphene oxide suspensions to promote their direct reduction, formation of graphene–metal nanoparticle hybrids and dye degradation," *Carbon N Y*, vol. 50, no. 3, pp. 1014–1024, Mar. 2012, doi: 10.1016/j.carbon.2011.10.005.

[194] R. Jakhar, J. E. Yap, and R. Joshi, "Microwave reduction of graphene oxide," *Carbon N Y*, vol. 170, pp. 277–293, Dec. 2020, doi: 10.1016/j.carbon.2020.08.034.

[195] X. Mei, X. Meng, and F. Wu, "Hydrothermal method for the production of reduced graphene oxide," *Physica E Low Dimens Syst Nanostruct*, vol. 68, pp. 81–86, Apr. 2015, doi: 10.1016/j.physe.2014.12.011.

[196] A. Zhou, J. Bai, W. Hong, and H. Bai, "Electrochemically reduced graphene oxide: Preparation, composites, and applications," *Carbon N Y*, vol. 191, pp. 301–332, May 2022, doi: 10.1016/j.carbon.2022.01.056.

[197] D. J. Mullan, *Physics of the Sun*. Boca Raton: CRC Press, 2022. doi: 10.1201/9781003153115.

[198] G. G. Howes, "A dynamical model of plasma turbulence in the solar wind," *Philosophical Transactions of the Royal Society A: Mathematical, Physical and Engineering Sciences*, vol. 373, no. 2041, p. 20140145, May 2015, doi: 10.1098/rsta.2014.0145.

[199] M. Barbarino, "A brief history of nuclear fusion," *Nat Phys*, vol. 16, no. 9, pp. 890–893, Sep. 2020, doi: 10.1038/s41567-020-0940-7.

[200] L. Chen *et al.*, "Modeling and plasma characteristics of high-power direct current discharge," *Plasma Sources Sci Technol*, vol. 29, no. 2, p. 025016, Feb. 2020, doi: 10.1088/1361-6595/ab681c.

[201] J. Schulze, E. Schüngel, Z. Donkó, and U. Czarnetzki, "Charge dynamics in capacitively coupled radio frequency discharges," *J Phys D Appl Phys*, vol. 43, no. 22, p. 225201, Jun. 2010, doi: 10.1088/0022-3727/43/22/225201.

[202] J. Hopwood, "Review of inductively coupled plasmas for plasma processing," *Plasma Sources Sci Technol*, vol. 1, no. 2, pp. 109–116, May 1992, doi: 10.1088/0963-0252/1/2/006.

[203] Y. A. Lebedev, "Microwave discharges: generation and diagnostics," *J Phys Conf Ser*, vol. 257, p. 012016, Nov. 2010, doi: 10.1088/1742-6596/257/1/012016.

[204] R. Brandenburg, "Dielectric barrier discharges: progress on plasma sources and on the understanding of regimes and single filaments," *Plasma Sources Sci Technol*, vol. 26, no. 5, p. 053001, Mar. 2017, doi: 10.1088/1361-6595/aa6426.

[205] Wblanchard, "Inductively Coupled Plasma," CC BY SA 3.0, https://commons.wikimedia.org/wiki/File:Inductively_Coupled_Plasma.jpg.

[206] E. Igors, "ICP torch," CC BY SA 4.0, https://commons.wikimedia.org/wiki/File:ICP_torch.svg.

[207] V. A. Godyak, R. B. Piejak, and B. M. Alexandrovich, "Experimental setup and electrical characteristics of an inductively coupled plasma," *J Appl Phys*, vol. 85, no. 2, pp. 703–712, Jan. 1999, doi: 10.1063/1.369150.

[208] K. C. Sabat, "Hydrogen Plasma - Thermodynamics," *J Phys Conf Ser*, vol. 1172, p. 012086, Mar. 2019, doi: 10.1088/1742-6596/1172/1/012086.

[209] C.-R. Yang, S.-F. Tseng, and Y.-T. Chen, "Characteristics of Graphene Oxide Films Reduced by Using an Atmospheric Plasma System," *Nanomaterials*, vol. 8, no. 10, p. 802, Oct. 2018, doi: 10.3390/nano8100802.

[210] V. K. Abdelkader-Fernández, M. Melguizo, M. Domingo-García, F. J. López-Garzón, and M. Pérez-Mendoza, "Hydrogen cold plasma for the effective reduction of graphene oxide," *Appl Surf Sci*, vol. 464, pp. 673–681, Jan. 2019, doi: 10.1016/j.apsusc.2018.09.121.

Bibliography

Publications Related to the Thesis

Journal Articles

A. Kurtishaj Hamzaj, E. Donà, N. M Santhosh, V. Shvalya, M. Košiček, and U. Cvelbar, "Plasma-Modification of graphene oxide for advanced ammonia sensing," *Applied Surface Science*, vol. 660, p. 160006, Jul. 2024, doi: 10.1016/j.apsusc.2024.160006.

E. Donà, G. J. Mohr, and A. Lobnik, "Dimethoate detection through a fluorescent coumarin dye," *Microchemical Journal*, vol. 207, p. 112205, Dec. 2024, doi: 10.1016/j.microc.2024.112205.

E. Donà, and A. Lobnik, "Chlorpyrifos detection based on 9-fluorenone oxime," *Chemosensors*, vol. 13, no. 5, p. 170, May 2025, doi: 10.3390/chemosensors13050170.

Conference Paper

E. Donà, G. J. Mohr, and A. Lobnik, "Design of experiment methodology to optimize dimethoate hydrolysis and improve fluorescence detection efficiency", in *16th Jožef Stefan International Postgraduate School Students' Conference*, Piran, Slovenia, May 2024.

Biography

Doctoral candidate Edoardo Donà completed his master's degree in chemistry at the University of Padua in 2018, with a thesis titled *"Electrolytes for Magnesium Secondary Batteries Based on Ionic Liquids"*, under the supervision of Prof. Vito Di Noto. He then moved to industry for a graduate program at Stevanato Group, a worldwide leader in pharmaceutical primary packaging. As a process engineer in the glass syringe production department, he was part of the continuous improvement team, successfully leading two 5S projects and a project focused on reducing microcracks.

As part of the graduate program, he later transitioned to regulatory affairs, assisting pharmaceutical companies with regulatory compliance by providing detailed process information, including raw material data, stability studies, and migration studies, as well as supporting the registration process for new drugs. He also worked at Lorenzi Srl as a researcher, investigating microfiber applications to enhance the performance of shoes and bags.

After this period in the industry, he decided to return to academia, and in 2021, he was awarded with the prestigious Marie Curie fellowship under the FoodTraNet project (https://www.foodtranet.org/) with the title *"New chemical sensors for food quality and safety"*. He is currently enrolled in the "Sensor Technologies" program at Jožef Stefan Postgraduate School in Ljubljana, primarily conducting his research at the Institute of Environmental Protection and Sensors (IOS) in Maribor under the supervision of Prof. Dr. Aleksandra Lobnik.

He is the first author of three articles published in internationally recognized peer-reviewed journals.

Training and Professional Development

In addition to his research, the candidate also participated in the following advanced training programs:

- Summer School on "Food quality, authenticity and traceability" in Trento, Italy, organized by Fondazione Edmund Mach, 22-24 June 2022;
- Winter School on "Advanced study course on optical chemical sensors", in Obergurgl, Austria, organized by Ulm University, 15-22 October 2022;
- Summer School on "Advanced solution in food production and safety" in Almeria, Spain, organized by University of Almeria, 19-23 June 2023;
- Winter School on "Advanced solutions in food production and safety" in Thessaloniki, Greece, organized by Aristotele University of Thessaloniki, 26-28 March 2024.